Next Generation Polymers of Intrinsic Microporosity with Tunable Moieties

for Ultrahigh Permeation and Precise Molecular CO2 Separation

Ahmad Arabi Shamsabadi¹, Mashallah Rezakazemi², Farzad Seidi³, Hossein Riazi¹,

Tejraj Aminabhavi⁴, Masoud Soroush^{1,*}

¹Department of Chemical and Biological Engineering, Drexel University, Philadelphia, PA 19104,

USA

² Faculty of Chemical and Materials Engineering, Shahrood University of Technology, Shahrood,

Iran

³ Jiangsu Co-Innovation Center of Efficient Processing and Utilization of Forest Resources,

College of Light Industry and Food Engineering, Nanjing Forestry University, Nanjing 210037,

China

⁴ Pharmaceutical Engineering, Sonia College of Pharmacy, Dharwad 580 002, India

January 4, 2020

FOURTH REVISED VERSION

Submitted for Publication in *Progress in Energy and Combustion Science*

*Corresponding author: <u>ms1@drexel.edu</u>

0

Abstract

Polymers of intrinsic microporosity (PIMs) with high free volumes have been synthesized by

incorporating contorted rigid moieties into polymers backbones. Despite their many appealing

properties, membranes made of these polymers have not been used industrially because of their

fast physical aging. The unprecedented CO₂ permeability and satisfactory CO₂/N₂ and CO₂/CH₄

selectivity of PIMs have led to establishing the new 2019 upper bounds for the gas mixtures. This

article reviews recent advances in the field of PIM-based membranes. It discusses polymer

synthesis strategies to modify PIM structures such that the resulting membranes have improved

CO₂ separation performance and lower physical aging. The strategies include the use of monomers

with suitable side chains, kinked moieties, and stable structures.

Keywords: Polymer membranes; polymers of intrinsic microporosity; sustainability, CO₂ capture;

CO₂/N₂ separation; CO₂/CH₄ separation

1

Table of Contents

1. Introduction	4
2. Current Challenges in PIM Membranes for CO ₂ Separation	9
3. PIM Membranes Containing Different Contortion Sites	10
3.1. Spirobisindane (SBI)-based PIM Membranes	12
3.1.1. Interlocked SBI-based PIM Membranes	12
3.1.2. Phenazine SBI (PSBI)-based PIM Membrane	13
3.1.3. SBI-based PIM Membranes with Different Side Chains	13
3.2. Spirobifluorene (SBF)-based PIM Membranes	16
3.3. Hexaphenylbenzene (HPB)-based PIM Membranes	17
3.4. Tetraphenylethylene (TPE)-based PIM Membranes	18
3.5. Tröger's base (TB)-based PIM Membranes	18
3.6. 2, 2', 3, 3'-Tetrahydroxy-1, 1'-Dinaphthyl (THDN)-based PIM Membranes	19
3.7. Triptycene-based PIM Membranes	19
3.7.1. Benzotriptycene-based PIM Membranes	19
3.7.2. Triptycene-based PIM Membranes	23
3.7.3. Poly(norbornene) Membranes	25
3.8. PIM Membranes Containing Two Contortion Sites	26
3.8.1. Tröger's base PIM Membranes Containing PIM-X-TB	26
3.8.2. PIMs with Different Combinations of Ethanoanthracene, Spirobisindane, Contortion Sites	
4. Polyimide-based PIM (PIM-PI) Membranes	33
4.1. PIM-PI Membranes Containing Diamine Contortion Sites	33
4.2. PIM-PI Membranes Containing Dianhydride Contortion Sites	43
5. Post-Modification of PIM Membranes	56
5.1. Crosslinking	57
5.2. Thermal Treatment	59
5.3. Photo-oxidative Modification	64
5.4. Chemical Post-modification.	66
5.4.1. Carboxylated Functionalized PIMs	67
5.4.2. Amidoxime Functionalized PIMs	68
5.4.3. Heterocyclic Tetrazole Functionalized PIMs	69
5.4.4. Amine Functionalized PIMs	69
5.4.5. Thioamide Functionalized PIMs	70

6. PIM Blending	72
7. Physical Aging of PIM Membranes	77
7.1. Effect of Contortion Site on Physical Aging	81
8. PIM-based Mixed-Matrix Membranes	85
8.1. Membranes Containing Silica and Its Derivatives	88
8.2. Membranes Containing Carbon Nanotubes (CNTs)	92
8.3. Membranes Containing Organic Nanoparticles	94
8.4. Membranes Containing 2D Nanoparticles	96
8.5. Membranes Containing Covalent Organic Frameworks (COFs)	98
8.6. Membranes Containing Metal-organic Frameworks (MOFs)	99
8.7. Effect of Filler Shape on PIM-based MMMs Performance for CO ₂ Separation	108
9. Potential of PIM Membranes for Industrial Implementations	110
10. Critical Insight into Gaps and Areas of Weakness	110
11. Concluding Remarks	116
References	120

1. Introduction

The level of CO₂ emission has been increasing globally with industrialization and modernization. More than 50% of the CO₂ is released by the electric power, chemical, petrochemical, and petroleum industries, as these industries still consume fossil fuels [1, 2]. The importance of lowering CO₂ emission is well-understood globally [3-5]. CO₂ is produced in enormous amounts as a side product in many industries, is a pollutant, and is not an economic chemical precursor. Thus, there are major environmental, economic, and operational incentives for separating CO₂ from other gases right after its generation in an industrial process and for using it. For example, CO₂ has been injected into oil/gas wells to enhance oil/gas recovery [6], reacted with metallic ions to obtain less soluble carbonates [7], and fed to microorganisms [8, 9]. Efforts to lower CO₂ emission include improving the efficiency of the existing fossil-fuel-consuming industrial plants, developing new efficient, fossil-fuel-consuming industrial plants, replacing the current CO₂ emitting technologies with modern, less CO₂ emitting alternative, and introducing innovative cost-effective capture technologies [10-12].

To decrease CO₂ emission, more efficient CO₂-capture methods are needed [13, 14]. Absorption is currently the most widely used technology for gas sweetening [15-19] to lower CO₂ levels in natural gas, improving the heat value of natural gas, reducing pipeline corrosion, and preventing the operational inconvenience in chemical and petrochemical processes. While absorption has been used widely and is effective, it is a relatively expensive (in terms of both operating and capital costs), bulky, and difficult-to-operate process. The operational difficulty is due to its susceptibility to foaming, entrainment, and flooding [14]. Alternatively, the membrane technology is modular and more compact, requires less energy, and has lower operating costs [20-26]. Furthermore, the membrane technology can tolerate changes in a feed composition easily, as

it does not involve phase change or solvent regeneration [27-29]. Currently the largest market for CO₂ separation membranes is CO₂ removal from natural gas. Emerging applications are the separation of CO₂ from N₂ and CO₂ from H₂ [30, 31]. The market has a lot of room to grow, as currently only 10% (by mass) of gases are separated using the membrane technology [32-36].

Membranes formed from metals, ceramics [37-40], zeolites, carbon products, and polymers [41-44] all have shown great potentials for gas separation [45-50]. Currently, commercial membranes are mostly made from polymers. These membranes separate CO₂ according to the solution-diffusion mechanism [51-53], which has three steps: (a) permeant dissolution in the membrane, (b) permeant diffusion through the membrane, and (c) permeant desorption on the other side of the membrane. In this mechanism, the permeant concentration gradient across a membrane generates a chemical potential gradient [54]. Then the permeability of gas i in a polymer, P_i , is defined as $P_i = LN_i/\Delta p$, where Δp , N_i , and L are the pressure differences across the membrane, steady-state gas flux, and membrane thickness, respectively [55, 56]. Permeability is commonly expressed in Barrer unit, where 1 Barrer = 10^{-10} cm³ (STP).cm/(cm².s.cmHg) [57, 58]. Any increase in the gas flux (cm³ (STP)/(cm².s)) lowers the operating and capital costs of membrane processes. This is achievable by increasing a membrane permeability or decreasing a membrane thickness [59]. This has motivated the development of defect-free selective thin film composite (TFC) membranes with a thickness of 0.1–1 μm. Generally, highly-permeable scalable membranes (>1000 GPU), GPU = 10⁻⁶ cm³ (STP)/(cm².s.cmHg) with sieving ability of 40 and descent plasticization resistance are needed for CO₂ separation from a real gas mixture containing various components [60-62]. Cellulose acetate, perfluoro polymers, and P84 polyimide (PI) have been used commercially for natural gas sweetening, as they exhibit good chemical, mechanical, and thermal stability, as well as excellent processability [63]. However, their major weakness is that their permeability and selectivity cannot be improved simultaneously [64, 65]. Additionally, the separation of CO₂ from natural gas is very challenging, as natural gas usually includes water vapor, H₂S, heavy aliphatics, and aromatics, which cause membrane plasticization.

Different types of membranes have been studied and introduced to attain high CO₂ permeability and CO₂/gas selectivity. They include mixed-matrix membranes (MMMs), thermally-rearranged membranes [66], and carbon molecular sieve (CMS) membranes [67]. MMMs typically have defects, restricting their commercialization [68-70]. By applying high temperatures (350-450 °C and >500 °C), thermally-rearranged membranes [66] and carbon CMS membranes [67] have been fabricated, but their fragility, high cost, and complexity have impeded their industrial applications. To fabricate a polymer membrane with a high CO₂ permeance, an amorphous and solution-processable polymer with a high surface area is required. Freeman [65] theoretically showed that suppressing the chain mobility and increasing the chain rigidity of a polymer improve the gas-separation performance of membranes made from the polymer.

By creating high free-volume (increasing the intra-chain rigidity) and constructing ultra-microporosity (precisely controlling interconnected pores), highly permeable polymers of intrinsic microporosity (PIMs) have been fabricated [71]. The manipulation of intra-chain and inter-chain rigidities has resulted in the synthesis of microporous polymers with tailored free-volumes and transport properties. Budd *et al.* designed and fabricated the first PIM membrane (named PIM-1) [72]. Their work was a major advance in membrane gas separation. PIM-1 has a quasi-ladder spirobisindane (SBI), known as spiro, which has two cyclopentane rings containing two methyl groups connected and linked with arene rings [73, 74]. The high surface area of PIM-1 (>700 m²/g) allows for high gas uptakes and provides extremely high gas permeability [75-83]. The high permeability (up to 52800 Barrer) of PIM membranes is due to their high specific surface area (up

to 1,050 m²/g) and high microporosity [84, 85]. This high level of gas permeability shows that, in addition to the solution-diffusion mechanism, the convective-diffusion mechanism contributes to gas transport in PIM membranes [86]. At low pressures, the gas uptake of PIM membranes is through ultra-micropores. However, at high pressures, the gas uptake is through micropores [87]. So, the gas solubility coefficients of PIM membranes are higher than those of low-free-volume commercial membranes.

The effects of the gas-molecule size on the gas-transport properties of PIM membranes can be explained by using the relationships between diffusion and sorption coefficients, and the critical volume, temperature, effective kinetic diameter, and van der Waals volume of gases [86]. In addition to the dual-mode sorption model for CO₂ uptake, Anderson and de Boer (GAB) layered-adsorption model can be used [86]. Sorption kinetics imply the occurrence of the convective-diffusion mechanism with different natures, compared to the solution-diffusion mechanism. The exceptional gas transport properties of PIM membranes have led to the establishment of the new upper bounds for CO₂ separation from fuel and flue gases, and a new upper bound for CO₂/CH₄ separation under mixed-gas conditions (Figure 1) [88, 89]. However, so far, a limited number of PIM membranes have surpassed the 2008 Robeson upper bounds for CO₂/N₂ and CO₂/CH₄ separations [88, 90].

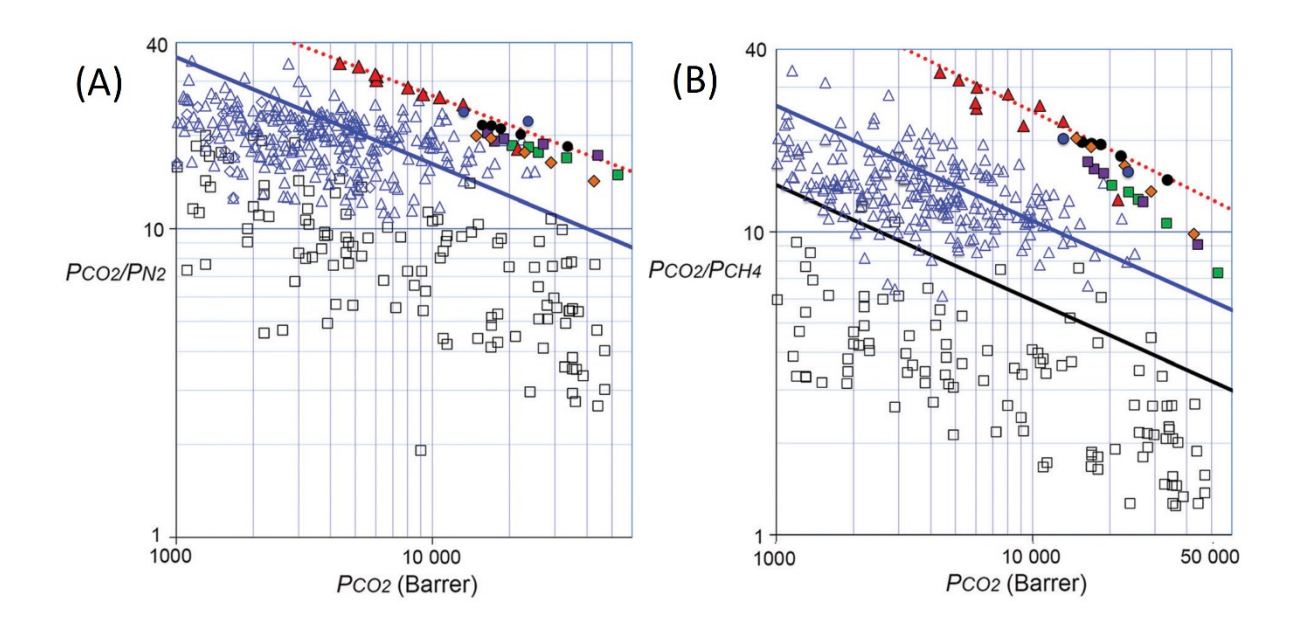


Figure 1. Upper bound plots for (A) CO_2/N_2 and (B) CO_2/CH_4 gas pairs. Colored filled symbols show gas permeation properties of films developed by new members of benzotriptycene family; non-filled symbols show gas permeation of previous non-PIM (\square) and PIMs (\triangle) membranes; 1991 upper bounds are represented by black lines, 2008 upper bounds by blue lines, and 2019 proposed revised upper bounds by dotted red lines [88]. Reprinted with permission from B. Comesaña-Gándara, Jie Chen, C. G. Bezzu, M. Carta, I. Rose, M.-Ch. Ferrari, E. Esposito, A. Fuoco, J. C. Jansen, N. B. McKeown, Redefining the Robeson upper bounds for CO_2/CH_4 and CO_2/N_2 separations using a series of ultrapermeable benzotriptycene-based polymers of intrinsic microporosity, Energy and Environmental Science, (2019) under the terms of the Creative Commons Attribution 3.0 Unported License (https://creativecommons.org/licenses/by/3.0/).

This review paper puts recent advances in PIMs and CO₂-separation PIM-based membranes into perspective. It evaluates the CO₂ separation performance of novel PIMs in terms of updated/redefined upper bounds for CO₂ containing gas streams. It identifies strategies that allow for modifying polymer structure and properties such that the resulting polymer membranes have high CO₂-separation performance. The potentials of PIM membranes for use in industrial-

scale separations of CO₂/N₂ and CO₂/CH₄ gas mixtures are elaborated. The scope of this review paper is limited to PIM membranes treated with methanol or ethanol.

2. Current Challenges in PIM Membranes for CO₂ Separation

The performance of PIM membranes can be improved to some extent via substituting the spiro moiety with different building blocks. Thus, the selection of a good moiety is certainly important regardless of the type of PIM materials. The performance of PIM-based membranes has been found to be above the 2008 Robeson upper bounds. However, the fabrication of highly permeable and highly selective microporous membranes has always been challenging, and the industrial use of these membranes is still rare. Furthermore, physical aging and plasticization are still two main drawbacks of these membranes, which have primarily hindered the industrial use of PIM-based membranes for gas separation [91]. Physical aging is the phenomenon of membrane transportproperty deterioration. It alters the free volume of glassy polymers. It is faster and occurs continuously over several years when the membrane has a high free volume. Physical aging can be mitigated with an appropriate design of the polymer backbone architecture, post-modifications, and the use of hybrid materials [92]. Plasticization is the drop in the selectivity of the desired gas due to the rearrangement of the polymer molecular structure caused by the high uptake of CO₂ and/or condensable gases. A balance between inter- and intra-chain rigidities mitigates the plasticization. In the case of PIM MMMs, there is an additional challenge; that is, the need for good compatibility of the polymer and the filler, the absence of which leads to the aggregation of the nanoparticles and their poor dispersion in the polymer matrix. This review covers strategies to mitigate physical aging, plasticization, and poor polymer-filler compatibility.

3. PIM Membranes Containing Different Contortion Sites

Many efforts have been made to improve the performance of PIM membranes by incorporating desired moieties into the backbone of the polymers [93]. PIM-based membranes are classified according to their type of sterically hindered building block. By introducing PIMs with rigid bulky contortion sites into PI backbones, PIM-PIs are prepared. Figure 2 shows the structure of PIM-based polymers containing different rigid moieties. This section covers PIMs consisting of different building blocks with distinct rigidity and rotational freedom. The 2008 Robeson and the redefined 2019 upper bounds are used as benchmarks to evaluate the performance of the PIM membranes for CO₂ separation.

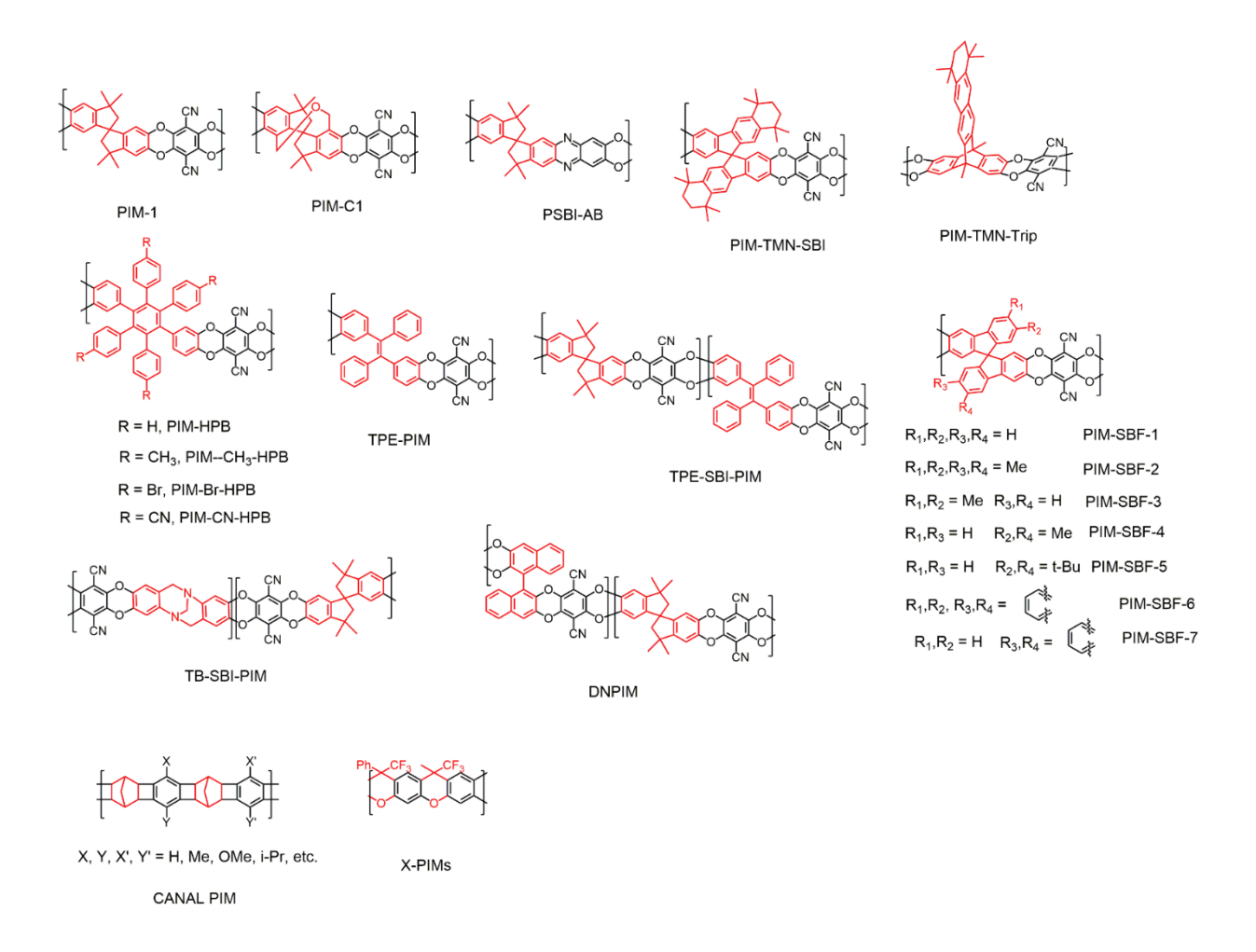


Figure 2. Molecular structures of PIM-based polymers with different moieties [89, 92, 94].

3.1. Spirobisindane (SBI)-based PIM Membranes

The discovery of PIM-1 [55] showed a new path to fabricating high-performance membranes. PIM-1 is the product of the condensation reaction of 5,5′,6,6′-tetrahydroxy-3,3,3′,3′-tetramethyl-1,1′-spirobisindane (TTSBI) and tetrafluoroterephthalonitrile (TFTPN), introducing the SBI moiety to the backbone of the polymer. PIM-1 has an extraordinary surface area and considerably higher permeability than low free-volume commercial PIs and cellulose acetate. The CO₂ separation performance of PIM-1 has been reported to be both below and above the 2008 Robeson upper bounds. These discrepancies arise from different sample history, preparation conditions, etc. For example, gas separation performance of a PIM membrane strongly depends on its thickness, casting solvent, thermal history, non-solvent (methanol, ethanol) treatment, and so on. Crosslinked PIM-SBI nanofilms can be formed by the interfacial polymerization [95].

3.1.1. Interlocked SBI-based PIM Membranes

The interlocked SBI-based monomer is synthesized via polycondensation, leading to the formation of interlocked PIM-1 called PIM-C1. PIM-C1 has an interlocked polycyclic structure generated by an eight-membered dihydrooxocine ring locking into the spiro-carbon hinge point. High molecular weight PIM-C1 has good solubility in several solvents (CHCl₃, CH₂Cl₂, and chlorobenzene) and has a Brunauer–Emmett–Teller (BET) surface area of 818 m² g⁻¹. The smaller dihedral angle between the two benzene rings of PIM-C1 compared to that of PIM-1 confirms the more twisted nature of the moiety of the interlocked polymer. The higher rigidity parameter value of the interlocked SBI (20 kcal mol⁻¹ rad⁻²) compared to that of SBI (8.6 kcal mol⁻¹ rad⁻²) confirms that PIM-C1 is more inflexible than PIM-1 [96]. Compared to PIM-1, the suppression of

vibrational planes around the SBI center results in a higher inter-chain distance and a higher free-volume. The PIM-C1 membrane has shown a high CO₂ permeability of 18,900 Barrer, a moderate CO₂/N₂ selectivity of 19.3, and a modest CO₂/CH₄ selectivity of 14.4, which place the performances of this membrane close to the revisited 2019 CO₂/N₂ and CO₂/CH₄ upper bounds [96].

3.1.2. Phenazine SBI (PSBI)-based PIM Membranes

Phenazine SBI (PSBI)-AB is a solution-processable, high molecular weight, and thermally stable microporous polymer, which can be synthesized via self-polymerization of an AB monomer (AB: monomer containing two types of reactive groups) [97]. SBI tetraol reacts in four reaction steps and forms a monomer containing catechol and aromatic dichloride groups. PSBI-AB bears both dioxane and phenazine rings. Compared to PIM-1, PSBI-AB has one dioxane ring, one phenazine ring, but no nitrile groups. Although the dioxane ring of PIM-1 can be replaced with the more rigid phenazine ring, the absence of two nitrile side groups induces more chain intermolecular packing for PSBI-AB. The CO₂ permeability and CO₂/CH₄ selectivity of PSBI-AB are lower than those of PIM-1, which can be attributed to the lack of side groups of the benzene ring connected to the phenazine. This shows the importance of side groups of PIM membranes for providing more free volume even with less rigid backbones.

3.1.3. SBI-based PIM Membranes with Different Side Chains

SBI-based homopolymers and copolymers can be synthesized using tetrafluoroterephthalo monomers. The less tetrafluoroterephthalonitrile is used, the lower is the free volume of the resulting polymers and copolymers. The synthesis of a homopolymer (TFMPSPIM1) and a series

of microporous copolymers (TFMPSPIM2-4) from tetrafluoro monomers such as heptafluoro-ptolylphenylsulfone (HFTPS) and TFTPN monomers have been reported (Figure 3) [98]. As the level of HFTPS in the copolymers increases, the mechanical and thermal stability of the copolymers increase, but their molecular weights decrease. The homopolymers and copolymers have extraordinarily high fractional free volumes (FFVs). As the HFTPS content increases, the CO₂ permeability decreases, but the sieving ability increases. The CO₂ permeability and the CO₂/N₂ selectivity are in the range of 731–3616 Barrer and 17–22, respectively. As the HFTPS content increases, the d-spacing related to the chain distances, the inter-chain distance and the intra-chain rigidity decrease. This type of tight chain packing reduces the CO₂ permeability but enhances the CO₂/N₂ selectivity. Moreover, unexpectedly, the presence of –CF₃/–SO₂C₆H₅ as rigid and long side chains cannot improve the free volume of the copolymers. This may be caused by the phenylsulfone groups occupying the free volume created by the SBI moiety, causing reduction in the CO₂ permeability while improve the CO₂/N₂ selectivity.

Figure 3. Molecular structures of copolymers made of TTSBI, TFTPN, HFTPS, disulfonyl monomers, and tetrafluorotetraoxide thianthrene (TFTOT) monomers [98-100].

Various homopolymers and copolymers called DSPIM can be prepared using TTSBI, TFTPN, HFTPS, disulfonyl monomers, and tetrafluorotetraoxide thianthrene (TFTOT) monomers (Figure 3) [99]. The copolymers containing TFTPN/disulfone-based monomers (3:1) exhibit good film-forming property, great thermal stability, and high molecular weight. Electronic and steric effects of disulfonyl-based cause little crosslinking in the homopolymers. The pendant disulfone groups increase the CO₂/N₂ selectivity but decrease the CO₂ permeability. Disulfone-based

monomers decrease the free volume via space-filling, especially when a benzene ring linked to the disulfone group exists. Increasing the size of the disulfonyl groups leads to filling the inter-chain space and lowering FFV. So, the gas permeability can be tuned by adjusting the monomer contents and the size of disulfonyl groups. The use of the disulfone monomers containing ethyl groups results in higher selectivity and permeability of the copolymers.

Tetrafluorotetraoxide thianthrene (TFTOT) has been used to develop a homopolymer (TOTPIM) and several copolymers (Figure 3) [100]. TOTPIM and the copolymers of TTSBI, TFTOT, and TFTPN exhibit high microporosity and high conformational flexibility. Increasing TFTOT content improves the efficient chain packing and consequently lowers CO₂ permeabilities of the copolymers to below that of PIM-1 but cannot affect the CO₂/N₂ selectivity significantly. The homopolymer has the lowest CO₂ permeability, but its CO₂/N₂ selectivity is above those of PIM-1 and the copolymers. Therefore, integrating TFTOT into a copolymer structure lowers the CO₂ permeability without any considerable improvement in the CO₂/N₂ selectivity. Almost the same behavior is observed for copolymers containing TTSBI, TFTPN, and THDN [100].

3.2. Spirobifluorene (SBF)-based PIM Membranes

The presence of spirobifluorene (SBF) moiety [101] can increase the CO₂ separation performance of PIM membranes significantly. Replacing the SBI moiety in PIM-1 with the more rigid SBF, which has a lower dihedral-angle variation, restricts chain movements due to the additional fused arene rings of SBF [101]. The SBF moiety can be generated via adding 2-lithio anion of 3, 4-dimethoxybiphenyl to 2, 3-dimethoxyfluorenone followed by acid-mediated cyclization [102].

The BET surface area of the PIM-SBF is 803 m².g⁻¹ [75-79]. The gas permeability and selectivity of PIM-SBF are higher than PIM-1. The CO₂/CH₄ solubility selectivity of PIM-SBF is similar to that of PIM-1, while its diffusivity selectivity is higher. On the other hand, its CO₂/N₂ solubility selectivity is higher than PIM-1, but its diffusivity selectivity is similar to PIM-1.

Different substituents such as methyl, t-butyl, and fused benzo groups can be placed onto the SBF moiety leading to the derivation of various PIM-SBF membranes [103]. The PIM derived from the tetramethyl substituted SBF shows a CO₂ permeability of 22,300 Barrer, which is the highest value reported to date for PIM membranes bearing SBF moiety, placing the performance of this membrane close to the redefined 2019 CO₂/N₂ Robeson upper bound.

PIM-TMN-SBF is another PIM membrane in which two TMN units coupled to the SBF moiety [88]. It has a high BET surface area of 1,015 m² g⁻¹, excellent CO₂ uptake, a high FFV of 0.276, and 3D contorted chains, endowing this membrane with a CO₂ permeability of 17,500 Barrer and a CO₂/N₂ selectivity of 16.2.

3.3. Hexaphenylbenzene (HPB)-based PIM Membranes

High molecular weight PIM-hexaphenylbenzene (HPB) polymers containing methyl (PIM-CH₃-HPB), bromine (PIM-Br-HPB), and nitrile (PIM-CN-HPB) substituents have BET surface areas in the range of $410 - 560 \text{ m}^2 \text{ g}^{-1}$. PIM-Br-HPB and PIM-CN-HPB have lower surface areas than PIM-CH₃-HPB, due to their more efficient chain packing originated from their stronger dipolar interactions. Their CO₂ permeabilities are in the range of 2,130 - 3,800 Barrer (PIM-HPB > PIM-

CH₃-HPB > PIM-Br-HPB > PIM-CN-HPB). Gas diffusivity and permeability in these membranes are tuned by changing the polarity of the substituents in the polymer chains [104, 105].

3.4. Tetraphenylethylene (TPE)-based PIM Membranes

Tetraphenylethylene (TPE)-PIM and TPE-SBI-PIM membranes have high solution processability, excellent thermal resistance, and high surface area (550 to 660 m² g⁻¹) [106]. The wider dihedral angle of the TPE compared to that of the SBI moiety results in larger conformational freedom and lower free volume of the TPE-PIM than PIM-1. A CO₂ permeability of 862 Barrer, a CO₂/N₂ selectivity of 26, and a CO₂/CH₄ selectivity of 20.9 were obtained for TPE-PIM. As the SBI moiety content increases, the gas permeability increases but the selectivity declines [106].

3.5. Tröger's base (TB)-based PIM Membranes

Tröger's base (TB)-PIM and TB-SBI-PIM [107] are two other classes of PIM membranes. TB-PIM100 is not soluble in common solvents. However, when the TB content of a TB-SBI-PIM is more than 40 wt%, the TB-SBI-PIM is partially soluble in organic solvents. TB-PIM25 (tetrahydroxyl-TB (THTB)/TTSBI, 1/3) and TB-PIM33 (THTB/TTSBI, 1/2) have high BET surface areas of 760 and 698 m² g⁻¹, respectively, and good solution processability. As the level of TB in the copolymer increases, CO₂ permeability decreases, while the gas selectivity increases. A high level of TB in the copolymer results in a narrow pore size distribution and a low accessible free volume for gas transport. Compared to PIM-1, a 33 % loss in CO₂ permeability and a 30 % gain in CO₂/N₂ selectivity were obtained for TB-PIM33 membrane [107].

3.6. 2, 2', 3, 3'-Tetrahydroxy-1, 1'-Dinaphthyl (THDN)-based PIM Membranes

Combining the bulky and non-planar 2, 2′, 3, 3′-tetrahydroxy-1, 1′-dinaphthyl (THDN) moiety with SBI leads to the synthesis of high-molecular-weight copolymers with a low polydispersity index (PDI) [108]. The spatially distorted THDN bond between its two rings and the twisted SBI core block disrupt chain packing, leading to improved intrinsic microporosity. The moieties incorporated into the copolymer backbone provide high FFV and render high CO₂ permeability because of inefficient chain packing. Excellent solution processability, thermal stability, and film-forming properties can be acquired for DNPIM-25 (THDN/TTSBI molar ratio of 1/3), and DNPIM-33 (THDN/TTSBI molar ratio of 1/2), copolymers containing THDN and TTSBI [108], where DN denotes to dinaphthyl groups. Under similar operating conditions, the DNPIM-33 has a higher selectivity, but a lower CO₂ permeability, compared to the PIM-1. DNPIM-25 is more selective than PIM-1, while its CO₂ permeability is slightly lower [100]. DNPIM-50 (THDN/TTSBI molar ratio of 1/1) showed a CO₂ permeability of about 70% less than PIM-1.

3.7. Triptycene-based PIM Membrane

3.7.1. Benzotriptycene-based PIM Membranes

The benzotriptycene (BTrip)-based PIM membranes have excellent gas separation performance [88], as such they have provided researchers with new opportunities for the preparation and design of novel PIMs. Membranes made from new members of the BTrip PIM family can exhibit so high gas separation properties, necessitating the introduction of new CO₂/CH₄ and CO₂/N₂ upper bounds. These new membranes contain sterically crowded, solubilizing groups like hexamethylindane and trifluoromethyl [88]. Recently, the Robeson upper bounds for CO₂/N₂ and

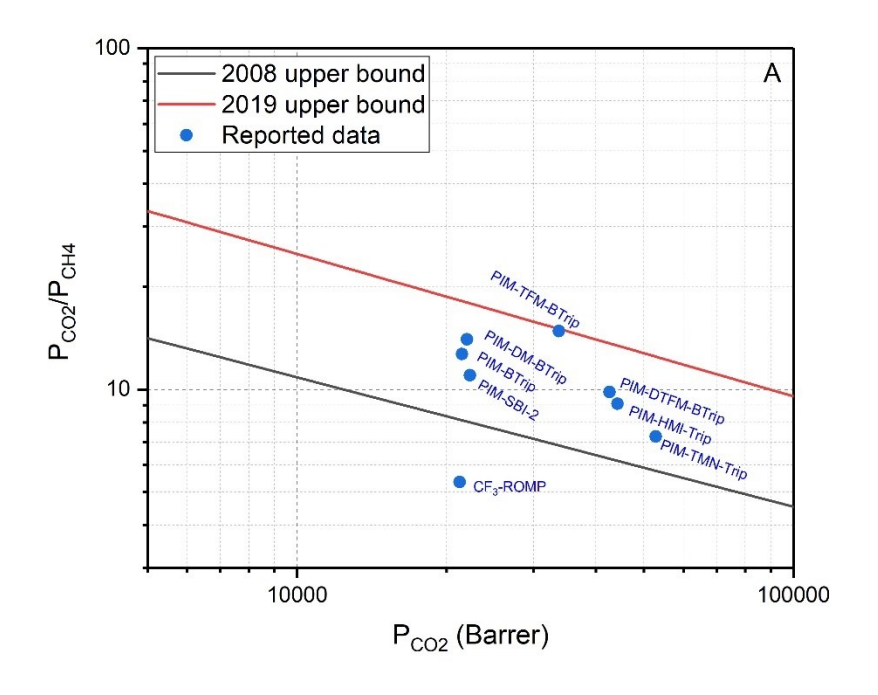
CO₂/CH₄ membrane gas separations have been updated and redefined using a series of ultrapermeable BTrip-based PIM membranes. This improvement will ensure the superiority of ultrapermeable PIM membranes (up to 52,800 Barrer) for CO₂ separation applications compared with existing competing technologies (Table 1 and Figure 4A, B). The CO₂/CH₄ separation performances of BTrip PIM membranes are well above the 2008 Robeson bound, and the CO₂/N₂ separation performances of benzotriptycene PIM membranes also lie above the 2008 Robeson bound. Interestingly, PIM-BTrip is the most attractive among them. Membranes in this family (whether thin or thick, new or aged, etc.) have shown $P_{CO2} > 4,000$ Barrer and CO_2/N_2 selectivity higher than 30. The remarkable separation performance of PIM-BTrip membrane seems to be originated from its high CO_2/N_2 diffusivity selectivity. However, the high separation performance of the other members of this family containing substituted groups are due to their high CO_2/N_2 solubility selectivities [88].

Attaching the tetramethyltetrahydronaphthalene (TMN) moiety to a blade of the Trip moiety results in PIM-TMN-Trip, which is a solution-processable polymer. Fusing TMN as a bulky substituent, makes the polymer soluble in common solvents. Regarding PIM-TMN-Trip, a high BET surface area of 1,050 m² g⁻¹ is obtained due to inefficient chain packing [109]. The coexistence of large micropores (7-10 Å) and interconnected small ultra-micropores (< 7Å) in the structure of PIM-TMN-Trip together provide an exceptional CO₂ permeability of 33,000 Barrer and a moderate selectivity. The dibenzodioxin group connects each Trip moiety co-planar to its neighbor via 2D ribbon-like chains. The high FFV of PIM-TMN-Trip (0.314) is almost the same with PTMSP (0.32) [109, 110]. In addition to ultra-permeability, higher selectivity, improved

membrane robustness, lower aging rate, and enhanced thermal stability of PIM-TMN-Trip, compared to PTMSP, extend the potential of the PIN-TMN-Trip toward industrial gas separation applications [110].

Table 1. Separation performances of the most permeable PIM membranes for CO₂ separation.

Polymer	P _{CO2} (Barrer)	P _{CH4} (Barrer)	P _{N2} (Barrer)	CO ₂ /CH ₄	CO ₂ /N ₂	Ref.
PIM-TMN-Trip	52800	7250	3540	7.28	14.9	[88]
PIM-HMI-Trip	44200	4870	2560	9.08	17.3	[88]
PIM-DTFM-	42600	4340	3000	9.82	14.2	[88]
BTrip						
PIM-TFM-BTrip	33700	2280	1830	14.8	18.4	[88]
PIM-SBI-2	22300	2020	1150	11	19.4	[103]
PIM-DM-BTrip	22000	1570	1020	14	21.8	[88]
PIM-BTrip	21500	1690	1190	12.7	18.1	[88]
CF ₃ -ROMP	21266	3970	2367	5.35	8.98	[111]



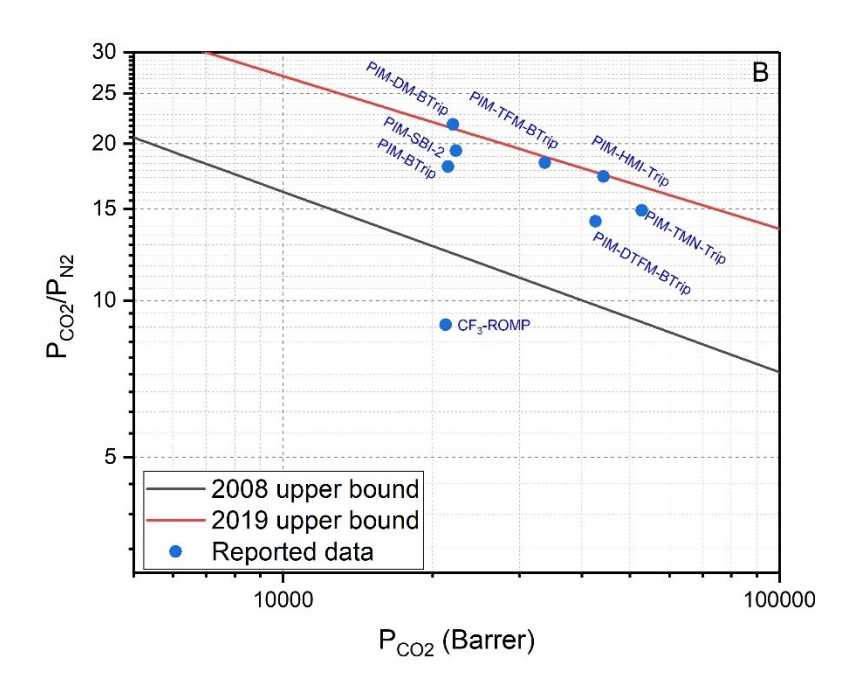


Figure 4. Data from Table 1 showing gas separation performances of the most permeable PIM membranes. (a) CO_2/CH_4 ; (b) CO_2/N_2 .

3.7.2. Triptycene-based PIM Membranes

Self-polymerization of AB-type monomers irrespective of the stoichiometry of the reactants may result in high-molecular-weight, film-forming polymers [71]. The monomers possess difluoro and diol functionalities. Triptycene-based PIMs (TPIMs) bearing 9,10-iso and linear propylsubstituted triptycene moieties are called TPIM-1 and TPIM-2, respectively (Figure 5a, b). Planar and contorted ribbon-like chain configurations are observed in molecular simulation of TPIMs [71]. The fused-ring and highly-rigid Trip moiety, the restricted rotation of the phenazine moiety, and the conformational barrier of their backbone provide TPIM-1 and TPIM-2 with intra-chain rigidity higher than PIM-1 and PIM-PIs. The surface areas of TPIM-1 and TPIM-2 are 862 and 612 m² g⁻¹, respectively. The higher N₂ adsorption of TPIM-1 than TPIM-2 (Figure 5c), especially in low pressures, confirms the narrow pore size distribution (Figure 5d) and high ultramicroporosity of TPIM-1. The high surface area and ultra-microporosity of TPIM-1 are attributed to the chain packing disruption caused by the Trip core block and the large sizes of the bridgehead substituents. The molecular sieving ability of TPIMs is ascribed to chain rigidity and ultramicroporosity. The CO₂ permeabilities of TPIM-1 and TPIM-2 are 1545 and 434 Barrer, respectively. The higher permeability of TPIM-1 is due to its higher solubility coefficient provided by its larger surface area and greater diffusivity coefficient. The lower permeability of TPIM-2 compared to TPIM-1 is due to accessible free-volume of TPIM-2 being filled partially with more flexible linear propyl groups of TPIM-2. Furthermore, TPIM-1 is more selective than TPIM-2, because a larger portion of its pore size distribution is inside the ultra-microporosity region.

The simultaneous improvement of the CO₂ permeability and the CO₂/CH₄ selectivity of TPIM-1 indicates the effectiveness of the short, branched isopropyl substituent of TPIM-1. The presence of the isopropyl substituent improves the surface area of the polymer. It increases the membrane ultra-microporosity and disrupts chain packing of TPIM-1. In CO₂/CH₄ separation, high selectivity and permeability can be achieved simultaneously through substituting flexible groups with stiffer ones such as phenazine and through connecting branched, short and bulky groups to the bridgehead of rigid moieties.

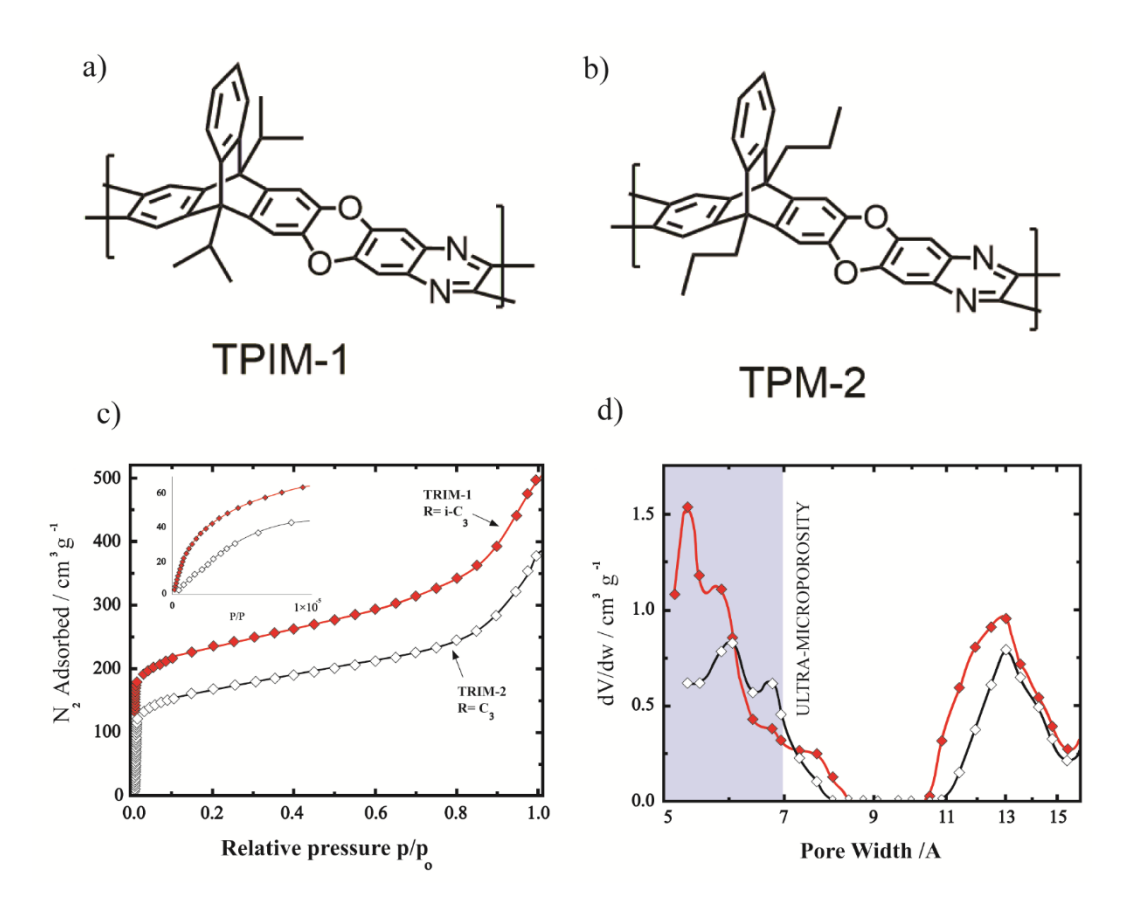


Figure 5. (a) Molecular structure of TPIM-1, (b) molecular structure of TPIM-2, (c) nitrogen adsorption isotherms for TPIM-1 and TPIM-2, and (d) pore-size distributions of TPIM-1 and TPIM-2 determined using non-local density functional theory (NLDFT) [112]. Reprinted with

permission from Ghanem BS, Swaidan R, Ma X, Litwiller E, Pinnau I., Energy-efficient hydrogen separation by AB-type ladder-polymer molecular sieves, Advanced Materials, 26:6696-700 (2014). Copyright 2014 John Wiley and Sons.

3.7.3. Poly(norbornene) Membranes

Ring-opening metathesis polymerization (ROMP) can be used to synthesize porous, flexible polymers like poly(norbornene) with –CF₃ and –OMe pendant species (Figure 6a, b) [111]. The pendants are made via an iterative Diels–Alder reaction, which forms a mixture of oligomers with different chain lengths (2–9 repeating units). The flexible backbone with inflexible fluorinated side chains leads to ultra-high CO₂ permeability of >21,000 Barrer. Compared to –OMe groups, the – CF₃ counterparts increase CO₂ permeability and improve the physical aging resistance of the corresponding membrane. Excellent CO₂ permeability is attributed to high gas uptake. More physical aging resistance of CF₃-ROMP compared to PIM-1 despite higher intrinsic microporosity (Figure 6d) represents a promising new platform of materials for CO₂ separation. Exceptional CO₂ plasticization resistance (plasticization pressure > 51 bar) can be attained for both OMe-ROMP and CF₃-ROMP membranes which is the highest to date for PIM membranes (Figure 6c).

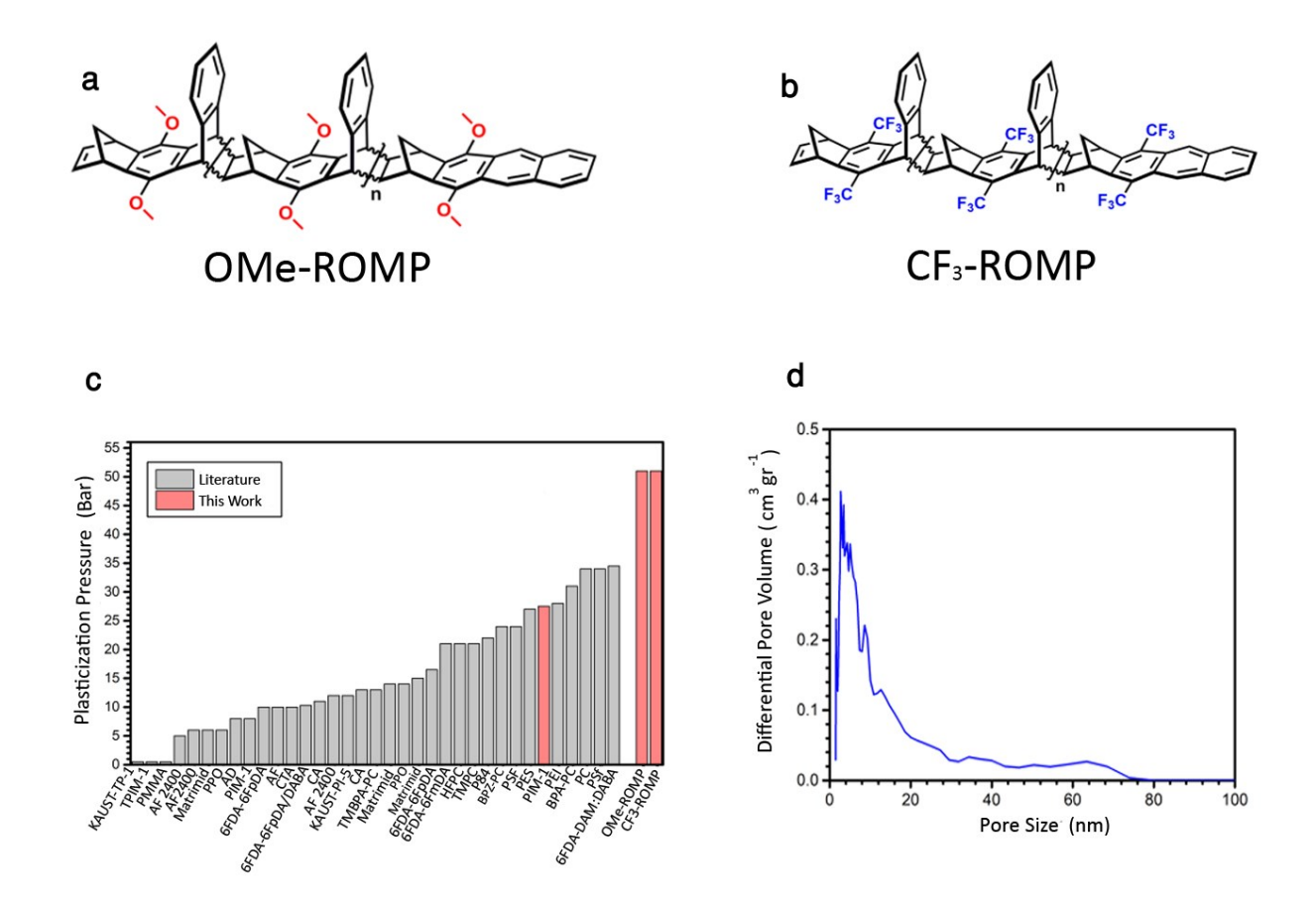


Figure 6. (a) Molecular structure of OMe-ROMP, (b) molecular structure of CF₃-ROMP, (c) exceptional CO₂ plasticization resistance of OMe-ROMP and CF₃-ROMP membranes compared to other PIM and commercial membranes, and (d) pore-size distributions of CF₃-ROMP [111]. Reprinted with permission from He Y, Benedetti FM, Lin S, Liu C, Zhao Y, Ye HZ, et al., Polymers with side chain porosity for ultrapermeable and plasticization resistant materials for gas separations, Advanced Materials, 31:1807871 (2019). Copyright 2019 John Wiley and Sons.

3.8. PIM Membranes Containing Two Contortion Sites

3.8.1. Tröger's base PIM Membranes Containing PIM-X-TB

The inclusion of methano-1, 5-diazocine (TB moiety) into PIMs improves microporosity and gas transport properties. The reason is high rigidity of this building block, which prevents the

formation of the coplanar pattern [113]. Also, the incorporation of the TB contortion site in the polymer backbone increases its CO₂-philic property [96]. High CO₂ permeability (7,696 Barrer) and moderate CO₂/N₂ selectivity (<13.3) can be achieved by incorporating ethanoanthracene (EA) and TB contortion sites simultaneously in the polymer backbone. PIM-EA-TB has a high surface area (1,028 m²/g) and a rigid backbone [114]. The higher rigidity of the EA and TB than SBI and dioxane moieties allows for the preparation of highly intrinsic microporous fused-ring polymers [115]. The high CO₂ permeability can be obtained thanks to the combined effects of high diffusivity and high solubility coefficients.

To create more free volume and intrinsic microporosity within the polymers, Trip can be an appropriate alternative moiety. The substitution of EA by Trip, containing no methyl substituents at its bridgehead, which has more rigidity, provided the PIM-Trip-TB membrane with improved CO₂ permeability (9,709 *vs.* 7,696 Barrer for PIM-EA-TB), CO₂/N₂ selectivity (15.9 *vs.* 13.3 for PIM-EA-TB), and CO₂/CH₄ selectivity (10.7 *vs.* 9.9 for PIM-EA-TB) [114]. The use of Trip building block preserves inter-chain distances, without a need for methyl substituents. The apparent BET surface area of PIM-Trip-TB is 899 m²/g. The attachment of additional benzene ring to the Trip further increases the internal free volume of Trip with the formation of BTrip moiety [116-119]. PIM-BTrip-TB has a high BET surface area (870 m²/g) and good processability, which forms robust membranes. The high rigidity, bulky structure, and high internal free volume of the BTrip moiety in PIM-BTrip-TB lead to a high CO₂ permeability of 13,200 Barrer [118]. A robust free-standing PIM-MP-TB membrane containing a rigid methanopentacene (MP) core block unit can be fabricated by dissolving the polymer in chloroform [120]. Compared to other PIM-TB

membranes, PIM-MP-TB with a BET surface area of 743 m²/g has lower CO₂ permeability. Figure 7 shows molecular structures of several PIM-X-TB polymers.

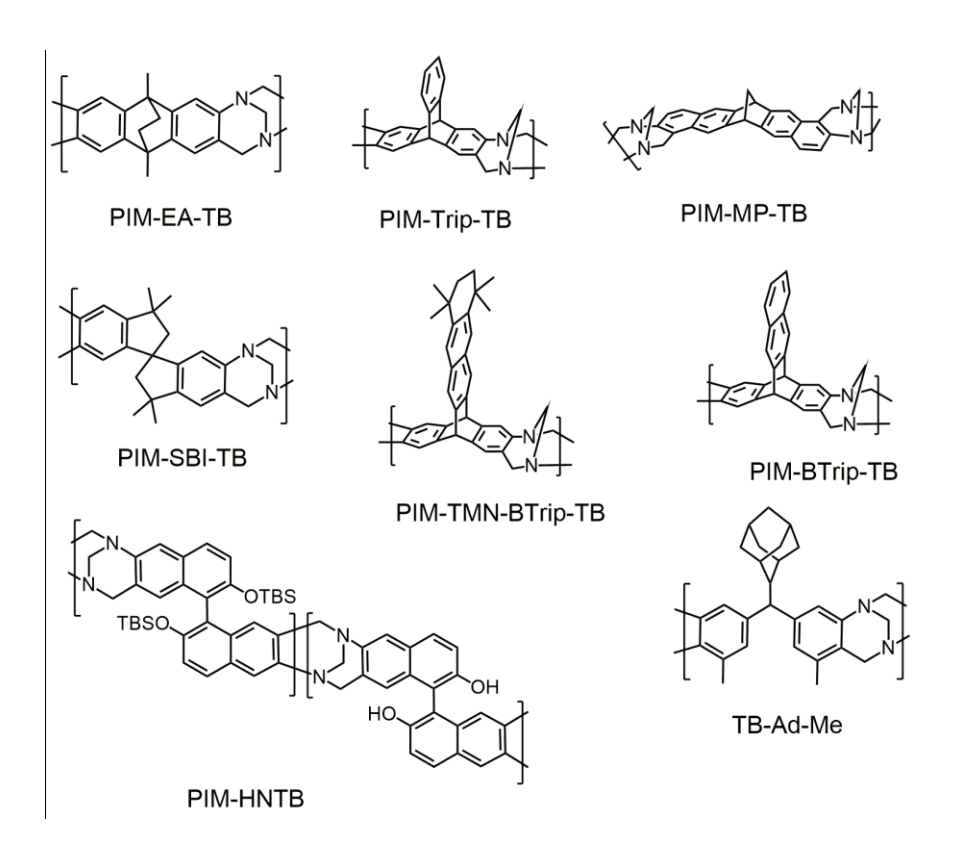


Figure 7. Molecular structures of several PIM-X-TB polymers [89, 92, 94].

3.8.2. PIMs with Different Combinations of Ethanoanthracene, Spirobisindane, and Cardobased Contortion Sites

Reactive tetrachloride monomers containing phenazine, SBI, and EA moieties can react with tetrahydroxy SBI, SBF, and EA monomers, leading to the synthesis of PIM-7 to PIM-10, and Cardo-PIM-1 and Cardo-PIM-2 [121] (Figure 8). PIM-7 and Cardo-PIM-1 have the film-forming

ability, high BET surface area (> 620 m² g⁻¹), and high pore volume (> 0.51 cm³ g⁻¹). The high CO_2 permeability of PIM-7 (1,100 Barrer) points to the creation of a stiff backbone in PIM-7. The presence of Cardo units in Cardo-PIM-1 backbone results in more conformational freedom and flexibility. This leads to low CO_2 permeability (430 Barrer) and satisfactory selectivity for CO_2/N_2 (33).

 $\label{eq:table 2} \begin{tabular}{ll} Table 2 and Figure 9 show gas separation performance of the PIM membranes for CO_2/CH_4 and CO_2/N_2 separations. \end{tabular}$

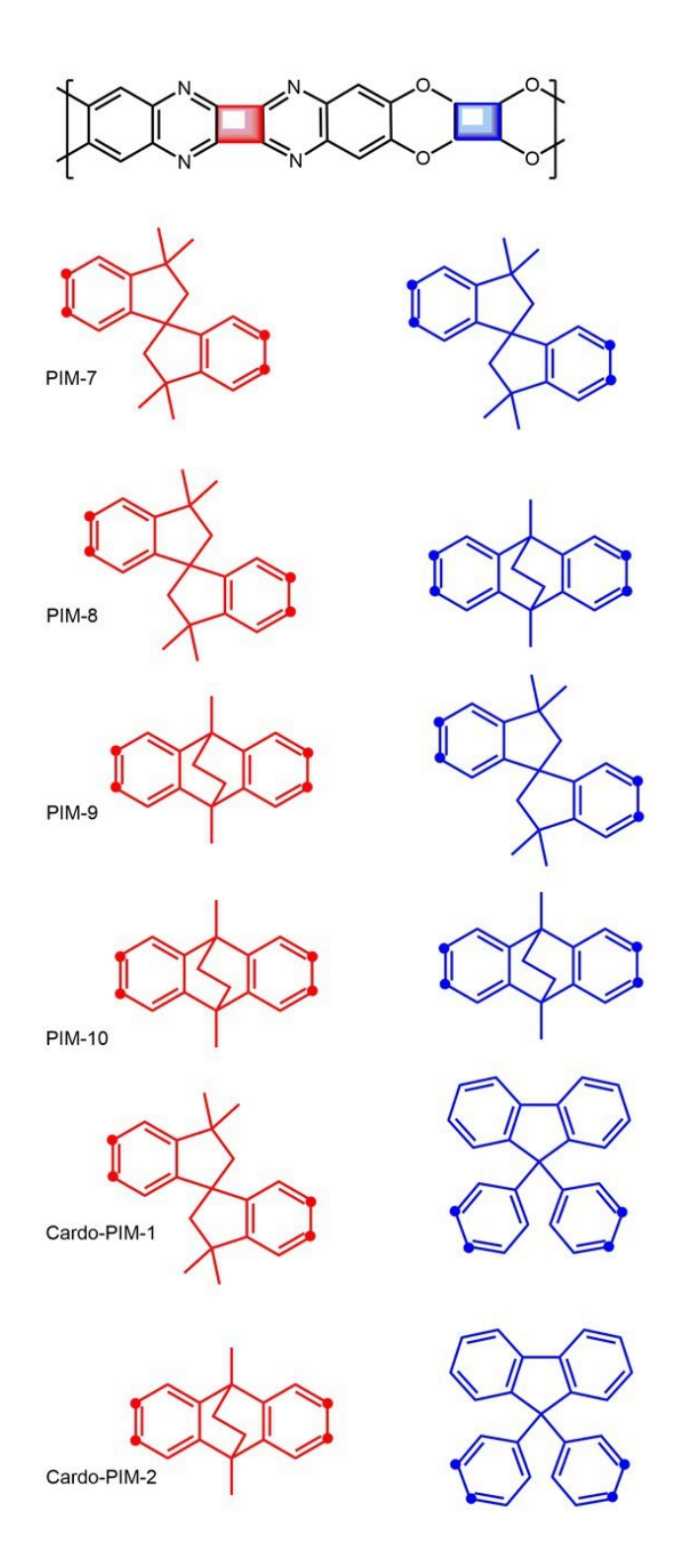
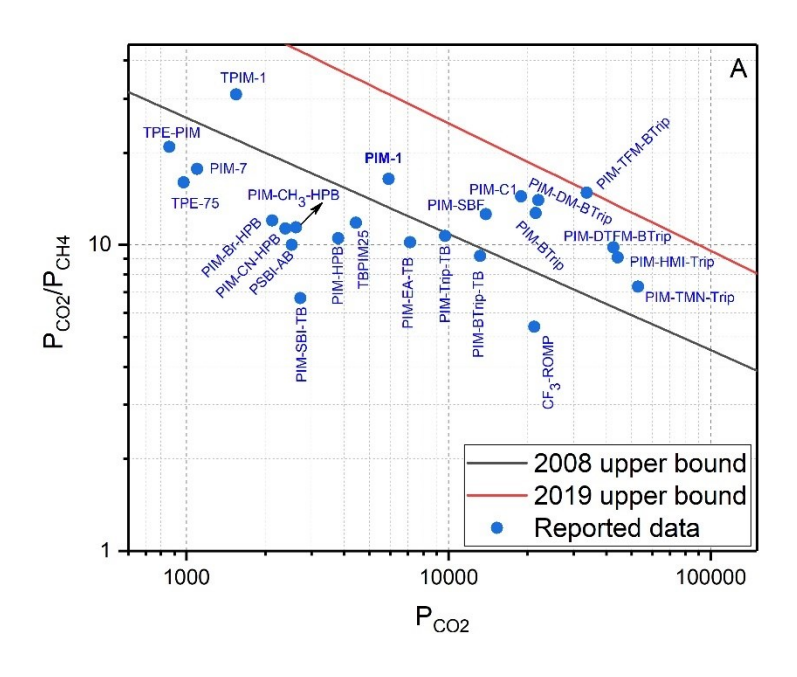


Figure 8. Molecular structures of PIM-7 to PIM-10 and Cardo-PIM-1 and Cardo-PIM-2 [121].

Table 2. Performance of the PIM membranes for CO₂ separation.

Polymer	Perm	Permeability (Barrer)			Selectivity	
	CO ₂	CH ₄	N_2	CO ₂ /CH ₄	CO ₂ /N ₂	
PIM-1	5,919	362	248	16.4	23.9	[122]
PSBI-AB	2,523	257	141	10.0	17.9	[97]
PIM-C1	18,900	1,310	980	14.4	19.3	[123]
PIM-SBF	13,900	1,100	786	12.6	17.7	[101]
PIM-HPB	3,800	361	190	10.5	20.0	[105]
PIM-CH ₃ -HPB	2,620	230	122	11.4	21.5	[105]
PIM-Br-HPB	2,130	177	92	12.0	23.2	[105]
PIM-CN-HPB	2,390	212	123	11.3	19.4	[105]
TPE-PIM	862	41	33.4	20.9	25.8	[106]
TPE-75	977	61	42	16.0	23.3	[106]
TBPIM25	4,441	375	262	11.8	17.0	[107]
PIM-BTrip	21500	1,690	1,190	12.7	18.1	[124]
PIM-TMN-Trip	52,800	7,250	3,540	7.3	14.9	[124]
PIM-HMI-Trip	44,200	4,870	2,560	9.1	17.3	[124]
PIM-TFM-BTrip	33,700	2,280	1,830	14.8	18.4	[124]
PIM-DTFM-BTrip	42,600	4,340	3,000	9.8	14.2	[124]
PIM-DM-BTrip	22,000	1,570	1,020	14.0	21.8	[124]
TPIM-1	1,549	50	54	31	28.7	[112]
TPIM-2	434	18	18	24	24.1	[112]
CF ₃ -ROMP	21,266	3,970	2,367	5.4	9	[111]
PIM-BTrip-TB	13,200	1,440	926	9.2	14.2	[118]
PIM-Trip-TB	9,709	905	629	10.7	15.4	[117]
PIM-EA-TB	7,140	699	525	10.2	13.6	[117]
PIM-SBI-TB	2,720	406	215	6.7	12.7	[114]
PIM-7	1,100	62	42	17.7	26.2	[121]
Cardo-PIM-1	430	22	13	19.5	33.1	[121]



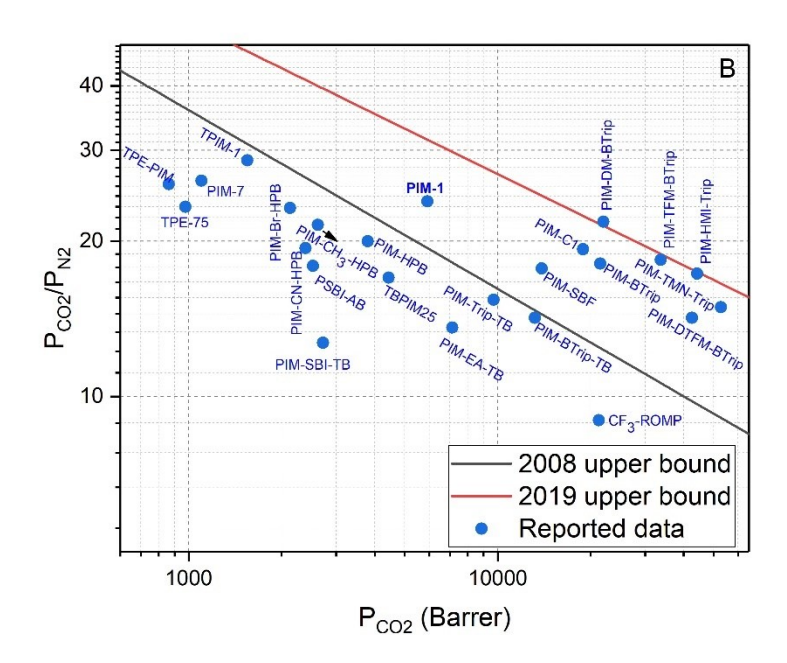


Figure 9. Data from Table 2 showing gas separation performances of the PIM membranes. (A) CO_2/CH_4 and (B) CO_2/N_2 .

4. Polyimide-based PIM (PIM-PI) Membranes

PIs with intrinsic microporosity allow for fabricating highly-permeable and adequately-selective membranes with high mechanical and thermal stabilities [74]. Dianhydrides and diamines containing a rigid moiety introduce motion-restricted segments to PIM-PIs structures. Diamine and dianhydride structures allow for tuning a polymer's free-volume via changing rotation limits of the imide bonds [66, 125, 126].

4.1. PIM-PI Membranes Containing Diamine Contortion Sites

Various diamines with different rigid moieties are synthesized [114, 116, 118, 127-131]. Figure 10 shows the structures of the mostly used diamines. It is believed that introducing a bulky moiety into the polymer backbone improves membrane permeability. To achieve this, two PIs containing iptycene diamine [Trip-based diamine (DAT1) or BTrip-based diamine (DAT2)] and 2, 2-bis-(3,4-dicarboxyphenyl) hexafluoropropane dianhydride (6FDA), called 6FDA-DAT1 and 6FDA-DAT2, can be prepared [116, 132]. Compared to 6FDA-DAT1, 6FDA-DAT2 has a higher free volume, a higher surface area, but less chain packing due to the additional aromatic ring stacked on the Trip moiety. 6FDA-DAT2 has a higher CO2 permeability than that of 6FDA-DAT1 (210 Barrer for 6FDA-DAT2 and 120 Barrer for 6FDA-DAT1), but a lower CO2/CH4 selectivity (30 vs. 38). The two PIs also have moderate CO2/N2 selectivities (lower than their CO2/CH4 selectivities). Since they have similar CO2 solubility coefficients, the higher CO2 permeability of 6FDA-DAT2 is attributed to its higher diffusion coefficient. 6FDA-DAT1 and 6FDA-DAT2 have similar

microporosity obtained from CO₂ adsorption, but different microporosity from N₂ adsorptiondesorption (6FDA–DAT2 has wider pores than 6FDA–DAT1).

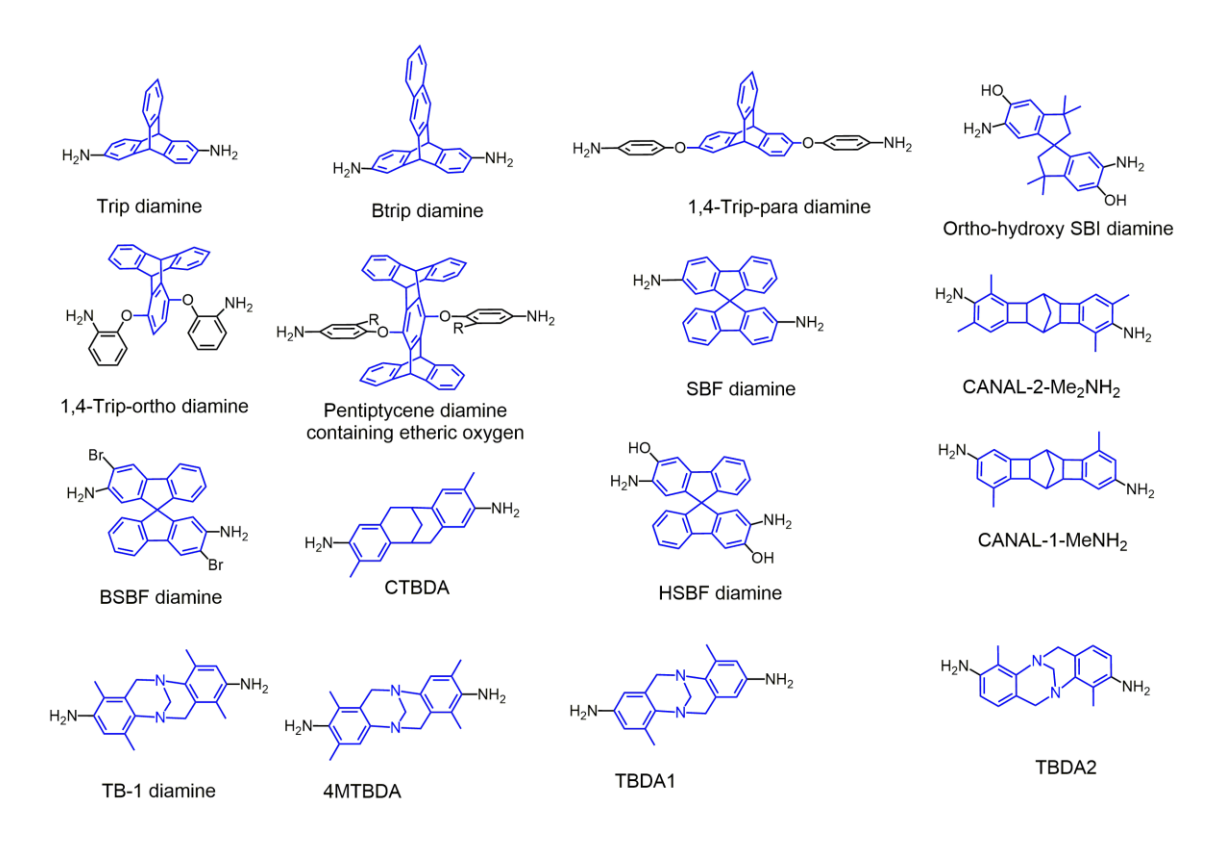


Figure 10. Molecular structures of mostly used diamines containing a rigid moiety [89, 92, 94].

The free volume of PIs containing iptycene moieties can be tailored by several methods. Using 1, 4-triptycene diamines with different substituent groups adjacent to the Trip moiety, several Trip-based PIs can be designed and synthesized [133, 134]. The synthesized polymers show high solubility in solvents, high processability, and tailored free volume. The introduction of Trip block near substituent groups in PIs results in moderate FFV ranging from 0.151 to 0.183.

This free volume range allows for gas permeabilities even higher than those of commercial membranes with similar free volumes, revealing the importance of Trip open fissures. In addition to micro-cavities created by inefficient chain packing, the presence of the opened clefts leads to a bimodal pore size distribution in these polymers.

Three PIs with different backbone geometries containing 1,4-trip-para (symmetric) and 2,6-trip-ortho (asymmetric) diamines were investigated [135]. The more contorted backbone of the 6FDA-2,6-trip-ortho results in more chain packing disruption and higher accessible volume. It was found that 6FDA-1,4-trip-para has the lowest d-spacing, the highest glass transition temperature (T_g), and the smallest cavities. The change in the alignment of the PI backbone from para to ortho led to a 29% reduction in the CO₂ permeability. Also, physical aging did not affect the gas transport properties of the PIs significantly. Trip-based diamines containing amine groups that are connected directly to the Trip moiety can be used to produce copolymers with different backbone rigidities [136].

To increase the moiety participation and decrease the ethereal oxygen density, the type of triptycene diamines (with or without ethereal oxygen) can be adjusted. Diamines without ethereal oxygen increase the inter- and intra-chain rigidities and the free volume. The permeability improvement without sacrificing the sieving ability is attained by increasing the triptycene level and decreasing the ethereal oxygen content due to the formation of more ultra-microporosity. The substitution of Trip with pentiptycene in 1, 4-triptycene diamines, possessing different substituent groups, does not alter the trend. In addition, 6FDA-(pentiptycene diamine) PPDA PIs exhibit bimodal pore size distributions [127]. The replacement of the Trip moiety with the pentiptycene

one in the polymer backbone results in higher free volume and larger inter-chain distances[137]. The CO₂ permeabilities of 6FDA-PPDA PIs are in the range of 55-132 Barrer. Although pentiptycene moiety causes inefficient chain packing, the ethereal oxygen in the backbone of polymers might have an opposing effect on it [127]. Therefore, the low permeability (compared to that of microporous PIMs) and the flexibility of the resulting polymer are attributed to the ethereal oxygen [127].

Mechanically robust membranes can be synthesized using copolymers consisting of 6FDA, PPDA, and linear polyethylene oxide (PEO)-based diamines [138]. The incorporation of the PEO leads to a decrease in the CO₂ permeability due to the lower free volume of these copolymers, compared to 6FDA-PPDA. These confirm the potential of Trip and pentiptycene moieties for tuning free volume and increasing the aging resistance of PIs. However, the CO₂ permeabilities of these membranes are lower than those of other PIM-PIs due to the existence of etheric oxygens in their backbones, which lower their free volumes. Figure 11 represents structures of PIM-PIs containing contortion sites in diamines.

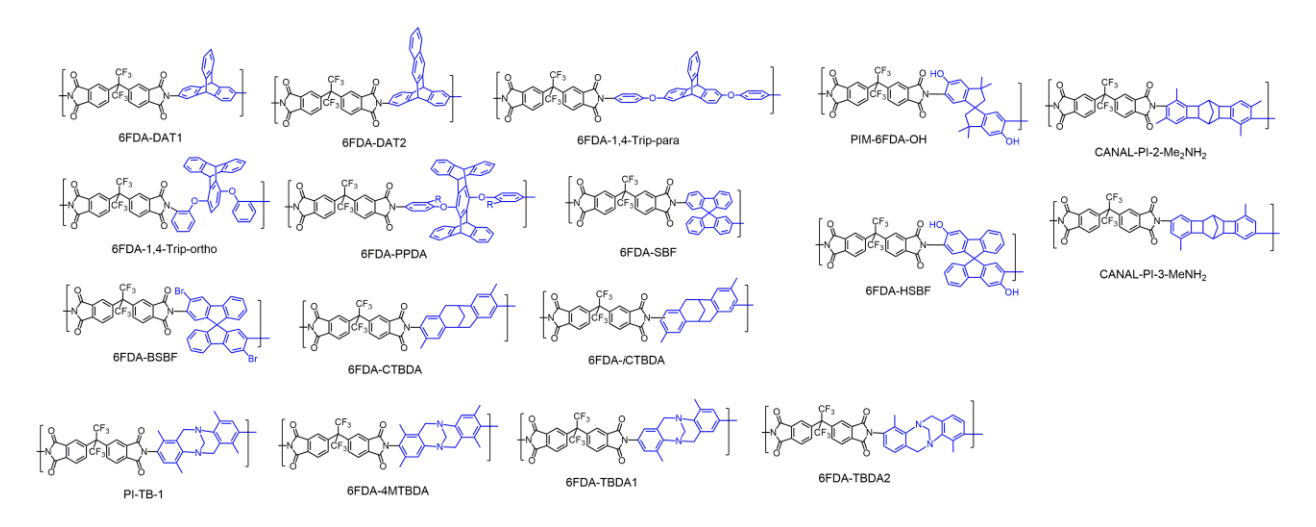


Figure 11. Molecular structures of PIM-PIs containing contortion sites in diamines [89, 92, 100].

Microporous PI membranes can be designed and synthesized using SBF-based diamines (SBF), brominated SBF (BSBF), and three different dianhydrides [6FDA, pyromellitic dianhydride (PMDA), and spiro-based dianhydride (SPDA)] [139]. The brominated polymers exhibit large surface areas. Bromination has no considerable effect on the thermal stability. However, the char yield of the brominated PIs is 10% less than that of the pristine PI. The dianhydride type has a significant effect on the gas permeabilities and the order of the permeabilities. 6FDA-SBF has CO_2 permeability of 182 Barrer and the permeability order is $CO_2 > N_2 > CH_4$. However, SPDA-SBF shows CO_2 permeability of 614 Barrer and the permeability order is $CO_2 > CH_4 > N_2$. Bromination increases the chain stiffness of the polymer due to the impeded single bond rotation of bromine [96]. The incorporation of the bromine groups into the SBF diamine increases the CO_2 permeability due to the gas diffusivity and solubility enhancements without sacrificing the selectivity, especially for CO_2/CH_4 separation.

Taking the advantage of the type, the position and the number of substituents of TB-based diamines, researchers have attempted to tune gas transport properties of PIs with various structures [122, 128, 140]. To synthesize TB-based PIs, two TB-based diamines containing two methyl groups in two different positions [2,8 diamino-4,10-dimethyl,11-methanodibenzo-diazocine (TBDA1) and 3,9-diamino-4,10-dimethyl,11-methanodibenzo-diazocine (TBDA2)] can be designed and synthesized. Four TB-based PIs can be prepared from these diamines, 6FDA, and 4,4-oxidiphthalic anhydride (ODPA). In addition to good film-forming, 6FDA-TBDA1-PI has a CO₂ permeability of 285 Barrer with satisfactory selectivity. Free volume and d-spacing results agree with permeability data. The kinked structure of TB, the closeness of the methyl group to the

amine unit, and the presence of bulky groups in the 6FDA structure cause high solubility and diffusivity coefficients, as well as high CO₂ permeability without sacrificing the selectivity.

Good processability, extraordinary thermal stability, high Tg, and good mechanical properties can be achieved by incorporating the TB moiety into the polymer structure using polymerization of imide containing diamines obtained from commercial dianhydrides [107, 141-143]. The introduction of TB building block into the polymer backbone creates significant microporosity and high FFV. The TB moiety endows the membrane with the anti-plasticization property. Two intrinsically microporous 6FDA-based PIs containing two TB-based di-osubstituted diamine monomers (PIM-PI-TB-1 and PIM-PI-TB-2) are synthesized possessing high molecular weight, outstanding thermal stability, and excellent solution processability. In addition to four methyl groups in different positions, PIM-PI-TB-1 has two bromine atoms in its repeating unit. PIM-PI-TB-1 and PIM-PI-TB-2 have good solution processability, which is ascribed to the presence of the TB moiety, the bulky -CF₃ groups, and the o-substituents that limit rotation around the imide bonds. Fast nitrogen adsorption at very low pressures reveals the ultra-microporous structure of the polymers created by the TB moiety, and the pendant o-methyl and o-bromine groups. BET surface area for PIM-PI-TB-1 and PIM-PI-TB-2 is 440 and 580 m²/g, respectively. Satisfactory permeability with low-to-moderate sieving ability is attained for these two membranes [140].

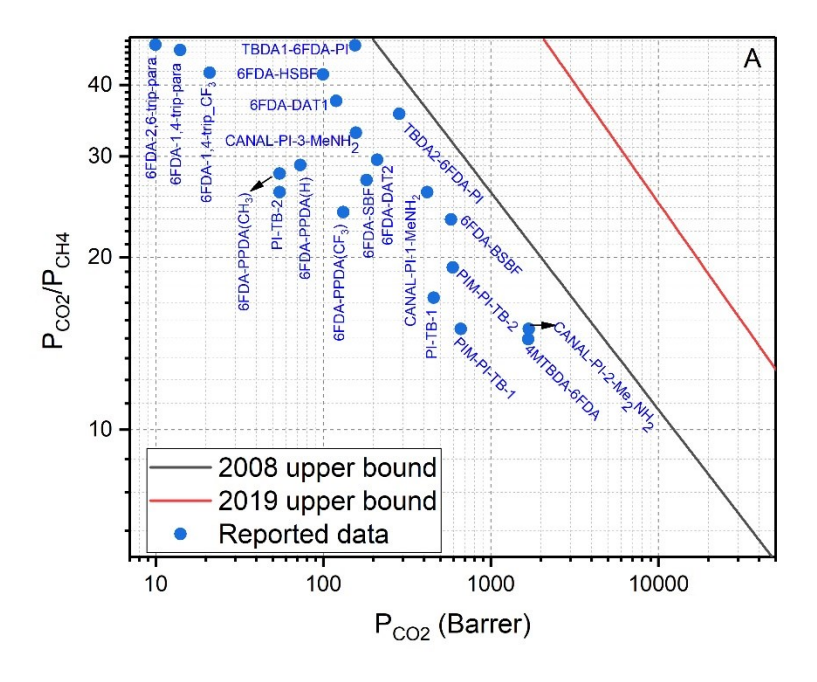
Considering the large microporosity that TB moiety creates, a TB diamine with four methyl groups (4MTBDA) is synthesized and used to prepare four TB-based PIs [122]. Restricted rotation around the imide bond provides intrinsic microporosity and BET surface areas between 584 and

739 m²/g. In addition to their microporous structure, the four PIs possess film-forming abilities and high molecular weights. High permeabilities and low selectivities are obtained for these PIs. Their permeability order agrees with their dianhydride rigidity order: PMDA > SBF-based dianhydride (SBFDA) > SPDA > 6FDA. PMDA is a promising monomer, as its polymerization produces chains with a rigid backbone and high microporosity. In addition, the fabricated membranes have high CO_2 permeability and excellent selectivity. Table 3 and Figure 12 show gas separation performance of the PIM-PI membranes containing contortion sites in diamines for CO_2/CH_4 and CO_2/N_2 separations.

Table 3. Performance of the PIM-PI membranes containing contortion sites in diamines for CO₂ separation.

Polymer	Permeability (Barrer)			Selectivity		Ref
	CO ₂	CH ₄	N ₂	CO ₂ /CH ₄	CO ₂ /N ₂	Ku
6FDA-DAT1	120	3.2	4.7	37.5	25.5	[96,
6FDA-DAT2	210	7.1	9.0	29.6	23.3	116]
6FDA-1,4-trip_ortho	7.7	0.15	0.28	51	28	
6FDA-1,4-trip_para	14	0.31	0.52	46	27	[135]
6FDA-2,6-trip_para	10	0.21	0.40	47	25	=
CANAL-PI-1-MeNH ₂	419	16.3	20.7	26	20	
CANAL-PI-2-Me ₂ NH ₂	1,691	108	91	15	18	[131]
CANAL-PI-3-MeNH ₂	157	4.8	7	33	22	-
6FDA-1,4-trip_CF ₃	21	0.49	0.87	42	24	[144]
6FDA-PPDA(H)	73	2.50	3.20	29	23	
6FDA-PPDA(CH ₃)	55	2.00	2.40	28	23	[127]
6FDA-PPDA(CF ₃)	132	5.50	7.00	24	19	1

6FDA-SBF	182	6.4	7.8	27.3	23.3	[139]
6FDA-BSBF	580	24.9	27	23.3	21.5	[137]
4MTBDA-6FDA	1,672	116	133	14.4	12.5	[145]
TBDA1- 6FDA-PI	155	3.3	6.5	46.9	23.8	[146]
TBDA2- 6FDA-PI	285	8	12	35.6	23.7	[1:0]
PIM-PI-TB-1	662	44	42	15	15.7	[122]
PIM-PI-TB-2	595	31	34	19.2	17.5	[122]
6FDA-SBF	182	6.4	7.8	27.3	23.3	[147]
6FDA-HSBF	100	2.4	3.8	41.7	26.3	[1./]
PI-TB-1	457	27	31	17	15	[141]
PI-TB-2	55	2.1	2.5	26	22	[[]]



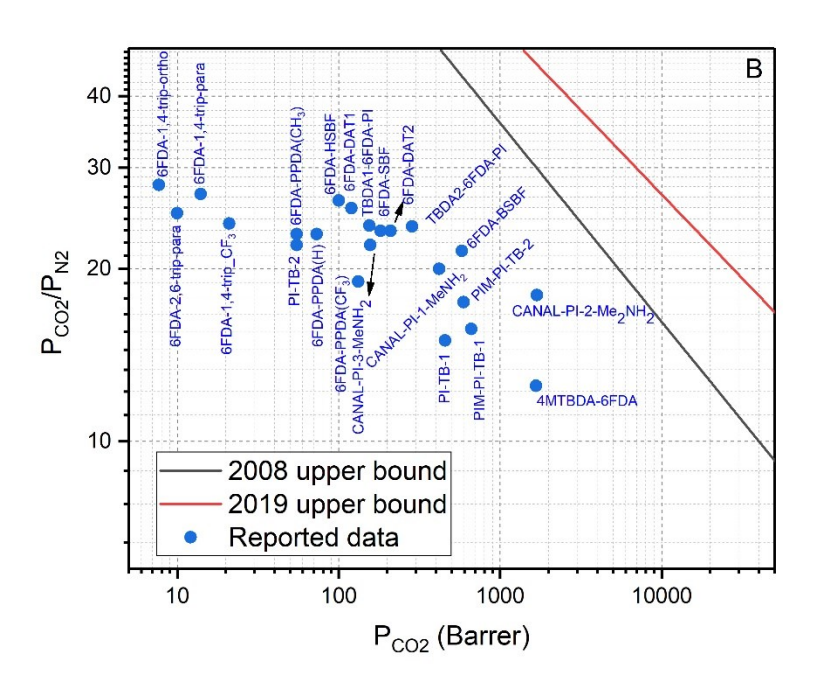


Figure 12. Data from Table 3 showing gas separation performances of the PIM-PI membranes containing contortion sites in diamines. (A) CO_2/CH_4 and (B) CO_2/N_2 .

4.2. PIM-PI Membranes Containing Dianhydride Contortion Sites

So far, only SBI-, SBF-, EA-, Trip- and pentiptycene-based dianhydrides have been synthesized and embedded into PIM-PIs structures [148-152]. Figure 13 shows the structures of all existing dianhydrides containing contorted moieties. Different PIM-PIs (PIM-PI-1 to PIM-PI-8) based on the SBI dianhydride with dioxane rings can be prepared using various diamines [149]. The PIs have BET surface areas of 471–683 m²/g, high thermal stability, CO₂ permeabilities of 210–3700 Barrer, CO₂/N₂ selectivities of 22.6–26.8, and CO₂/CH₄ selectivities of 13.4–23.3. Among them, PIM-PI containing 3, 3'-dimethylnaphthidine (DMN) has the highest CO₂ permeability (3,700 Barrer) and a moderate CO₂/N₂ selectivity (23.1) [149]. Modest performances of these membranes motivate the synthesis of SBI-based dianhydrides without dioxane rings. Among these PIs, PIM-PI-10 that contains DMN has a CO₂ permeability of 2,154 Barrer and a CO₂/N₂ selectivity of 25.6 [126].

Membranes prepared from a SBI-based dianhydride and a SBI-based diamine (PIM-PI-11) have CO₂ permeability and selectivity lower than that PIM-PI-10. Eliminating the dibenzodioxin units in the polymer backbone and connecting the anhydride groups to the SBI moiety increase the polymer rigidity and CO₂ permeability. However, PIM-PI-10 (based on SBI anhydride without dioxane rings) has lower CO₂ permeability, compared to PIM-PI-8 (based on SBI anhydride with dioxane rings).

The substitution of the SBI moiety for SBF in the dianhydride structure leads to the synthesis of the SBFDA. Highly microporous SBFDA-DMN (BET surface area of 686 m²/g) PI can be prepared via the imidization reaction of SBFDA and DMN. SBFDA-DMN has high microporosity,

good processability, and exceptional thermal stability. The presence of a great number of ultramicropores (<7 Å) and pores larger than 1 nm provide the membrane with a high CO₂ permeability of 6,674 Barrer, a moderate CO₂/N₂ selectivity of 18, and a low CO₂/CH₄ selectivity of 11.5 [153]. Figure 14 represents structures of PIM-PIs containing contortion sites in dianhydride.

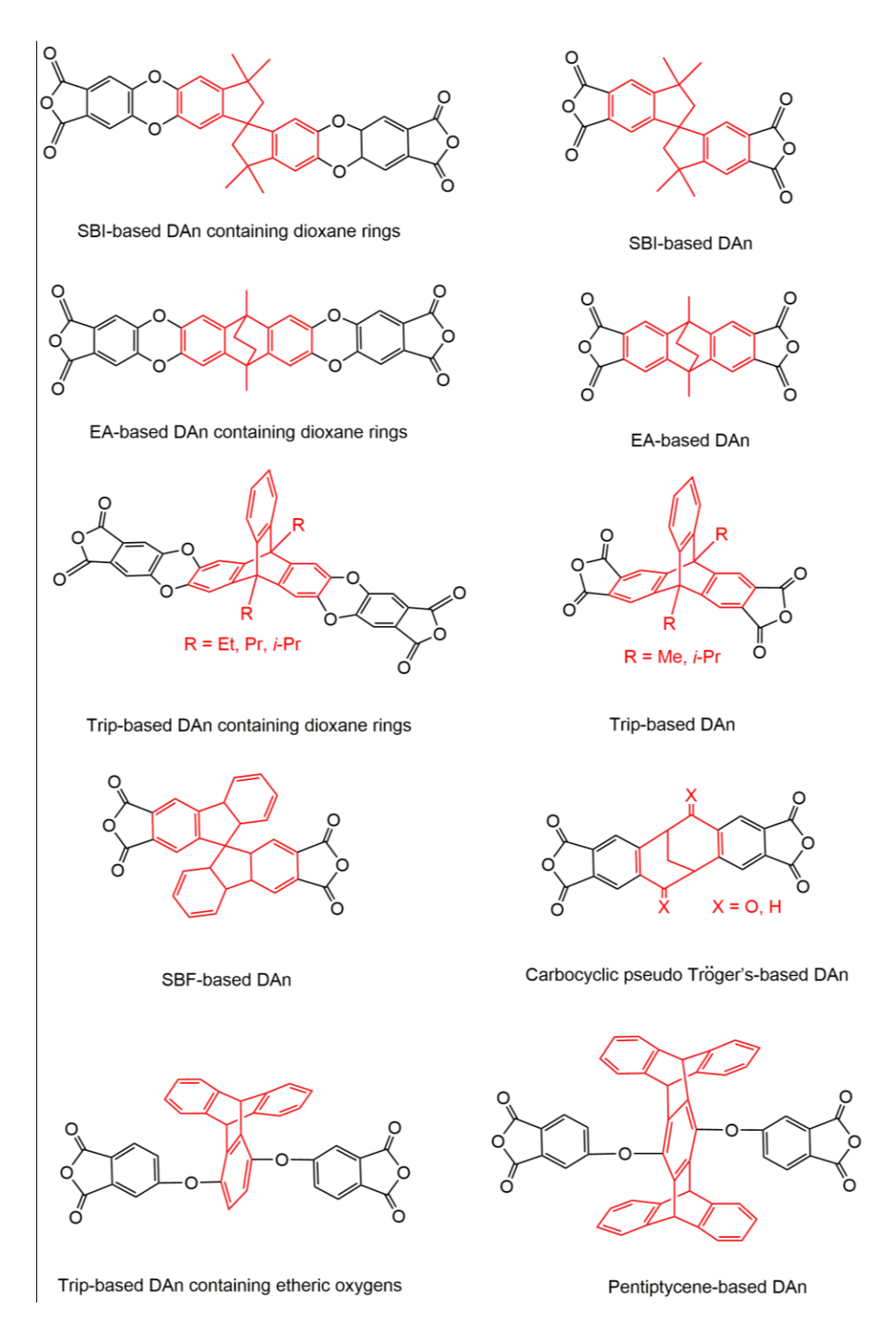


Figure 13. Molecular structures of dianhydrides containing contorted moieties [70, 89, 92].

Figure 14. Sample PIM-PIs containing contortion sites in dianhydrides [70, 89, 92, 154].

The inability of previous polymers with SBI and SBF moieties in their dianhydride structures to surpass the 2008 Robeson upper bounds has motivated the synthesis of polymers with rigid moieties in dianhydrides [125]. For example, an EA-based dianhydride (EADAn) from 2, 3, 6, 7, 9, 10-hexamethylethanoanthracene reacts with DMN via a polycondensation reaction [150]. The resulting polymer, PIM-PI-EA (PIM-PI-12), has a high molecular weight, a BET surface area of 616 m²/g, an exceptional CO₂ permeability (7,340 Barrer), and moderate CO₂/N₂ and CO₂/CH₄ selectivities (20 and 16, respectively) [150]. Its permeabilities have the order of CO₂ > CH₄ > N₂. Its CO₂/N₂ and CO₂/CH₄ performances are above the 2008 Robeson upper bounds [150]. The PIM-PI-EA has excellent CO₂ separation performance due to its impressive diffusivity and solubility selectivities. The presence of the EA moiety (in the dianhydride monomer) and the rigid diamine (DMN) lead to excellent CO₂/N₂ and CO₂/CH₄ separation performances of PIM-PI-EA membrane [150].

Rigid dibenzodioxane containing EA dianhydride (EAD-DA) has been used for the preparation of a microporous PI having DMN (EAD-DMN) [155]. EAD-DMN has a BET surface area of 800 m² g⁻¹. As anticipated, adding the dibenzodioxane units to the polymer backbone decreases the polymer rigidity and, consequently, its CO₂ permeability.

Excellent performances of PI membranes containing EA-based dianhydrides have motivated researchers to synthesize other kinds of dianhydrides containing rigid contortion sites. Amorphous and solution-processable Trip-based PIM-PIs (KAUST-PI-series) having high free volume and good sieving ability have been synthesized (Figure 15) [125, 151]. To tune the pore size distribution, the macromolecular rigidity, and inter-chain distances, Trip-based dianhydrides with 9, 10-bridgehead-substituents (diisopropyl, dipropyl, and diethyl) are synthesized. In these dianhydrides, the less rigid SBI moiety in the SBI-based dianhydride containing dioxane rings is

replaced with the more rigid, bulky, torsion-resistant bridged bicyclic Trip moiety. The degrees of torsional freedom in different contortion sites are shown in Figure 16. As this Figure shows, the torsional freedom of the bridged bicyclic moieties such as EA and Trip is less than those of the SBI and SBF moieties. Furthermore, an additional vertical aromatic ring makes the triptycene moiety the most torsion-resistant among the building blocks shown in Figure 16. Seven diamines can be utilized to obtain various PIs with different properties. More selective and permeable gas separation membranes can be designed and synthesized by the substitution of the SBI dianhydride with 9, 10-diisopropyl-substituted triptycenes dianhydride (i-C₃TPDA) [125]. KAUST-PI-1 and KAUST-PI-2 can be prepared from i-C₃TPDA and diamines containing methyl groups in the ortho position related to the C-N bond [N, N, N', N'-tetramethylphenyl-diamine (TMPD) and 3,3',5,5'tetramethylbenzidine (TMBZ)]. The presence of the stiff diamines rigidifies the polymer backbone and confines the chain rotation. Incorporating isopropyl bridgehead substituents, diamines with asymmetric methyl groups and Trip moiety into KAUST-PI-1 and KAUST-PI-2 resulted in a ribbon-like chain growth of these polymers, and consequently, inefficient chain packing and significant ultra-microporosity [125].

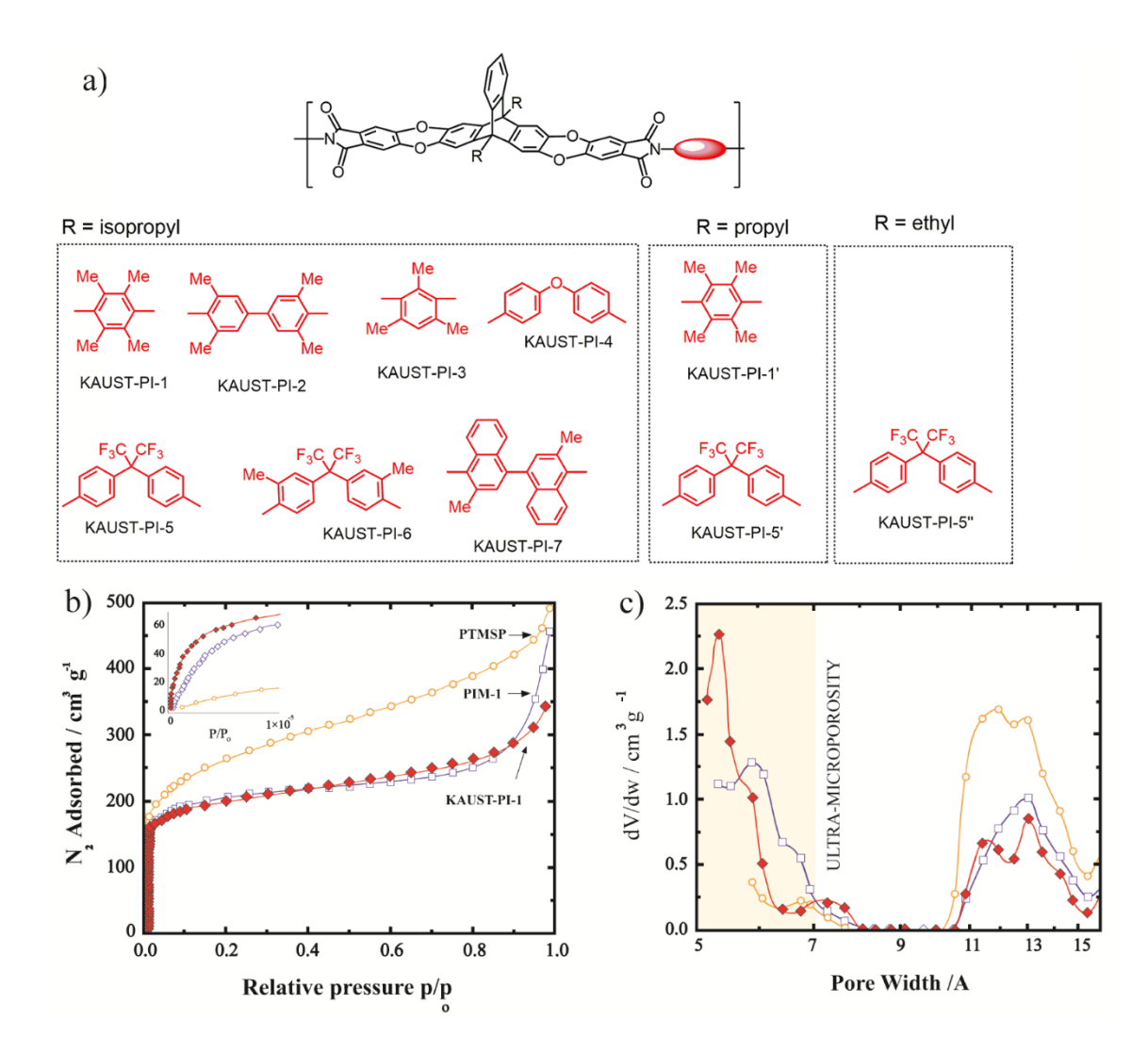


Figure 15. (a) Molecular structures of KAUST-PIs, (b) nitrogen adsorption isotherms of PTMSP, PIM-1 and KAUST-PI-1, and (c) their pore-size distributions [125, 151]. (a) Reprinted with permission from Swaidan R, Al-Saeedi M, Ghanem B, Litwiller E, Pinnau I., Rational design of intrinsically ultramicroporous polyimides containing bridgehead-substituted triptycene for highly selective and permeable gas separation membranes, Macromolecules, 47:5104-14, (2014). Copyright 2014 American Chemical Society. (b) & (c) Reprinted with permission from M. Ghanem BS, Swaidan R, Litwiller E, Pinnau I. Ultra-Microporous Triptycene-based Polyimide Membranes for High-Performance Gas Separation, Advanced Materials, 26:3688-92, (2014). Copyright 2014 John Wiley and Sons.

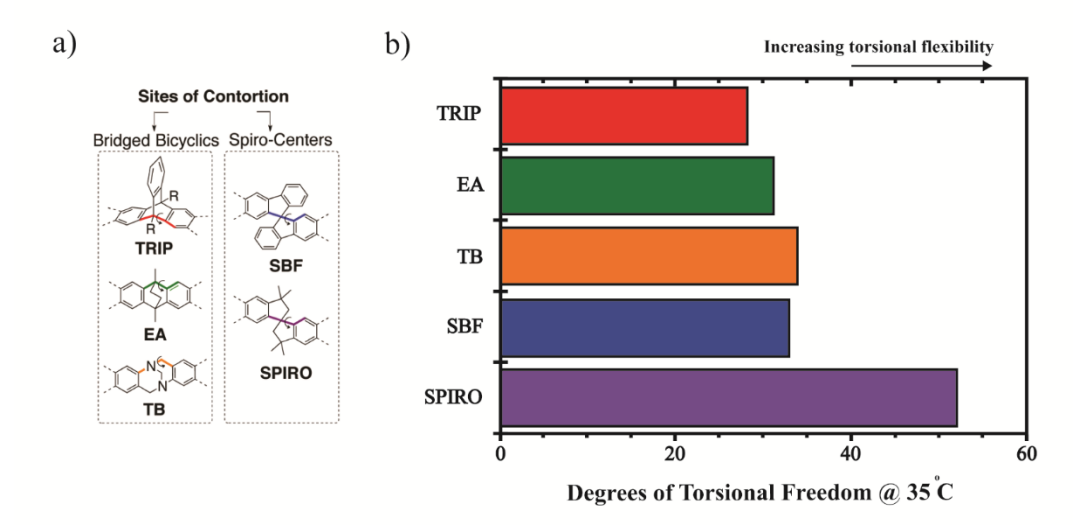


Figure 16. Comparison of dihedral angle distributions of the bridged-bicyclic and spiro-based moieties [125]. Reprinted with permission from Swaidan R, Al-Saeedi M, Ghanem B, Litwiller E, Pinnau I., Rational design of intrinsically ultramicroporous polyimides containing bridgehead-substituted triptycene for highly selective and permeable gas separation membranes. Macromolecules. 47:5104-14 (2014). Copyright 2014 American Chemical Society.

KAUST-PI-1, 2 and 3 have high BET surface areas of 740–760 m² g⁻¹, which points to the effect of the presence of the isopropyl-substituted Trip moiety. The high BET surface areas of KAUST-PI-1, 2, 3 and 8 imply that the bulkiness, rigidity, and substituent groups of the diamine increase the surface area via restricting the rotation around the imide bond. KAUST-PI-7 (i-C₃TPDA-DMN), bearing a pair of two fused benzene rings with two methyl groups in the diamine structure, has the highest BET surface area among PIs (840 m²/g).

Among all KAUST-PIs, KAUST-PI-7 has the highest CO₂ permeability and the highest diffusivity coefficient due to the bulky structure of DMN, which provides a high surface area and an open structure. However, KAUST-PI-7 has the lowest selectivity and solubility selectivity. The higher microporosity of KAUST-PI-1 than KAUST-PI-1' and KAUST-PI-5 than KAUST-PI-5' and 5'' indicates the efficacy of the isopropyl-substituent compared to linear diethyl and dipropyl substituents. TMPD is a rigid aromatic diamine with four methyl groups adjacent to amines. It has

been used to develop PIs with extraordinary permeability and good selectivity [125, 126, 149]. KAUST-PI-1 (i-C₃TPDA-TMPD) has a high CO₂/CH₄ selectivity and a great CO₂ permeability placing its performance on the 2018 mixed-gas upper bound [125].

The outstanding permeability and the satisfactory selectivity of KAUST-PI-1 are due to the bimodal pore-size distribution and the porous structure of the polymer, pointing to ultramicroporosity of KAUST-PI compared to PIM-I and PTMSP (Figure 15). Small micropores improve the sieving ability due to the narrow paths, and the large pores boost the CO₂ permeability via fast gas adsorption and desorption. The branched methyl groups, the small size, and the rigidity of TMPD generate more ultra-microporosity and sorption sites. This causes improvement in permeability and selectivity. KAUST-PI-1 has a higher selectivity and a higher CO₂ permeability than KAUST-PI-2, even with its lower diffusivity coefficient. Switching from rigid diamines to more flexible diamines lowers the CO₂ permeabilities of KAUST-PI-4 and KAUST-PI-6 but increases their selectivities. The KAUST-PI-4 derived from Trip dianhydride and 4, 4'oxydianiline has a considerably low CO₂ permeability (286 Barrer) compared to other KAUST-PI-series, while KAUST-PI-1 derived from the same dianhydride and TMPD has a high CO₂ permeability. It is commonly understood that the ethereal oxygen of 4, 4'-oxydianiline is responsible for the low permeability and diffusivity [125]. KAUST-PI-1 and 2 can fill the gap between commercial membranes (highly selective and low permeable) and highly permeable and low selective PIM membranes.

PI membranes containing Trip-based dianhydride (without dioxane rings), dimethyl- and diisopropyl-triptycene-based dianhydride monomers (TDA1 and TDA*i*3, respectively) have superior CO₂ separation performance (Figure 17). Among these monomers, only anhydride groups are connected directly to the Trip moiety, and therefore the dianhydride monomers do not include

any dioxane rings [129, 156]. Diisopropyl-substituted-triptycene-TMPD (TDA*i3*-TMPD) is not solution-processable in comparison with KAUST-PI-1. PIs developed based on the dianhydride monomers and the highly sterically-hindered DMN diamine are solution-processable. TDA-DMN polymers have high molecular weights, processability, and excellent thermal stability. The presence of DMN in the structure of PIs leads to the formation of highly permeable membranes with outstanding surface areas. Introducing dimethyl bridgehead groups to the Trip moiety leads to a surface area of 760 m²/g for TDA1-DMN. Both PIs have bimodal pore size distributions. TDA1-DMN (3,700 Barrer) and TDA*i*3-DMN (3,154 Barrer) have high CO₂ permeabilities with moderate selectivities. The higher CO₂ permeability of TDA1-DMN is due to the higher free volume verified by broader peaks in the powder X-ray diffraction (PXRD) patterns agreed with its higher affinity to CO₂ (Figure 17). Furthermore, the better sieving ability of TDA1-DMN is due to the lower intersegmental distance, indicated by the smaller d-spacing in its PXRD pattern. The microporous structure, the pore size distribution, and the gas transport properties can be tuned with appropriate bridgehead substituents.

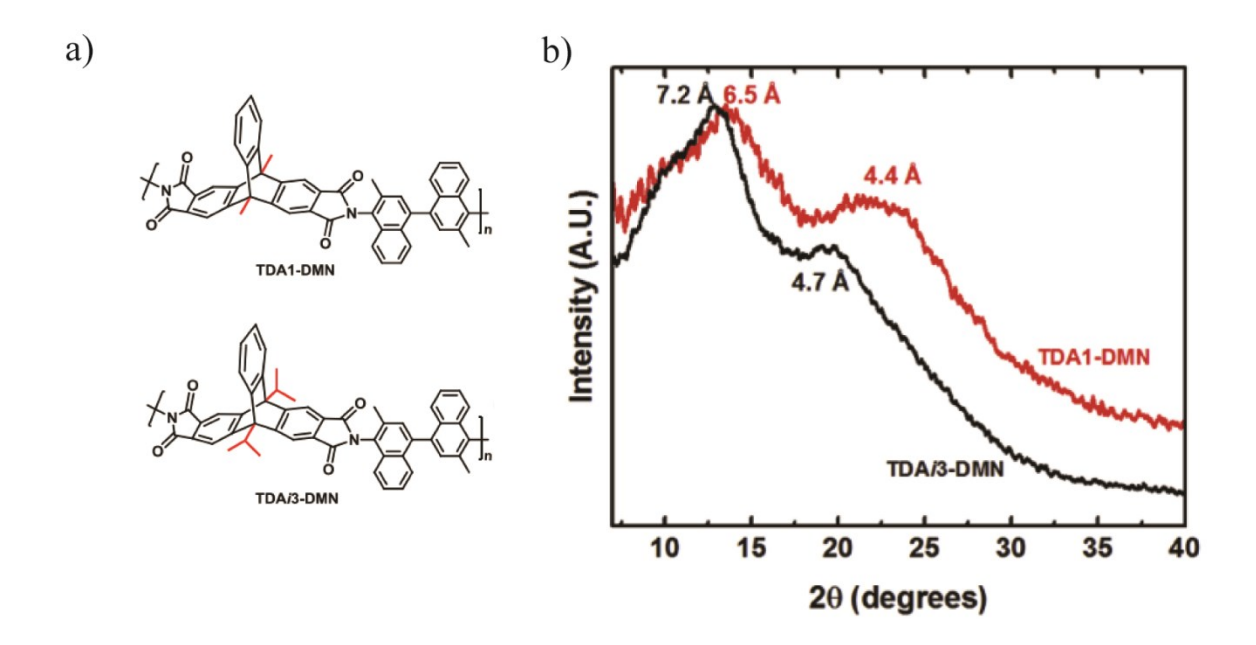


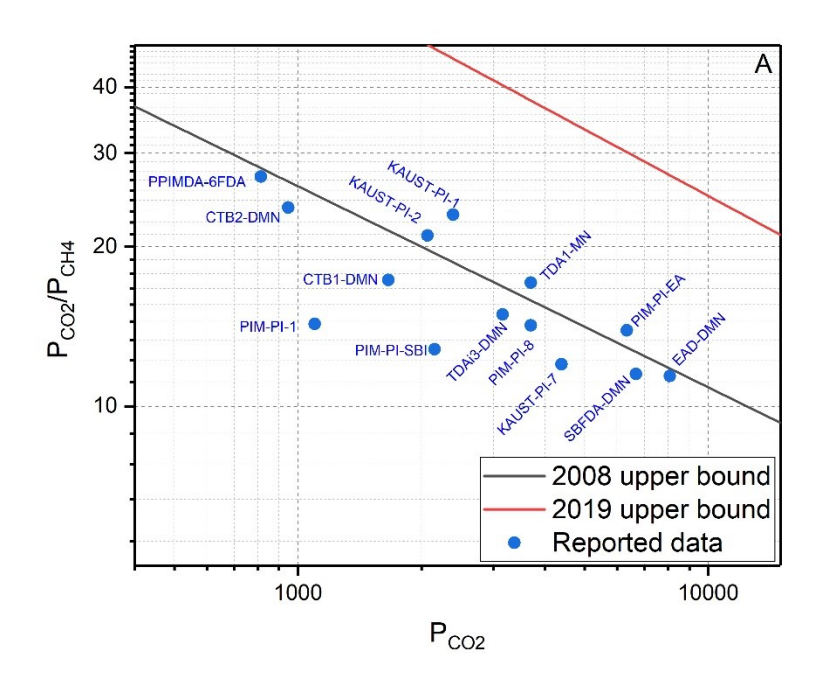
Figure 17. (a) Structure of TDA1-DMN and TDA*i*3-DMN membranes, and (b) PXRD patterns of TDA1-DMN and TDA*i*3-DMN membranes [129]. Reprinted with permission from Ghanem B, Alghunaimi F, Ma X, Alaslai N, Pinnau I., Synthesis and characterization of novel triptycene dianhydrides and polyimides of intrinsic microporosity based on 3, 3'-dimethylnaphthidine. Polymer, 101:225-32. (2016). Copyright 2016 Elsevier.

The Trip moiety affects dianhydride properties strongly. Trip-containing dianhydride (TPDAn) can react with two iptycene-containing diamines (i.e., TPDAm and PPDA) to synthesize iptycene-containing PIs [157]. A bimodal pore-size distribution with maxima at 3 and 7 Å indicates the ultra-microporosity of the prepared PIs. Low free volumes of these polymers are due to the flexible ether linkages in their backbone, leading to CO₂ permeabilities less than 39 Barrer, which is much lower than those of microporous polymers.

The rigid groups have a remarkable effect on veiling the effects of flexible groups, which may lead to improved CO₂ permeability. Ethereal oxygen has a negative impact on pentiptycne-based polymers. A pentiptycene dianhydride (PPDAn) can be synthesized from a pentiptycne diol. One-step imidization reaction of PPDAn with TMPD forms an insoluble low molecular weight polymer. Using excess TMPD, an imide containing pentiptycene diamine (PPImDA) is prepared

followed by its polymerization with 6FDA to obtain PPImDA-6FDA as a processable polymer for membrane fabrication. This polymer has outstanding thermal stability, excellent solubility, and a moderate BET surface area of 302 m²/g. Like other pentiptycene polymers, PPIMDA-6FDA has a bimodal pore size distribution. CO₂ permeability of 812 Barrer with moderate CO₂/CH₄ selectivity were achieved for PPIMDA-6FDA [152].

Two solution-processable PIs are 5,6,11,12-tetrahydro-5,11-methanodibenzo(a,e)(8) annulene-2,3,8,9-tetracarboxylic anhydride (CTB1)-DMN and 6,12-dioxo-5,6,11,12-tetrahydro-5,11-methanodibenzo(a,e)(8) annulene-2,3,8,9-tetracarboxylic dianhydride (CTB2)-DMN, which can be synthesized from separate polycondensation reactions between two carbocyclic pseudo Tröger's base dianhydrides and DMN [135]. Both CTB1-DMN and CTB2-DMN have commendable thermal stability and high BET surface area of 580 and 469 m²g⁻¹, respectively. Because of the high microporosity, CTB1-DMN and CTB2-DMN have shown high CO₂ permeabilities of 1,661 and 948 Barrer, respectively. Their gas selectivities were found to be moderate. These properties have placed the CO₂/N₂ and CO₂/CH₄ gas separation performances of CTB1-DMN and CTB2-DMN below the Robeson upper bounds. Furthermore, CTB2-DMN has the highest gas selectivity and the lowest gas permeability among the DMN-based PIs prepared from dianhydrides with other contorted moieties. The studies have shown that PIM-PIs prepared from diamines containing a rigid moiety are unable to surpass the Robeson upper bounds (Figure 12). Incorporating ladder-type moieties into the dianhydride structure is a promising strategy to prepare PIM-PI membranes whose performances are above the Robeson upper bounds (Figure 18). Table 4 shows CO₂ separation performance of the PIM-PI membranes containing contortion sites in dianhydrides. PIM-PI membranes containing two moieties at both dianhydride and diamine molecules can be synthesized (Figure 19).



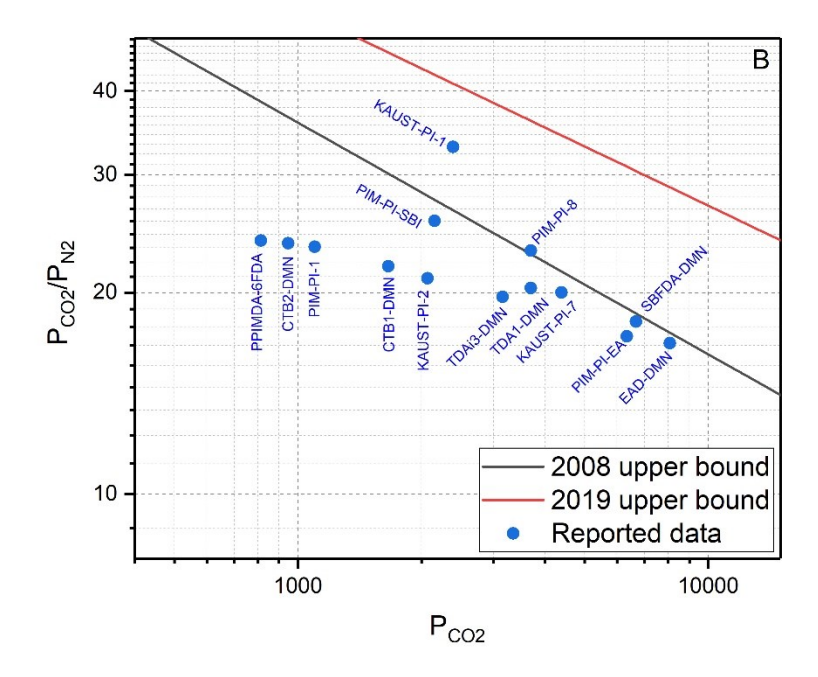


Figure 18. Data from Table 4 showing gas separation performances of the PIM-PI membranes containing contortion sites in dianhydrides. (A) CO_2/CH_4 and (B) CO_2/N_2 .

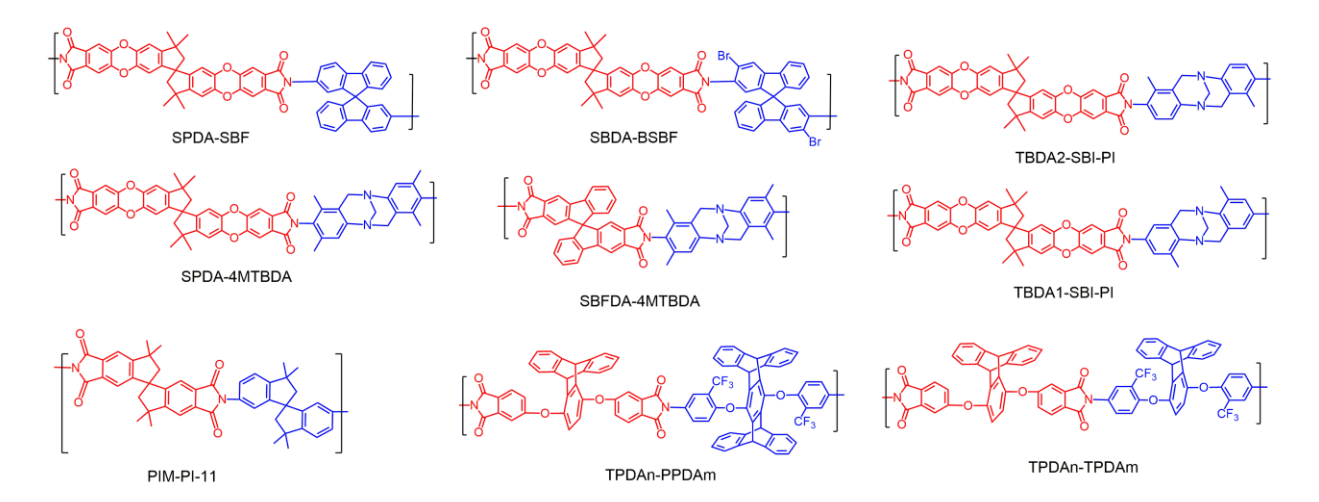


Figure 19. Molecular structures of PIM-PIs containing contortion sites in both diamine and dianhydride [89, 92, 94].

Table 4. Performance of the PIM-PI membranes containing contortion sites in dianhydride for CO₂ separation.

Polymer	Permeability (Barrer)			Selectivity		Ref
	CO ₂	CH ₄	N ₂	CO ₂ /CH ₄	CO ₂ /N ₂	Kei
PIM-PI-1	1,100	77	47	14.3	23.4	[149]
PIM-PI-8	3,700	260	160	14.2	23.1	[158]
PIM-PI-SBI	2,154	168	84	12.8	25.6	[126]
SBFDA-DMN	6,674	581	369	11.5	18.1	[153]
PIM-PI-EA	6,340	457	369	13.9	17.2	[150]
EAD-DMN	8,070	707	480	11.4	16.8	[155]
KAUST-PI-1	2,389	105	107	23.0	33.0	[125]
KAUST-PI-2	2,071	101	98	21.0	21.0	[125]
KAUST-PI-7	4,391	354	225	12.0	20.0	[125]
TDA1-DMN	3,700	216	182	17.1	20.3	[129]
TDAi3-DMN	3,154	211	160	14.9	19.7	[129]
TPDAn-PPDAm	39.0	1.50	1.80	26.0	21.6	[157]
TPDAn-TPDAm	9.7	0.31	0.44	31.3	22.0	[157]
TPDAn-6FAP	4.7	0.09	0.19	52.2	24.7	[157]

PPIMDA-6FDA	812	30	34	27.1	23.9	[152]
CTB1-DMN	1,661	96	76	17.3	21.9	[159]
CTB2-DMN	948	40	40	23.7	23.7	[159]

5. Post-Modification of PIM Membranes

5.1. Crosslinking

Crosslinking allows for preparing highly selective membranes for gas separation [160]. Polymer solubility and membrane gas-transport properties can be controlled via adjusting the degree of crosslinking. Thermal crosslinking is a method for preparing crosslinked membranes. In this method, the degree of crosslinking of a membrane depends on the reaction temperature, catalyst type and amount, and/or reaction time [161]. Thermal stability increases with increased degree of crosslinking, which rises with both the reaction temperature and duration. Thermal crosslinking of PIM-1 under vacuum at 300 °C with a 2-day reaction time improved the CO₂ permeability by 18%, the CO₂/N₂ selectivity by 104%, and the CO₂/CH₄ selectivity by 230% [161]. Increasing crosslinking time from 12 to 48 h at 300 °C and from 12 to 24 h at 250 °C resulted in a uniform CO₂/CH₄ selectivity enhancement of PIM-1 [161]. The formation of stable planar triazine rings (Figure 20a) without releasing any volatile product, increases the PIM-1 stability. The creation of triazine rings decreases the inter-chain distance and free volume. Therefore, the formation of contracted cavities leads to selectivity enhancement. Figure 20b shows how pores change during thermal crosslinking. The permeability enhancement has been attributed to the conformational freedom limitations caused by increased inefficient chain packing. The use of a longer crosslinking time led to the creation of more triazine rings, and consequently to a higher CO₂ permeability of 4,000 Barrer, a higher CO₂/N₂ selectivity of 41.7, and a higher CO₂/CH₄ selectivity of 54.8 [161].

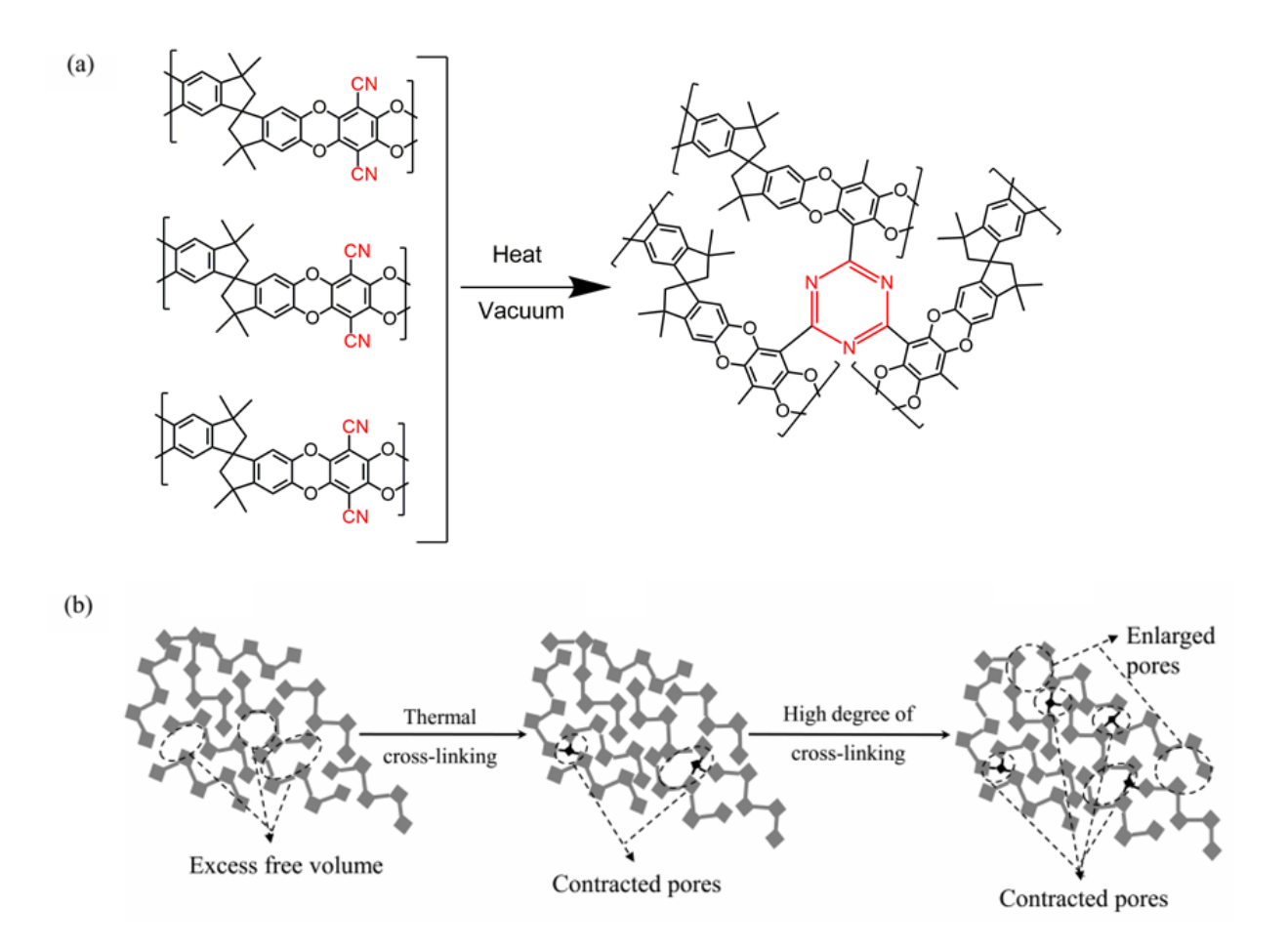


Figure 20. (a) Formation of a triazine ring during thermal crosslinking of PIM-1, and (b) change in PIM-1 structure during thermal crosslinking [161]. Reprinted with permission from Li FY, Xiao Y, Chung T-S, Kawi S., High-performance thermally self-cross-linked polymer of intrinsic microporosity (PIM-1) membranes for energy development. Macromolecules, 45:1427-37. (2012). Copyright 2012 American Chemical Society.

Thermal crosslinking in an inert atmosphere containing tiny amounts of atmospheric oxygen leads to the formation of covalently crosslinked polymer chains and increased molecular sieving ability [162]. The O₂ plays a prominent role in the crosslinking process. The degree of crosslinking is controlled by adjusting oxygen content, reaction time, and temperature. At a high oxygen level (air condition), the reaction time should be short (10 min), because the membrane may degrade or crack. The oxidative heat treatment of microporous membranes results in the formation of 3D networks with tighter pathways and lower chain-to-chain spacing, allowing for

higher selectivity. The high free volume of a membrane provides an opportunity for excellent sorption and diffusion of oxygen molecules through the spaces between the interconnected micropores. Performing the reaction under different conditions may affect the pore size distribution and the crosslinking extent differently.

Another method of preparing crosslinked membranes is converting the nitrile groups of PIM-1 to carboxyl groups, followed by decarboxylation and annealing [163]. The created carboxylic acid anhydride is then converted to aryl radicals, and radical combination generates biphenyl crosslinking. The abstraction of a hydrogen from a methyl group, the loss of a methyl group, and aromatic radicals provide possible sites for crosslinking. The carboxylated PIM-1 was crosslinked via annealing at 375 °C for 40 min [163]. The resulting membranes have higher CO₂/N₂ and CO₂/CH₄ selectivities but lower CO₂ permeabilities compared to the pristine PIM-1 [163].

5.2. Thermal Treatment

The post-thermal treatment of PI and polyamide [164] films containing ortho-positioned groups like hydroxyl results in polymers containing benzoxazole groups via thermal rearrangement (TR) and thermal cyclodehydration (TC) processes, respectively (Figure 21) [94, 165-169]. Thermally-treated membranes simultaneously possess favorable permeabilities, satisfactory selectivities, and good plasticization resistances, making the membranes attractive for CO₂ separation [170, 171].

Controlling the pore size distribution and the free volume is an effective approach to increase diffusion pathways [172]. Micropores formed during TR and TC processes provide membranes with attractive interconnected pores and a high free-volume content. The high free-volume is due to the conversion of the packed PIs to heterogeneous aromatic rigid-rod polymers

[173]. Both PIM and TR membranes possess low elongation at break, but TR membranes exhibit higher tensile strengths and better mechanical properties than PIM membranes [174, 175]. On the other hand, the need for a completely inert atmosphere, a high temperature for membrane preparation, and the brittleness of the obtained membranes are major drawbacks of this post-modification method [170, 176].

Figure 21. Molecular structures of PIM membranes prepared by TR and TC processes [89, 92, 94].

By combining TR and PIM membranes, four SBI-containing thermally-rearranged benzoxazole (SBI-TR-PBO) membranes were fabricated through the thermal treatment of the corresponding PIs [173]. Rearranging the PIs structure using thermal treatment lowers the density, increases the free volume, improves the surface area, and enhances the d-spacing of the SBI-TR-PBO more than those of SBI-PIs. Furthermore, SBI-TR-PBO has a higher elongation at break. 6FDA-SBI-TR-PBO has a significantly high CO₂ permeability of 675 Barrer, which is six times higher than that of 6FDA-SBI-PI (102 Barrer), and a higher CO₂/N₂ selectivity (22) than that of

6FDA-SBI-PI (19), while its CO₂/CH₄ selectivity is slightly lower [177]. The extraordinary improvement of the CO₂ permeability of 6FDA-SBI-TR-PBO is ascribed to its high free volume created by thermal rearrangement and to its high CO₂ solubility.

To synthesize thermally-rearranged SBF-based membranes, a general method can be used to prepare an o-hydroxyl-functionalized SBF-based diamine monomer (HSBF) [147, 178]. In this method, the precursor PIs for TR-PBOs are prepared using a reaction of HSBF, 6FDA, and SBDA. The TR-PBOs have higher thermal stability than the corresponding PIs. SPDA-HSBF has the highest CO₂ permeability (568 Barrer) among all hydroxyl-containing PIs. However, the BET surface area and the diffusion coefficient of SPDA-SBF-PBO are not considerably changed during the thermal processing. The SPDA-SBF-PBO has a 225% improvement in the CO₂ permeability compared to SPDA-HSBF due to its higher CO₂ solubility coefficient, but it has low-to-moderate selectivity. The thermal rearrangement of PBO-6FDA-HSBF improved the BET surface area of the polymer by 4.95 times [147, 178]. The microporosity generated by the thermal rearrangement provided a 5.09 times higher CO₂ diffusion coefficient and a 90% enhancement in the CO₂ solubility coefficient, leading to a 10.6 times higher CO₂ permeability (1,160 Barrer) [147, 178]. PBO-6FDA-HSBF has been reported to have a CO₂/N₂ selectivity of 21.1 and a CO₂/CH₄ selectivity of 20.7 [147, 178].

To investigate the effect of Trip moiety on the performance of a thermally-rearranged membrane, a Trip-based polybenzoxazole (PBO) was synthesized by thermal treatment of the microporous TAD1- 2, 2'-bis(3-amino-4-hydroxyphenyl)-hexafluoropropane (APAF) PI at 460 °C for 30 min under an inert atmosphere [179]. The full conversion of TDA1-APAF to PBO and the partial main-chain decomposition were verified using thermal gravimetric analysis (TGA) [179]. Nitrogen adsorption isotherms showed that heat treatment results in almost 160%

enhancement in BET surface area of the TR-TDA1-PBO compared to the TDA1-APAF PI, which had a BET surface area of 260 m² g⁻¹ [179]. Significantly enhanced microporosity, large d-spacing, and wide pore size distribution improved the CO₂ diffusion coefficient by 25.1 times and consequently the CO₂ permeability by 32.2 times [179]. The TR-TDA1-PBO membrane was reported to have an exceptional CO₂ permeability of 1,328 Barrer and a CO₂/CH₄ selectivity of 27. Furthermore, its CO₂ permeability of 1,000 Barrer and CO₂/CH₄ selectivity of 22 at 10 bar in mixed-gas permeation experiments pointed to its satisfactory transport properties. Because of its high microporosity and ultra-microporosity, TR-TDA1-PBO has a high CO₂ permeability and a satisfactory CO₂/CH₄ selectivity [179]. This performance is better than those of all previously prepared APAF-PI-based PBOs. Consequently, TDA1 is a promising monomer to fabricate APAF-PI-based PBOs membranes [179].

Trip-based PBO membranes were synthesized from Trip-containing polyhydroxyamide (TPHA) and poly(hydroxyimide) (TPHI) precursors using TC and TR processes, respectively [138]. A higher activation energy for the conversion of the imide to a benzoxazole group results in a higher temperature demand for the TR than TC. In addition to the lower required temperature of the TC process, a more mechanically robust membrane is obtained using the TC process due to the lower decomposition. The gas transport properties of TPHA-TC are not higher than TRHI-TRs due to the less structural change during the TC process. A major increase in the FFV evidenced with a higher d-spacing value, and generated ultra-microporosity upon the formation of TPHI-TR-450, leading to significant improvement in the CO₂ permeability (56 times higher) and a 28% increase in the CO₂/CH₄ selectivity (67) compared to its original PI. TPHI-TR-400 has a CO₂ permeability of 320 Barrer and a CO₂/CH₄ selectivity of 39 [180]. The exceptional sieving ability

of TPHI-TR-450 is due to the stiffness of the polymer and the interconnectivity of the free volume [180].

Excellent chemical and thermal stability of carbon molecular sieve (CMS) membranes along with their ability to surpass the 2008 Robeson upper bounds are promising for the development of advanced membranes [51, 181-183]. Generated microporosity between plates and ultra-microporosity between strands verified by bimodal pore size distribution allow for tailoring of gas transport properties [51]. To date, there have not been many reports on fabricating CMS membranes from an intrinsically microporous PI [177, 184]. Using heat treatment in three series of distinct stages, the PIM-6FDA-OH can be converted to the 6FDA-SBI-PBO (at 440 °C for 2 h), then to an intermediate amorphous carbon structure (at 530 °C for 30 min), and next to a graphitic carbon membrane (at above 600 °C for 30 min) [177, 184].

Although 6FDA-SBI-TR-PBO has a lower CO₂ solubility coefficient compared to its corresponding PI, its CO₂ permeability is three-fold higher due to its higher CO₂ diffusion coefficient, higher microporosity, and higher surface area (700 m² g⁻¹) [177, 184]. Despite its moderate CO₂/CH₄ selectivity (20), 6FDA-SBI-PBO rearranged at 530 °C displayed a CO₂ permeability of 4,140 Barrer [177, 184]. Increasing the thermal treatment temperature beyond 600 °C alters the PI membranes to CMS membranes with partial graphitization. The construction of a large portion of ultra-microporosity especially at 3.58 Å determined with CO₂ adsorption isotherms and verified with XRD allowed for high CO₂/CH₄ selectivities of 38 and 93 for PIM-CMS-600 and PIM-CMS-800, respectively [177, 184].

To achieve high gas permeance and selectivity, sub-100 nm CMS membranes were fabricated by depositing a thin layer of SBFDA-DMN on a γ -alumina-coated α -alumina ceramic support and using a protective polydimethylsiloxane (PDMS) layer, followed by the membranes

pyrolysis at different temperatures (Figure 22) [67]. Compared to the bulk, CO₂ permeability decreases three orders of magnitude, while selectivity increases significantly indicating enhanced physical aging. The membranes were stable within 1–1.5 months.

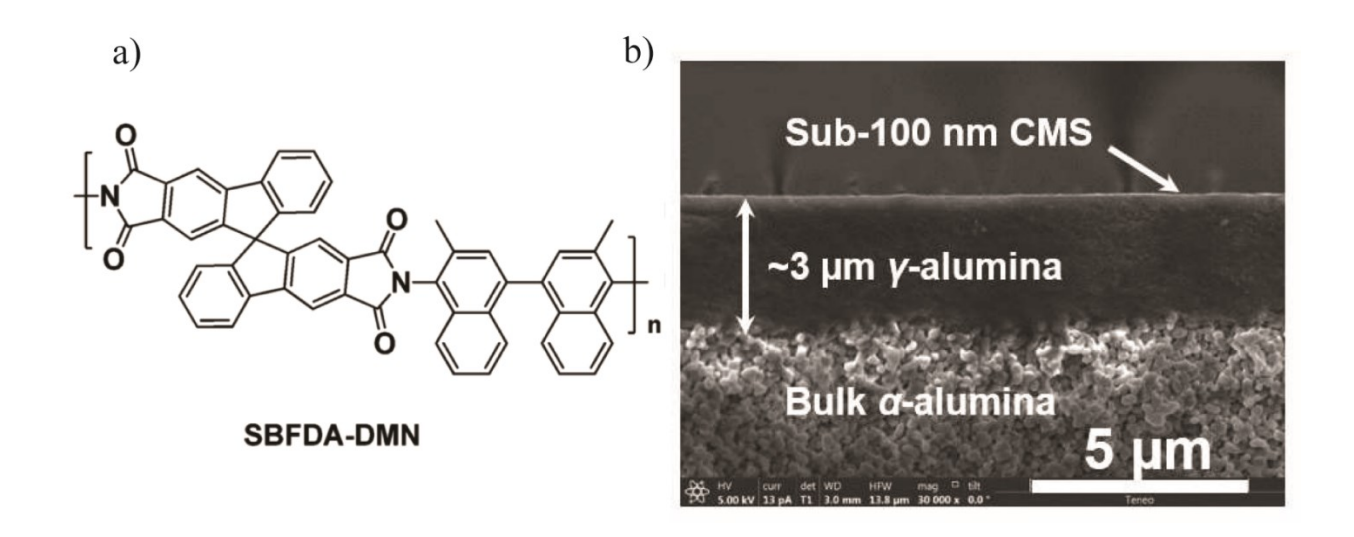


Figure 22. (a) Molecular structure of the SBFDA-DMN polymer, and (b) cross sectional scanning electron microscopy (SEM) image of the sub-100 nm CMS membrane prepared from SBFDA-DMN [67] Reprinted with permission from Ogieglo W, Puspasari T, Ma X, Pinnau I. Sub-100 nm carbon molecular sieve membranes from a polymer of intrinsic microporosity precursor: Physical aging and near-equilibrium gas separation properties, Journal of Membrane Science, 597:117752, (2020). Copyright 2020 Elsevier.

5.3. Photo-oxidative Modification

Photo-oxidative modification of a membrane involves the irradiation of its surface using short-wavelength ultraviolet (UV) light in an oxygen atmosphere. This post-treatment method changes membranes morphology and performance [79, 185, 186]. The exposure of the membrane surface to UV light densifies the near-top-surface region and forms an asymmetric structure in the UV-oxidized membranes. Irradiation time and atmosphere composition are two control knobs in UV surface modification of PIM-1 [187]. The surface modification led to a decrease in CO₂ permeability and increases in CO₂/N₂ and CO₂/CH₄ selectivities in the presence of air and oxygen

[187]. Performing the modification reaction in an oxygen atmosphere leads to larger changes in the membranes' performance than in air. In this technique, highly oxidizing ozone and atomic oxygen, generated from oxygen molecules, attack the free volume of the membrane, especially in UV-exposed regions. The oxidization then leads to chain scission, confirmed by the formation of carboxyl and hydroxyl groups [187].

The creation of shorter polymer chains increases the efficient chain packing via decreasing the intra-chain rigidity and the inter-chain distance. Therefore, the accessible microporous free volume declines due to the denser top layer. The exposure of PIM-1 to UV light for 5 and 10 min in the presence of O₂ resulted in higher CO₂/N₂ and CO₂/CH₄ selectivities without any decrease in the CO₂ permeability [187]. Increasing the exposure time from 20 to 40 min led to CO₂/N₂ and CO₂/CH₄ selectivity gains and CO₂ permeability losses [187].

UV post-modification of PIM-1 can change the contorted structure of the polymer [188]. Considerable CO₂ permeability loss and selectivity gain were observed after UV irradiation, which can be attributed to the reordering of the polymer chains toward efficient chain packing [188]. The absence of any significant changes in the gas solubility coefficients indicates that the membrane performance is controlled by diffusivity and diffusivity selectivity [188]. The rearrangement of the polymer backbone leads to conformational changes and decreases FFV. Two intermediates are formed during the formation of the UV-modified PIM-1 (Figure 23). The exposure of the membranes to a UV light for 20 and 30 min was found to improve their gas separation performances.

Figure 23. Photochemical reaction of PIM-1 membrane [188]. Reprinted with permission from Li FY, Xiao Y, Ong YK, Chung TS., UV-Rearranged PIM-1 Polymeric Membranes for Advanced Hydrogen Purification and Production. Advanced Energy Materials, 2:1456-66. (2012). Copyright 2012 John Wiley and Sons.

5.4. Chemical Post-modification

The post-functionalization of polymers with different groups that possess a high affinity towards CO₂ is a convenient approach to improve polymer sieving ability [189]. Tetrazole, triazine, amines, hydroxyls, and imidazole are known for their strong interactions with CO₂ [190]. Chemical functionalization is the most common, solubility-controlled method used for acid-gas removal [191, 192]. A carrier is provided to adsorb the target gas and form a complex to help the so-called solution-diffusion mechanism for achieving higher selectivity [193]. However, it is susceptible to carrier saturation especially at high pressures [194].

There are two kinds of functionalization carriers: (a) mobile carriers, which can freely move across the membrane, and (b) fixed carriers, which are connected to membrane structure via covalent bonds. Mobile carriers make membranes more selective than fixed carriers. However, the

volatility of the solution of mobile carriers is a disadvantage. Carriers that are suitable for CO₂ removal usually have basic groups such as amines and carboxylates. The amine can be primary, secondary, or tertiary. Reactions between CO₂ and several kinds of amines are [195]:

$$CO_2 + 2RNH_2 \longleftrightarrow RNHCOO^- + RNH_3^+$$

 $CO_2 + 2R_2NH \longleftrightarrow R_2NCOO^- + R_2NH_2^+$
 $R_3N + H_2O + CO_2 \longleftrightarrow R_3NH^+ + HCO_3^-$

Nitrile (-C=N) groups of PIM-1 are a promising type of functionality for incorporating different CO₂-philic groups. However, in most cases, the modifications lead to a decrease in surface area or available cavities [190]. Figure 24 shows different chemical post-modifications of PIM-1 for fabricating gas separation membranes.

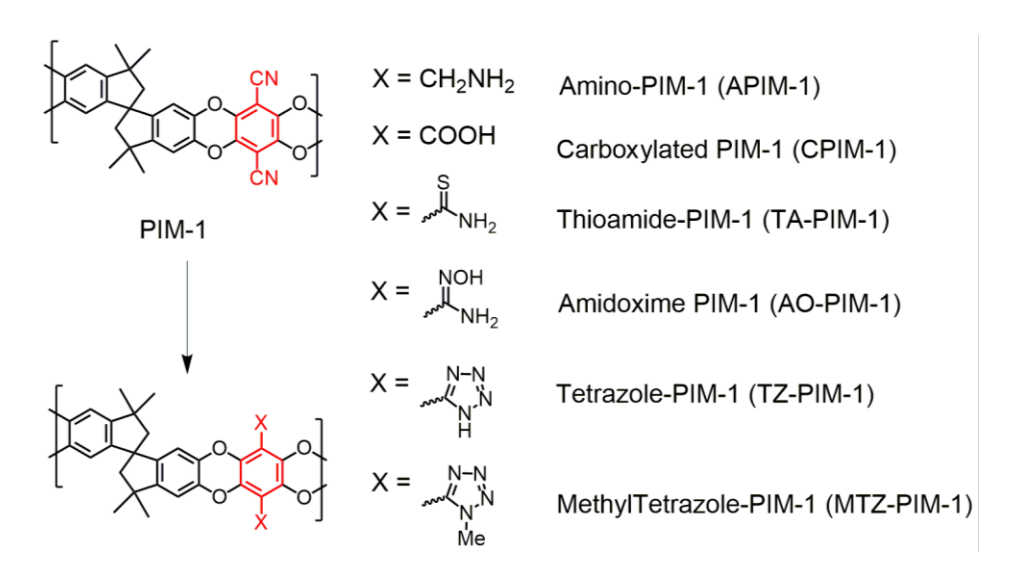


Figure 24. Different PIM-1 chemical post-modifications for fabricating gas separation membranes.

5.4.1. Carboxylated Functionalized PIMs

Carboxylate-functionalized PIMs (cPIMs) are attractive polymers for gas separation membrane. As cPIMs are soluble in different organic solvents like dimethyl sulfoxide and tetrahydrofuran, a free-standing cPIMs membrane can be fabricated using the conventional solution casting

technique. cPIMs with ~92 mol % of the –COOH were synthesized via a prolonged alkaline hydrolysis process [196]. Moreover, cPIM-1 can be obtained by the full hydrolysis of nitrile groups to carboxyl groups [197-199]. cPIM membranes have extra CO₂ affinity and less interchain gaps than PIM-1 membranes. As a result, these membranes efficiently separate small-size components, e.g. CO₂, of a gas mixture owing to the increased diffusivity selectivity and less cavity size. Besides, robust interactions between the –COOH and CO₂ enhance solubility selectivity. Consequently, the cPIM membrane has shown a CO₂/N₂ selectivity of 53.6, which is the highest reported selectivity among available chemically-modified PIMs [196]. cPIM-1 has high CO₂/N₂ and CO₂/CH₄ selectivities but a low CO₂ permeability. The surface area of cPIM-1 is about 50% less than that of PIM-1.

5.4.2. Amidoxime Functionalized PIMs

The substitution of nitrile groups with hydroxyl or amine-based moieties is an effective strategy to increase Lewis acid–Lewis base interactions with CO₂ [189]. The fast conversion of nitrile groups of PIM-1 to amidoxime moiety can be achieved using hydroxylamine in THF at the reflux temperature [190, 200]. The resulting amidoxime-functionalized PIM-1 (AO-PIM-1) has a 37% lower BET surface area (482 m²/g) and a 60% lower pore volume than PIM-1 [200]. An increase in CO₂ and N₂ adsorption at low pressures points to the creation of the interconnected cavities and shift towards ultra-microporosity compared to PIM-1 [200]. The CO₂/CH₄ and CO₂/N₂ selectivities of the AO-PIM-1 membrane were found to be 110% and 45% higher respectively, compared to those of PIM-1. The remarkable improvement in diffusivity selectivity indicates the narrow porosity of AO-PIM-1, which impedes the transport of gas molecules with a large kinetic diameter. The low solubility selectivity is related to the low CO₂ uptake by the polymer chains. The abundance of oxygen and nitrogen of –OH and –NH₂ groups as donors, and the dioxane rings as

the acceptor constructs a stable network via hydrogen bonds. Although created –OH and –NH₂ groups improve the polymer affinity towards CO₂, the restriction of accessible cavities results in lower gas solubility, especially for CO₂.

5.4.3. Heterocyclic Tetrazole Functionalized PIMs

Heterocyclic tetrazole rings can be introduced to PIM-1 via the so-called click chemistry reaction to increase the solubility selectivity of CO₂ over other gases [201]. The strong interactions of the tetrazole rings increase the affinity of the tetrazole modified PIM-1 (TZPIMs) toward CO₂. Adsorption results show an increase in the CO₂ uptake and a reduction in the N₂ solubility due to unprecedented improvement of the CO₂/N₂ solubility selectivity. However, the BET surface area of the modified PIM-1 decreases to 30 m²/g. The degree of the reaction and the average molecular weight can be adjusted by the ZnCl₂ amount and the reaction time. A CO₂/N₂ selectivity of 41, a CO₂/CH₄ selectivity of 22, and a CO₂ permeability of 3,000 Barrer were obtained for TZPIM-1. To obtain a PIM-based polymer with methyl tetrazol group (MTZ-PIM-1), the TZ-PIM-1 must be methylated [202]. MTZ-PIM-1 has a higher thermal resistance and better processability than TZ-PIM-1. Compared with PIM-1, the MTZ-PIM has a higher CO₂/N₂ sieving ability and a lower CO₂ permeability.

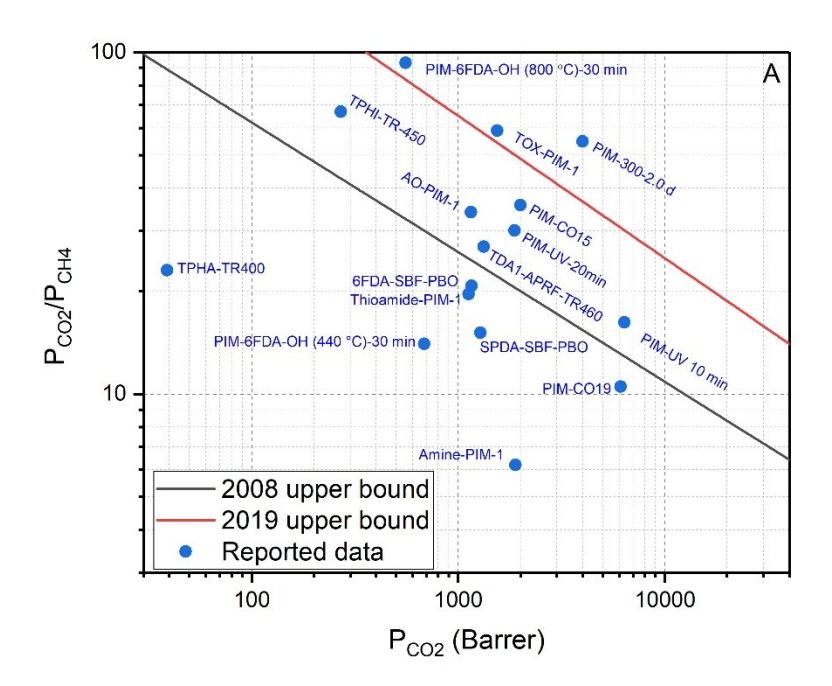
5.4.4. Amine Functionalized PIMs

The reduction of nitrile groups of PIM-1 to a primary amine using borane complexes is another post-modification method [203]. Although the introduction of –NH₂ groups increases the CO₂ uptake in the polymer and the solubility selectivity, the formation of hydrogen bonds between amine donor groups and oxygen acceptors in the dioxane rings decrease the free volume of the polymer. The CO₂ permeability and diffusivity decrease due to the strong interactions of the polymer chains and fewer pathways for gas transport. A simultaneous decrease in the permeability

and selectivity of amino-PIM-1 confirm that this modification is not adequately effective to overcome the upper bounds.

5.4.5. Thioamide Functionalized PIMs

Nitrile moiety can be replaced with thioamide using phosphorus pentasulfide and sodium sulfite in a dioxane/ethanol mixture [204]. The incorporation of thioamide leads to a 66 % reduction in the surface area of the modified polymers compared to the prototype PIM-1. In addition to the bulkier side-chain moiety, hydrogen bonding between –NH₂ donor groups, and S and O acceptors decreases the inter-chain distances and the free volume. Ethanol-treated thioamide-PIM-1 has been reported to have a CO₂ permeability of 1,150 Barrer and a CO₂/N₂ selectivity of 30.3 [204]. Table 5 and Figure 25 present CO₂ separation performances of the post-modified PIM membranes.



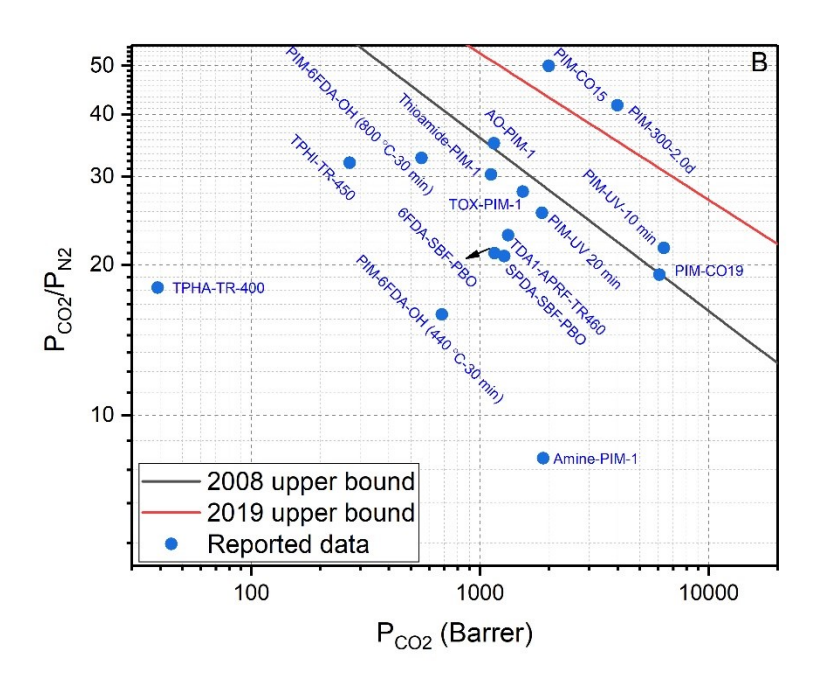


Figure 25. Data from Table 5 showing gas separation performances of the post-modified PIM membranes for (A) CO_2/CH_4 and (B) CO_2/N_2 .

Table 5. Performances of the post-modified PIM membranes for CO₂ separation.

Polymer	Permeability (Barrer)			Selectivity		Ref
	CO_2	CH ₄	N ₂	CO ₂ /CH ₄	CO ₂ /N ₂	
AO-PIM-1	1,153	34	33	34.0	35.0	[205]
Amine-PIM-1	1,890	303	230	6.2	8.2	[203]
Thioamide-PIM-1	1,120	56	37	19.6	30.3	[204]
TOX-PIM-1	1,540	26	55	59.0	28.0	[206]
PIM-UV 20 min	1,869	62	74	30.1	25.4	[188]
PIM-UV 10 min	6,374	393	296	16.2	21.6	[207]
PIM-CO19	6,100	580	320	10.5	19.1	[208]
PIM-CO15	2,000	56	40	35.7	50.0	[208]
TPHI-TR-450	270	4	8	67.0	32.0	[209]
TPHA-TR-400	39	2	2.2	23.0	18.0	[209]

PIM-300-2.0d	4,000	73	96	54.8	41.7	[161]
PIM-6FDA-OH (800°C)-30 min	556	6	17	93.0	32.7	[184]
PIM-6FDA-OH (440°C)-30 min	683	50	43	14.0	15.9	[184]
TDA1-APRF-TR460	1,328	49	58	27.0	22.9	[210]
6FDA-SBF-PBO	1,160	56	55	20.7	21.1	[147]
SPDA-SBF-PBO	1,280	85	62	15.1	20.8	[147]

6. PIM Blending

Polymer blending is a simple method to combine the strengths of two polymers to improve gas separation properties [211-214]. Based on the permeability of each polymer and their volume fractions, the CO₂ permeability of their miscible blends can be predicted using [215]:

$$\operatorname{Ln} P_b = \varphi_1 \operatorname{Ln} P_1 + \varphi_2 \operatorname{Ln} P_1 \tag{1}$$

where P_b , P_1 , and P_2 are the permeabilities of the blend and polymers 1 and 2. ϕ_1 and ϕ_2 are volume fractions of polymers 1 and 2, respectively. When specific interactions result in densification, Eq.1 poorly predicts the permeability of the blend [216].

To improve the selectivity of PIM-1-based membranes, PIM-1 can be blended with Matrimid-5218. Almost all PIM-1/Matrimid membranes have good miscibility. The introduction of 10% PIM-1 to Matrimid led to a 77% increase in the CO₂ permeability without sacrificing CO₂/CH₄ and CO₂/N₂ selectivities [217]. PIM-1 and Ultem PEI form a partially miscible blend at some specific ratios [218]. The addition of less than 20 wt% or more than 90 wt% PIM-1 to Ultem leads to the formation of homogeneous polymeric blends. PIM-1 as an organic dispersed phase

can increase gas permeabilities. The addition of just 10 % PIM-1 to Ultem matrix provides impressive improvement (167%) in the CO₂ permeability without a great loss in CO₂/CH₄ or CO₂/N₂ selectivities [218]. Dual-layer hollow fiber configuration can also be formed by blending these polymers [219]. The brittleness of PIM-1 and the jelly nature of MEEP80 polyphosphazene can be resolved by making composite membranes from them with excellent flexibility and toughness [220]. Oligo(ethylene oxide) side groups of MEEP80 enhance the interactions of the membranes with CO₂, leading to excellent performance of PIM-1/25 wt% MEEP80 under mixed gas conditions. Glass transition temperature (T_g) measurements verify good miscibility of the components achieved through chains entanglement. Taking the advantage of interactions between –CN groups of PIM-1 and N atoms in Tröger's base polymers, mechanically robust membranes with enhanced CO₂ selectivity and plasticization resistance can be fabricated [221].

To increase the selectivity and plasticization resistance of microporous polymers, carboxylated PIM (cPIM-1) can be mixed with a polyamide-imide (PAI) such as Torlon [222]. cPIM-1 is soluble in common polar solvents like N-Methyl-2-pyrrolidone (NMP). A 791% enhancement in CO₂ permeability with just a 17% decrease in CO₂/CH₄ selectivity were achieved with adding 30 wt% cPIM-1 to the Torlon. The creation of hydrogen-bonding between acceptors and donors of Torlon and cPIM-1, as well as the formation of charge transfer complexes improve the interactions, miscibility and compatibility of two polymers, leading to the increase of permeability. The embedment of Torlon restricts the chain mobility of Torlon/cPIM-1 membranes due to the formation of a partially miscible blend. This leads to an extraordinary advancement in the plasticization resistance up to 30 bar. Furthermore, the incorporation of Torlon enhances the gas separation performance of the membranes. cPIM-1 is also miscible with Matrimid-5218

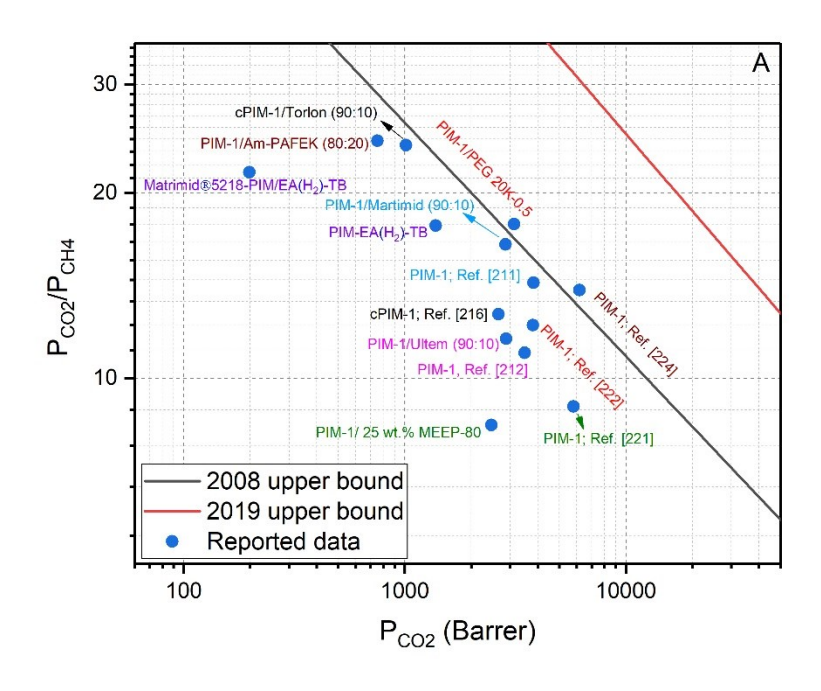
verified by polarized light microscopy (PLM), atomic force microscopy (AFM), and differential scanning calorimetry (DSC) [223].

Plasticization resistance of Matrimid can be significantly enhanced by the addition of cPIM-1. CO₂ permeability of Matrimid can be tailored over a wide range by its blending with PIM-EA(H₂)-TB [224]. PIM-EA(H₂)-TB/Matrimid membrane (1:1 w/w) shows higher CO₂ permeability and CO₂/N₂ selectivity for a gas mixture because of the competitive sorption. Physical aging leads to a slight deviation of the permeability trend from the logarithmic relationship expressed in Eq.1.

Crosslinking with chemicals and additives is another method for modifying microporous polymers. Good crosslinkers include diazides, pyrene, and 1-aminopyrene. (Figure 26). For instance, crosslinking with diazide molecules can be achieved after annealing at 175 °C after 7.5 h or at 250 °C for 1 h [225, 226]. Crosslinking with diazide increases CO₂/N₂ and CO₂/CH₄ selectivities and decreases the CO₂ permeability. Furthermore, adding crosslinkers results in the fabrication of plasticization-resistant membranes. Crosslinking PIM-1 with pyrene and 1-aminopyrene leads to a considerable improvement in the CO₂/N₂ solubility selectivity of the pristine polymer. Crosslinking PIM-1 with pyrene increases the CO₂ permeability and the CO₂/N₂ selectivity simultaneously, while PIM-1 crosslinking with 1-aminopyrene decreases the CO₂ permeability. PIM-aminopyrene membranes have higher CO₂/N₂ selectivities and aging resistance.

Figure 26. Molecular structures of two diazides, pyrene, and 1-aminopyrene used for PIM-1 crosslinking.

Table 6 and Figure 27 present CO₂ separation performances of the post-modified PIM membranes; the different CO₂ separation performances are due to the use of different preparation and solvent treatment methods, as well as different thicknesses and molecular weights of the membranes.



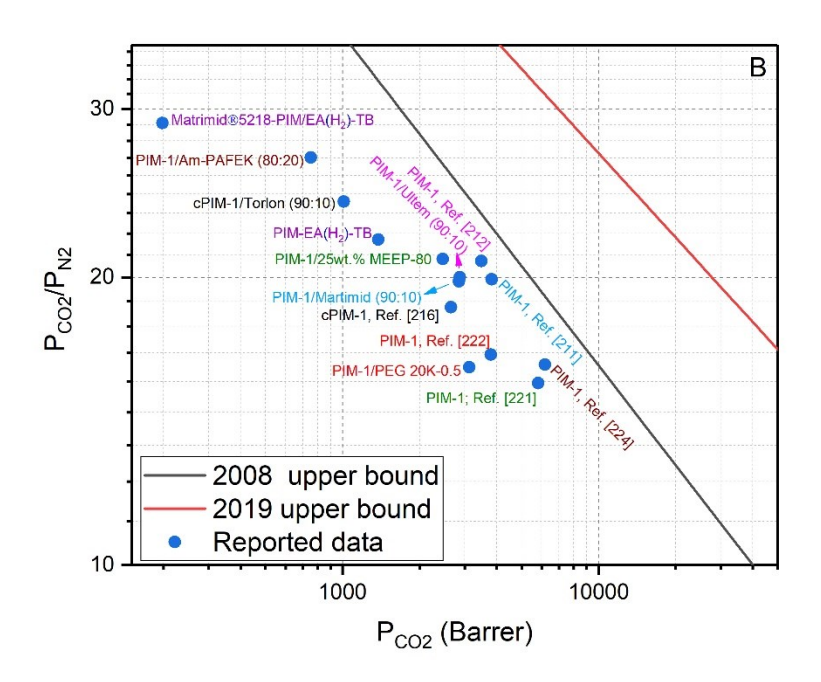


Figure 27. Data from Table 6 showing gas separation performances blended PIM membranes. (A) $\rm CO_2/CH_4$ and (B) $\rm CO_2/N_2$.

Table 6. Performance of the blended PIM membranes for CO₂ separation.

Membrane	Perme	ability (B	arrer)	Select	Ref	
	CO ₂	CH ₄	N ₂	CO ₂ /CH ₄	CO ₂ /N ₂	
PIM-1	5,811	644	375	9.0	15.5	[227]
PIM-1/25wt% MEEP-80	2,466	292	117	8.4	20.9	[227]
PIM-1	3,799	310	228	12.2	16.6	[220]
PIM-1/PEG 20k-0.5	3,125	176	194	17.8	16.1	[228]
PIM-1	3,825	268	192	14.3	19.9	[217]
PIM-1/Matrimid (90:10)	2,855	173	144	16.5	19.8	[217]
cPIM-1	2,654	209	143	12.7	18.6	[222]
cPIM-1/Torlon (90:10)	1,013	42	42	23.9	24.0	[222]
PIM-1	3,489	318	168	11.0	20.8	[210]
PIM-1/Ultem (90:10)	2,877	248	144	11.6	20.0	[218]
PIM-1/6FDA-m-PDA (7.5:92.5)	22	0.5	-	48.7	-	[229]
PIM-1	6,173	444	381	13.9	16.2	[220]
PIM-1/Am-PAFEK (80:20)	752	301	28	24.3	26.7	[230]
PIM-EA(H2)-TB	1,380	78	63	17.7	21.9	[221]
Matrimid®5218/PIM-EA(H2)-TB	198	9	7	21.6	29.0	[231]

7. Physical Aging of PIM Membranes

Aging has been a long-term challenge in glassy-polymer membranes and has particular importance in industrial applications [59]. First, it causes higher operation and maintenance costs. Second, it complicates the long-term operation of membrane processes [59]. Third, it alters membrane properties.

Physical aging is caused by a decline in the inter-chain distance and free volume of glassy polymers. In other words, at temperatures far below the polymer T_g, physical aging occurs due to a difference between polymer specific volume and the equilibrium volume [76]. As polymer chains have some mobility even at a temperature lower than their T_g, the difference leads to the densification of polymer chains via their segmental motions, porosity loss, and consequently decrease in permeability [77, 232, 233]. Stated differently, the densification results in a decrease

in both diffusivity and solubility, with the former being affected more. However, in some cases, physical aging leads to favorable well-adjusted permeability and selectivity [116]. Membranes exposed to gases with different effective kinetic diameters experience aging differently. To describe the effects of aging on membrane separation performance, it is better to consider the effective kinetic parameter instead of the kinetic diameter, as the latter is a temperature-dependent parameter [234]. Gas molecules with smaller effective kinetic diameter like H₂ and He experience different diffusion mechanisms in glassy polymers, compared with bigger counterparts like CO₂ and CH₄. The former group finds the FFV of PIM as an interconnected space and consequently, their permeation mechanism is more pore-diffusion dominant. The larger gas molecules, however, permeate through the membranes based on the solution-diffusion principles. This difference in permeation mechanism also affects the response rate of the molecules to aging. In other words, this difference causes smaller molecules to show less permeation reduction upon aging [180]. Thus, the permeability of a small gas through a membrane is affected less by the physical aging compared with the bigger counterparts. Aging is dependent on many parameters. For two membranes made of similar materials which are just different in term of thickness, aging happens faster for the thinner one. For example, carbon molecular sieve membranes (CMS) with 100 nm thickness made of a PIM precursor have three orders of magnitude faster aging, compared with bulk polymer [67].

When the thickness of a membrane is less than 100 nm, the gas permeability of the membrane decreases quickly due to physical aging. In other words, the high free-volume of microporous membranes makes them susceptible to physical aging [63, 116]. The physical aging of PIM membranes occurs over two (short and long) time horizons. During the short time horizon (typically 15 days), a quick permeability reduction happens due to the fast elimination of the

additional non-equilibrium free-volume generated by soaking of the membranes in a non-solvent during the membrane preparation [116, 235]. The gradual gas permeability decrease during the long-time horizon is related to the rearrangement of the membrane micropores [116]. Although physical aging causes a decrease in both diffusivity and solubility coefficients (the former being affected more), it leads to favorable well-adjusted permeability and selectivity [116].

Compared to thick films, PIM-1 thin films (<150 nm) undergo considerable initial aging [236]. In thin films, aging is faster in membranes cast from a more volatile solvent. Because of the high aging in PIM-1 thin films, their onset of plasticization is low. Additionally, CO₂ exposure showed that the aging effect can overcome plasticization after 1.2 min of exposure for thin films compared to 10 h for thick films.

Generally speaking, thermal crosslinking [161], the incorporation of nanofillers [237, 238], alcohol treatment followed by thermal treatment [232, 239], and appropriate storage [63] have been found to be effective methods to mitigate physical aging. The addition of nanofillers to PIMs is an effective method for suppressing aging due to the segmental motion restrictions imposed by an added nanofiller. Nanofillers can be directly incorporated into the PIMs or after a surface modification to tailor their surface chemistry. Silica is a good example here, as its both pristine and surface modified versions are added to PIMs to suppress aging. For example, silica functionalized with dimethylbenzoic acid helps PIM-1 to keep its enhanced CO₂ permeability without losing its CO₂/N₂ selectivity after 60 days while methanol-treated PIM-1 or PIM-1 membranes containing other kinds of silica cannot show such outstanding gas separation performance under the same operating condition [240]. Not only the chemical structure of the nanofiller affects the aging resistivity of a PIM membrane, but also its geometry is influential. For

example, sheet-like nanofillers suppress aging much more significantly than spherical or cylindrical counterparts.

Treating PIM membranes via supercritical carbon dioxide (scCO₂) is another method for aging suppression. ScCO₂ causes the contraction of large micro-cavities right after the treatment process. Thus, those large micro-cavities are already collapsed and there is no chance for them to contract more during membrane service life [241]. The fabrication of high-performance membranes with less vulnerability against aging allows for substituting currently-used membranes with more efficient ones and reducing the capital and operating costs significantly.

Aging also affects the mechanical properties of membranes by increasing Young modulus of a polymer [242]. There is a direct relationship between chain stiffness and Young modulus [243]. It has been shown that porous polymers like PIM-1 usually keep their ultimate tensile stress and strain even for a long time, e.g. after 400 days of aging [244]. Elastic moduli of PIM membranes is another important mechanical property that should be taken into account when these polymers are used as a gas storage media. AFM nanoindentation is used to measure elastic moduli of PIM-1 and it was found that elastic properties of this polymer vary over its thickness. This variation is due to different relaxation procedures of the chains at the surface compared with the ones in depth after solution casting [245]. In general, mechanical properties and aging resistance of PIM membranes strongly depend on their building block and chemical groups on their structure. It may be possible to synthesize a stiff PIM with high Young's modulus (1000 MPa), high tensile strength (47 MPa), and an acceptable elongation at break (45%) while keeping its aging resistivity high by tuning the functional groups in their structure [88, 243].

7.1. Effect of Contortion Site on Physical Aging

Aging is dependent on the moiety kind and its chemical groups. Rigid moieties like pentiptycene or triptycene are favorable in terms of aging resistance [246]. Moreover, chemical groups in a moiety can affect its aging resistivity. For example, –CF₃ groups in BTrip suppress aging in PIM membranes made from such moieties [88]. Similarly, the presence of the SBI moiety and two dioxane rings in the PIM-1 backbone permit for insufficient chain packing thereby getting high free volume. A more rigid structure imparted by the Trip moiety and the phenazine ring demonstrates that TPIMs suffer from physical aging more than PIM-1. The improved sieving ability of TPIMs may be ascribed to the propagation of TPIM macromolecules through space in 2D ribbon-like conformations [116].

Interestingly, morphological changes in membrane channels upon thermal-oxidative treatment decrease the first period of aging and improves the membrane stability against long term aging. In case of TOX-PIM-1 (thermal-oxidative crosslinked PIM-1), a decrease in permeability occurs over the initial 5 days and then gradually stabilizes over an extended time of about 1 year. TOX-PIM-1 has been reported to have a CO₂ permeability in the wide range of 297–6,470 Barrer with a CO₂/CH₄ selectivity in the range of 10.5–72.4 and a CO₂/N₂ selectivity in the range of 14.4–38.0 [162]. The aging knee for TOX-PIM-1 membranes is shorter than KAUST-PI-1 [162]. It was found that aging can be affected by the crosslinking atmosphere, especially O₂ concentration. For example, crosslinking of TOX-PIM-1 membranes under O₂ atmosphere accelerates the CO₂ permeability decline.

Physical aging can be also slowed by using moieties with stable architectures, possessing configuration-induced free-volume [247]. PIM-PEIs containing symmetric, H-shaped, contorted pentiptycene currently have the best aging resistance among all PIM membranes [88, 248]. UV-

treatment is also another method for the suppressing of aging in porous polymers [249]. Furthermore, the presence of the substituent groups lowers physical aging via decreasing the aging driving force and improves interconnections of pores. Table 7 compares the gas transport properties of different fresh and aged PIM membranes; it indicates that physical aging decreases the permeability but increases the selectivity.

Table 7. Gas transport properties of fresh and aged PIM and PIM-PI membranes.

Membrane	Age	Gas per	meability	(Barrer)	Sele	Ref.	
	(Day)	CO ₂	N_2	CH ₄	CO ₂ /N ₂	CO ₂ /CH ₄	
PIM-PI-12	0	7,340	369.0	457.0	19.8	16.0	[150]
PIM-PI-12	273	3,230	131.0	156.0	24.6	20.7	
O-PIM-PBO-1	0	1,176	64.0	69.0	18.0	17.0	[66]
O-PIM-PBO-1	270	564	26.0	26.0	22.0	22.0	
PIM-PBO-3	0	870	35.0	40.0	25.0	22.0	
PIM-PBO-3	197	235	7.2	7.4	33.0	32.0	
TDA1-APAF	0	40	1.5	0.7	26.6	55.0	[179]
TDA1-APAF	250	30	0.9	0.4	33.3	75.0	
PIM-Btrip-TB	0	13,200	926.0	1,440.0	14.3	9.2	[118]
PIM-Btrip-TB	166	4,150	216.0	283.0	19.2	14.7	
Amine-PIM-1	0	1,230	181.0	259.0	5.3	3.5	[203]
Amine-PIM-1	540	309	55.0	69.0	6.8	4.7	
PIM-HPB (methanol treated)	0	3,800	190.0	361.0	20.0	10.5	[105]
PIM- HPB (methanol treated)	145	2,390	107.0	192.0	22.3	12.4	
PIM-CH3- HPB	0	2,620	122.0	230.0	21.4	11.3	
PIM-CH3- HPB	147	1,630	60.0	132.0	27.3	12.3	
PIM-Br- HPB	0	2,130	92.0	177.0	23.0	12.0	
PIM-Br-HBP	146	1,430	54.0	102.0	26.5	14.0	

PIM-CN- HPB	0	2,390	123.0	212.0	19.5	11.2	
PIM-CN- HPB P	147	1,300	52.0	93.0	24.7	13.9	
TOX-PIM-1	0	1,104	30.0	16.0	37.0	69.0	[162]
TOX-PIM-1	455	310	8.1	4.0	38.0	76.0	
PIM-Trip-TB	0	9,709	629.0	905.0	15.9	10.7	[117]
PIM-Trip-TB	100	3,951	189.0	218.0	21.0	18.1	
PIM-EA-TB	0	7,696	580.0	774.0	13.3	9.9	
PIM-EA-TB	470	2,644	188.0	219.0	14.1	12.0	
6FDA-DAT1	0	120	4.7	3.2	25.5	38.0	[116]
6FDA-DAT1	150	102	4.0	2.7	25.5	38.0	
6FDA-DAT2	0	210	9.0	7.1	23.3	30.0	
6FDA-DAT2	150	160	7.7	5.3	20.7	30.0	
SBFDA-DMN	0	6,674	369.0	581.0	18.0	11.5	[153]
SBFDA-DMN	200	703	33.0	40.0	21.3	17.6	
6FDA-1,4-trip_CH3	0	9.3	0.4	0.2	26.0	45.0	[144]
6FDA-1,4-trip_CH3	270	12	0.4	0.3	27.0	47.0	
6FDA-1,4-trip_para	0	14	0.5	0.3	27.0	46.0	
6FDA-1,4-trip_para	270	8.5	0.3	0.2	28.0	50.0	
6FDA-1,4-trip_CF3	0	21	0.9	0.5	24.0	42.0	
6FDA-1,4-trip_CF3	270	28	1.2	0.7	24.0	42.0	
6FDA-PPDA(H)	0	73	3.2	2.5	22.8	29.0	[248]
6FDA-PPDA(H)	240	70	3.1	2.4	22.5	29.0	
6FDA-PPDA(CH3)	0	55	2.4	2.0	22.9	27.5	
6FDA-PPDA(CH3)	240	53	2.4	1.9	22.0	28.0	
6FDA-PPDA(CF3)	0	132	7.0	5.5	18.8	24.0	
6FDA-PPDA(CF3)	130	126	6.9	5.4	18.2	23.0	
PIM-HPB	0	1640	124.0	68.0	13.2	24.3	[105]
PIM-HPB	145	2,390	192.0	107.0	12.4	22.3	
PIM-CH3-HPB	0	990	82.0	46.0	12.1	21.5	
PIM-CH3-HPB	147	1,630	132.0	60.0	12.3	27.3	

PIM-Br-HPB	0	189	10.1	6.3	18.7	30.0	
PIM-Br-HPB	146	1430	102.0	54.0	14.0	26.5	
PIM-CN-HPB	0	228	12.8	7.8	17.8	29.2	
PIM-CN-HPB	147	1300	93.0	52.0	14.0	24.7	
PIM-TMN-Trip	0	33,300	3,420.0	2230.0	9.73	14.9	[109]
PIM-TMN-Trip	365	14,100	943.0	727.0	14.9	19.3	
PIM-SBF-1	0	8,850	532.0	340.0	16.6	26.0	[103]
PIM-SBF-1	2088	2,410	102.0	87.5	23.6	27.5	
PIM-SBF-2	0	22,300	2,020.0	1150.0	11.0	19.4	
PIM-SBF-2	1295	3,870	184.0	166.0	21.0	23.3	
PIM-SBF-3	0	10,900	878.0	463.0	12.4	23.5	
PIM-SBF-3	1294	4,850	248.0	219.0	19.6	22.2	
PIM-SBF-4	0	10,600	834.0	474.0	12.7	22.3	
PIM-SBF-4	1428	6,410	331.0	286.0	19.3	22.2	
PIM-SBF-5	0	16,400	2,480.0	1080.0	6.6	15.2	
PIM-SBF-5	1439	10,000	925.0	550.0	10.8	18.0	
PIM-BTrip	0	21,500	1,690.0	1190.0	18.1	12.7	[124]
PIM-BTrip	718	3,770	113.0	112.0	33.8	33.5	
PIM-TMN-Trip	0	52,800	7,250.0	3540.0	14.9	7.3	
PIM-TMN-Trip	426	20,400	1,440.0	1100.0	18.5	14.2	
PIM-HMI-Trip	0	44,200	4,870.0	2560.0	17.3	9.1	
PIM-HMI-Trip	426	16,400	967.0	804.0	20.4	16.9	
PIM-TFM-BTrip	0	33,700	2,280.0	1830.0	18.4	14.8	
PIM-TFM-Btrip	496	15,600	792.0	722.0	21.6	19.7	
PIM-DTFM-BTrip	0	42,600	4,340.0	3000.0	14.2	9.8	
PIM-DTFM-Btrip	636	14,800	728.0	741.0	20.0	20.3	
PIM-DM-BTrip	0	22,000	1,570.0	1020.0	21.8	14.0	
PIM-DM-Btrip	128	12,200	599.0	521.0	14.0	20.4	
PIM-MP-TB	0	3,500	264.0	200.0	13.3	17.5	[120]
PIM-MP-TB	370	378	14.7	13.3	25.7	28.4	

4MTBDA-6FDA	0	1,672	116.0	133.0	14.4	12.6	[145]
4MTBDA-6FDA	524	1,008	60.0	62.0	16.8	16.2	
4MTBDA-PMDA	0	4,460	390.0	290.0	11.4	15.4	
4MTBDA-PMDA	333	1,689	114.0	99.0	14.8	17.0	
4MTBDA-SBIDA	0	5,140	591.0	373.0	8.7	13.8	
4MTBDA-SBIDA	509	2,476	-	152.0	-	16.3	
4MTBDA-SBFDA	0	4,476	371.0	264.0	12.1	16.9	
4MTBDA-SBFDA	405	1,621	125.0	106.0	13.0	15.3	
PIM-PI-TB-1	0	662	44.0	-	15.0	-	[122]
PIM-PI-TB-1	180	361	16.0	-	23.0	-	
PIM-PI-TB-2	0	595	31.0	-	19.0	-	
PIM-PI-TB-2	180	376	18.0	-	21.0	-	
6FDA-1,4-ortho	0	8	51.0	0.2	0.3	28.0	[135]
6FDA-1,4-ortho	730	8	51.0	0.2	0.3	28.0	
6FDA-1,4-para	0	14	46.0	0.3	0.5	27.0	
6FDA-1,4-para	273	9	50.0	0.5	0.3	28.0	
6FDA-2,6-para	0	10	47.0	0.2	0.4	25.0	
6FDA-2,6-para	150	8	48.0	0.2	0.3	27.0	
PIM-PI-EA	0	7,340	457.0	369.0	16.0	19.9	[150]
PIM-PI-EA	273	3,230	156.0	131.0	20.7	24.6	
6FDA-DAT1-OH	0	70	1.4	2.7	50.0	25.9	[250]
6FDA-DAT1-OH	60	66	1.2	2.3	55.0	28.7	
6FDA-HTB	0	67	0.9	2.26	72.8	29.6	[251]
6FDA-HTB	30	65	0.7	1.80	76.4	36.1	

8. PIM-based Mixed-Matrix Membranes

Mixed-matrix membranes (MMMs), a promising family of hybrid membranes, contain nanoparticles and nanostructures in their polymeric matrices [154, 252-255]. The inorganic or

organic nanoparticles are dispersed within the continuous polymeric matrices [256-259]. Different kinds of nanomaterials such as metal oxides [252], graphene-based nanosheets [260, 261], metal organic frameworks (MOFs) [262], covalent organic frameworks (COFs) [263], and carbon nanotubes (CNTs) [264] have been used for the synthesis of PIM-based MMMs (Figure 28). MMMs offer a solution to the trade-off between the permeability and selectivity of the classical membranes [265]. Good processability of PIMs and excellent gas-separation ability of the inorganic materials result in high-performance PIM-based MMMs that can overcome the 2008 Robeson upper bounds [266]. These PIM-based MMMs have the advantages of both PIMs and inorganic materials in terms of performance and stability [267]. Compared to pristine PIM membranes, PIM-based MMMs may show enhanced performance [268]. However, the aggregation of the nanoparticles and their poor compatibility with PIMs are the main problems concerning PIM-based MMMs [269]. Detrimental voids at the nanoparticle/PIMs interface, rigidified PIMs chains around the nanoparticles, and partial pore blockage by nanofillers are nonidealities in the MMMs for gas separation [270]. Filler size, morphology, and preparation procedures are important factors affecting these non-idealities [270].

The effective permeability of a MMM, P_{MMM}, is predicted mostly by the Maxwell model:

$$P_{MMM} = P_c \left[\frac{P_d + 2P_c - 2\varphi_d(P_c + P_{cd})}{P_d + 2P_c + \varphi_d(P_c + P_{cd})} \right] \tag{2}$$

where φ_d is the volume fraction of the dispersed phase, and P_d and P_c are gas permeabilities of the dispersed and continuous phases, respectively.

Simplified Maxwell model for a non-permeable and highly-permeable continuous and dispersed phases, respectively, are:

$$P_{MMM} = P_c \left[\frac{1 - \varphi_d}{1 + 0.5 \varphi_d} \right] \tag{3}$$

$$P_{MMM} = P_c \left[\frac{1 + 2\varphi_d}{1 - \varphi_d} \right] \tag{4}$$

Porous organic cages (POCs), as a new family of porous nanomaterials, have been used rarely to fabricate PIM-based MMMs. The addition of POCs such as Cage 3-R (CC₃), nanocrystalline CC₃ (nanoCC₃), and redCC₃ within PIM-1 can significantly increase CO₂ permeation while retaining good CO₂/N₂ permselectivity and improve membrane's resistance against physical aging [271].

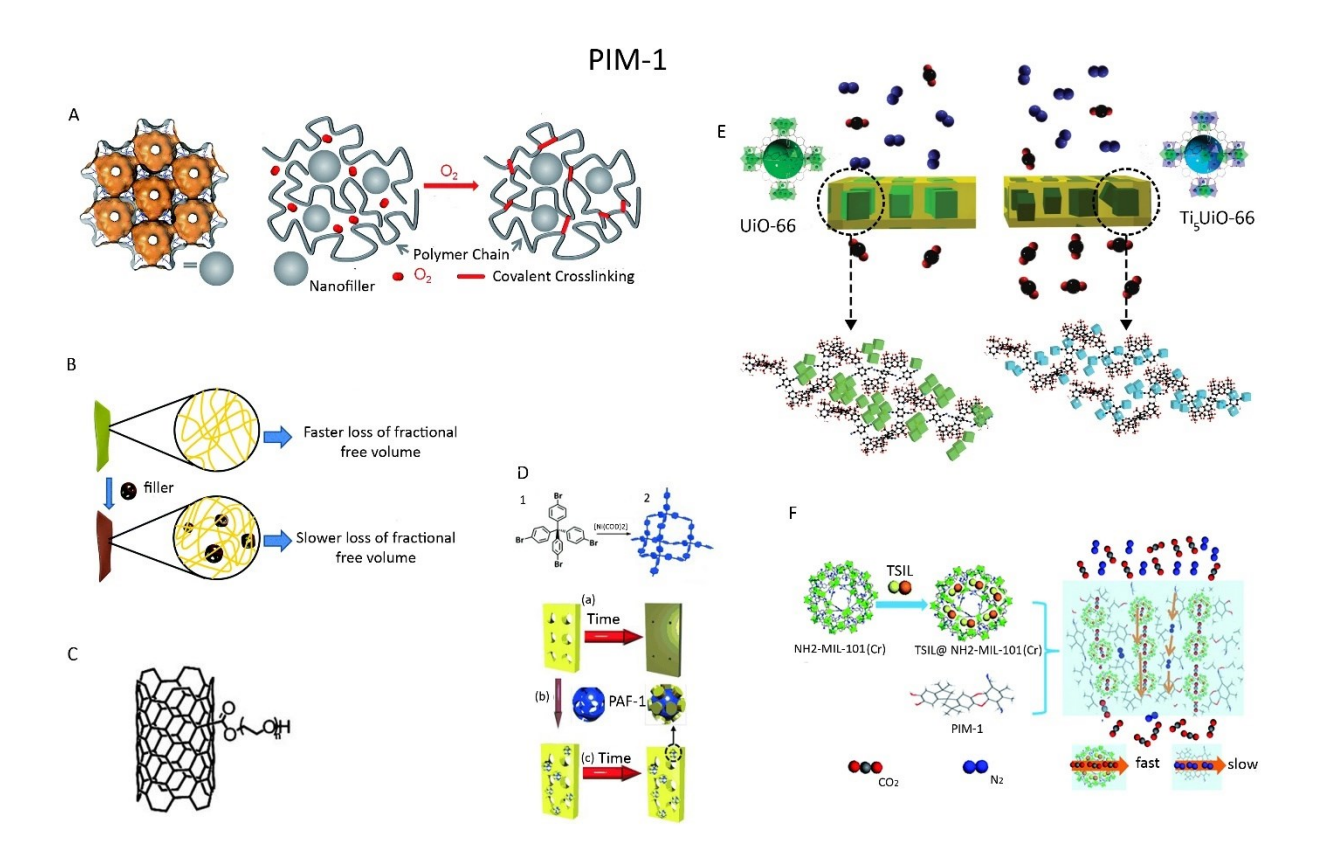


Figure 28. Different nanoparticles used for preparing PIM-1-based MMMs [264, 272-276]. (A) Reprinted with permission from Song Q, Cao S, Pritchard RH, Qiblawey H, Terentjev EM, Cheetham AK, et al., Nanofiller-tuned microporous polymer molecular sieves for energy and environmental processes, Journal of Materials Chemistry A., 4:270-9. (2016) which is an open access journal. (B) Reprinted with permission from Mitra T, Bhavsar RS, Adams DJ, Budd PM, Cooper AI. PIM-1 mixed matrix membranes for gas separations using cost-effective hypercrosslinked nanoparticle fillers, Chemical Communications, 52:5581-4. (2016) which is an open access journal. (C) Reprinted with permission from Khan MM, Filiz V, Bengtson G, Shishatskiy S, Rahman MM, Lillepaerg J, et al. Enhanced gas permeability by fabricating mixed

matrix membranes of functionalized multiwalled carbon nanotubes and polymers of intrinsic microporosity (PIM). Journal of Membrane Science, 436:109-20. (2013). Copyright 2013 Elsevier. (D) Reprinted with permission from Lau CH, Nguyen PT, Hill MR, Thornton AW, Konstas K, Doherty CM, et al., Ending aging in super glassy polymer membranes, Angewandte Chemie International Edition. 53:5322-6, (2014). Copyright 2014 John Wiley and Sons. (E) Reprinted with permission from Smith SJ, Ladewig BP, Hill AJ, Lau CH, Hill MR, Post-synthetic Ti exchanged UiO-66 metal-organic frameworks that deliver exceptional gas permeability in mixed matrix membranes, Scientific reports, 2015;5, Copyright 2015 Springer Nature. (F) Reprinted with permission from Ma J, Ying Y, Guo X, Huang H, Liu D, Zhong C, Fabrication of mixed-matrix membrane containing metal—organic framework composite with task-specific ionic liquid for efficient CO₂ separation. Journal of Materials Chemistry A., 4:7281-8. Copyright 2016 Royal Chemical Society.

8.1. Membranes Containing Silica and Its Derivatives

Silica and its derivatives such as fumed silica and polyhedral oligomeric silsesquioxanes (POSS) have been widely used in PIM membranes to fabricate MMMs. Fumed silica can increase the permeation and thermal stability of the PIM membranes. One of the main challenges is achieving of a homogenous dispersion of silica in the PIMs matrix especially at high silica concentrations, exceeding 24 vol.%. Usually, the poor dispersion of the inorganic nanoparticles in PIMs leads to an aggregate formation. Such aggregates may create voids in the system which finally affect permeation properties of the PIM-based MMMs. These voids usually are generated at PIM/filler interface or between filler aggregates. When the level of SiO₂ loading into PIM-1 exceeds 30 vol.%, brittle PIM membranes are formed, which are not useful from a practical point of view. Thus, the silica concentration at which flexible to brittle transition happens, usually 24 vol.%, is considered as the maximum threshold of the silica addition. Near 100% improvement in the CO₂ permeability is achieved when the volume fraction of silica is around 20 vol.%. On the other hand, the CO₂/N₂ selectivity decreases from 15.0 to 7.8 under the same circumstances. In summary, the incoporation of unmodified inorganic fillers like fumed silica improve the CO₂ permeability but

decreases the CO_2/N_2 selectivity due to the unselective voids in the PIM-based MMMs [252]. The Maxwell model is unable to the gas permeabilities of these membranes.

POSS nanoparticles were embedded into the PIM-1 matrix to improve its CO₂ permeability and CO₂/CH₄ selectivity [277]. These are very tiny nanoparticles in the range of 1.5–3.0 nm possessing a porous structure. Functionalization of the POSS with various functionalities including alkyl, olefin, epoxy, alcohol, acid, amine, and sulfonate allows for improving the filler dispersion in different polymeric matrices. Also, the filler has a cage-like structure in the size range of 1-3 nm, making it suitable for use as the dispersed phase of CO₂-separating MMMs. These 3D fillers are modified to create an organic outer layer on their surface. The presence of the layer improves the dispersion of the nanoparticles in the common solvents, enhances its dispersion in the PIM-1 matrix and eliminates filler/matrix interfacial non-selective gaps. The incorporation of 20 wt% unmodified POSS into PIM-1 matrix increased the CO₂ permeability up to 220% compared with the pure PIM-1 [277]. However, no improvement in the selectivity was observed. The enhancement in permeability without any improvement in selectivity is due to the generation of non-selective passages in the filler/PIM-1 interface. On the other hand, PIM-1 containing aminefunctionalized POSS (OAPS) particles shows a completely different behavior. The addition of OAPS slightly decreased CO₂ permeability but increased CO₂/N₂ selectivity up to 250% compared with the pure PIM-1 [277]. At 20 wt% loading of OAPS, a gradual agglomeration of the fillers happened, and a large selectivity increase was observed due to the strong hydrogen bond formation between the nitrile groups of PIM-1 and the amine groups of the filler. The strong hydrogen bonds change the PIM-1's chain rigidity, leading to the significant selectivity improvement. The addition of 5 wt% OAPS effectively suppresses aging of PIM-1through the formation of a fine dispersion in the polymer matrix and the establishment of interactions with PIM-1 [277]. The free volume

among rigid chains disappears more slowly than the flexible chains, and this is the rationale behind the resolution of the aging problem upon the addition of the modified, well-dispersed fillers. The modification of the POSS with an amine or nitro group is a successful strategy to improve POSS interactions with the PIM-1 matrix, which makes PIM-1 chains more rigidified and mitigates the aging problem.

The octa-phenethyl POSS (PhE-POSS) can be added to the PIM-1 matrix to prevent physical aging and improve the CO₂ transport of the nanocomposite membranes [278]. MMM containing 1 wt% of the filler has higher CO₂ permeability and diffusivity coefficient than the PIM-1 membrane. The presence of PhE-POSS decreases chain packing after film casting which causes higher membrane permeability compared to the pure PIM-1 membrane. At high upstream pressures near 20 bar, the CO₂ permeability of the PIM-1 with 1 wt% PhE-POSS decreases significantly to around 3,100 Barrer due to the collapse of open, loosened morphology of the PIM-1 containing 1 wt% PhE-POSS.

Poly(ethylene glycol) (PEG) functionalized POSS nanofillers can be incorporated into PIM-1 to take the advantage of dipole-quadrupole interactions between ethylene oxide units of PEG and CO₂ molecules [279]. Although the main improvement here originates from the interactions of CO₂ with ethylene oxide groups, the direct addition of PEG to PIM-1 is not useful enough as PEG/PIM-1 blend undergoes a phase separation. To address this issue, PEG chains can be covalently anchored on the nanofillers, and the modified nanofillers can then be added to PIM-1 matrix to obtain homogeneously dispersed solutions. Selecting POSS as an anchoring site is reasonable as it has nanometer size (1-3 nm) and can be dispersed finely in most of polymeric matrices. Also, POSS has an organic-inorganic structure and thus makes a favorable polymer-filler

interface [18, 280, 281]. Finally, POSS can be easily modified to bear different kinds of functionalities.

PEG anchored POSS were incorporated into PIM-1 membrane to enhance its CO2 selectivity [279]. CO₂ permeability decreased from 3,795 Barrer (pure PIM-1) to 1,309 Barrer (10 wt% filler containing), while CO₂/N₂ and CO₂/CH₄ selectivities increased from 19 to 31 and 12 to 30, respectively [279]. The main reasons behind CO₂ permeability drop with the filler incorporation are chain rigidification and induced barrier effects. By the barrier effect, it means that the POSS nanoparticles may partially block intrinsic pores of PIM-1, create more tortuous gas diffusion pathways and thereby make the gas diffusion process more difficult. Despite the reduction in CO₂ permeability, the CO₂/CH₄ selectivity increases significantly.

Disilanol isobutyl POSS (SO1440) is highly dispersible in dichloromethane, which is a common solvent for PIM-1 as well. The addition of just 0.5 wt% of the filler to the PIM-1 matrix increases the CO₂ permeability by 64% compared with pure PIM-1 [282]. This permeability improvement is due to the increased free volume caused by the presence of bulky SO1440 particles. In other words, the CO₂ permeability is improved because of an increase in the CO₂ diffusivity coefficient. However, a further increase in the filler level leads to a decrease in CO₂ permeability due to the PIM-1 chain rigidification and space-filling by the fillers. The presence of a high amount of the filler (> 0.5 wt%) blocks intrinsic pores of PIM-1 or narrows its pore size distribution, which makes it difficult for the CO₂ molecules to pass through the passages. On the other hand, both CO₂/N₂ and CO₂/CH₄ selectivities increase, as the filler loading content increases from 2 to 10 wt% [282]. In this filler loading range, not only d-spacing of PIM-1 chains decreases but also the chance of hydrogen bond formation between CO₂ and -SiOH groups of SO1440 increases. At a very high filler concentration, 20 wt%, filler agglomeration happens and both

permeability and selectivity decrease [282]. A –SiOH functional group can interact with both CO₂ and N₂, as it can establish hydrogen bonds with both of them. This implies that there is a competitive sorption between CO₂ and N₂. Under this condition, CO₂/N₂ selectivity is improved less than the CO₂/CH₄ selectivity.

8.2. Membranes Containing Carbon Nanotubes (CNTs)

Multiwall carbon nanotubes (MWCNTs) have also been dispersed in PIM-1 to make CO₂ permeable membranes [264]. As in the case of other fillers, a homogenous dispersion of MWCNTs is needed to prepare a high-performance membrane. This necessitates the functionalization of the MWCNTs by PEG chains. By using the "grafting to" method [264], the PEG chains can be covalently bonded to the surface of the MWCNTs, f-MWCNTs. Grafted PEG chains on the surface of the MWCNTs not only facilitate their fine dispersion in the PIM-1 matrix but also increase the affinity of the system for CO₂ adsorption through favorable interactions between PEG and CO₂ molecules.

Unfunctionalized MWCNTs cannot be dispersed in the PIM-1 matrix finely, as their π - π interactions are stronger than their interactions with the PIM-1 matrix. However, the PEG chains de-bundle their structure and facilitate their dispersion in the polymer matrix [283]. The dispersion of the functionalized MWCNTs is feasible up to 2 wt% of the filler. However, MMMs containing 3 wt% of MWCNTs showed filler aggregation, defects, and voids at the interface of the filler and the PIM-1 chains [283]. As a result, 2 wt% of the MWCNT is the optimum concentration for achieving the best gas transport properties. PIM-1, f-MWCNT/PIM-1, and pristine MWCNT/PIM-1 membrane have CO_2/N_2 and CO_2/CH_4 selectivities of (28.2, 15.4), (32.9, 10.4), and (16.3, 8.1), respectively [283].

Compared to pure PIM-1, f-MWCNT-loaded membranes have shown higher CO₂/N₂ and lower CO₂/CH₄ selectivities [283]. Improvement in the CO₂/N₂ selectivity can be expected, as PEG chains show a great affinity to CO₂ molecules but not to CH₄ ones. CO₂ permeabilities of 0.0 and 2.0 wt% f-MWCNT MMMs have been reported to be 5,360 and 8,230 Barrer, respectively [283]. Permeability increases due to the transport of CO₂ molecules through the free volume of PIM-1 and MWCNTs' channels. The main reason for the permeability improvement is a disruption in PIM-1 chain packing due to its interactions with PEG. This trend may be explained by analyzing the contribution of diffusivity to the overall permeation of CO₂. The diffusivity coefficient has been reported to increase from 7.91×10^{-7} cm²/s for pure PIM-1 to 19.4×10^{-7} cm²/s for PIM-1 containing 2 wt% functionalized MWCNTs. However, it decreased to 6.72 (10⁻⁷ cm²/s) when the filler concentration increased to 3 wt% [283]. This trend indicates that at lower filler concentrations (< 2 wt%), the interface between the functionalized MWCNTs and PIM-1 chains is continuous and there is no gas diffusion resistance. On the other hand, at higher concentrations of the filler (> 2 wt%), the generated nano-gaps between polymer chains and the MWCNTs become discontinuous, which serve as a barrier to gas diffusion. Nevertheless, the separation performance of all of the PIM-1 based MMMs containing 0.5–3.0 wt% of the functionalized MWCNTs surpass the 2008 CO₂/N₂ Robeson upper bound. It is worth noting that the solubility coefficient of CO₂ in the MMM increases slightly in the entire range of the filler addition (0.5–3.0 wt%). The reason is that there is a strong affinity between the ethylene oxide units of PEG and CO₂ molecules. Thus, the unexpected non-monotonic relationship between the permeability and the filler loading level originates from the polymer/filler interface and diffusivity resistance. The loading amount of the f-MWCNTs also affects selectivity greatly. The highest CO₂/N₂ selectivity was achieved at 3 wt% of the filler. It is believed that the interfacial interactions are highest at this concentration, leading

to the highest selectivity. In general, MMMs containing f-MWCNTs show better permeability, improved CO₂/N₂ selectivity, and higher long-term stability compared with MMMs containing pristine MWCNTs, thanks to homogenous dispersion in the PIM-1 matrix and the creation of defect-free filler/polymer interfaces [283]. The addition of f-MWCNTs to a bis(phenyl)fluorene-based PIM (Cardo-PIM-1) — synthesized via the dibenzodioxane polymerization reaction of 9,9-bis(3,4-dihydroxyphenyl) fluorene (BDPF), 2,3,5,6-tetrafluoroterephthalonitrile (TFTPN), and spirocyclic 5,5',6,6'-tetrahydroxy-3,3',3,3'-tetramethylspirobisindane (TTSBI) — improved the CO₂ separation performance of Cardo-PIM-1 [284]. The improved performance was attributed to the good dispersion of f-MWCNTs and enhanced affinity of the hybrid membranes for CO₂.

8.3. Membranes Containing Organic Nanoparticles

The addition of organic particles to PIM-1 leads to the creation of voids at the PIM/particle interface and causes selectivity reduction. Among organic particles is a highly crosslinked, porous, imidazole-functionalized particle named BILP-10. Two different kinds of amine are present in the chemical structure of this nanoparticle. The first one is a tertiary amine, which improves its affinity to CO₂, and the second one is a secondary amine, which facilitates hydrogen bond formation between the filler and PIM-1. This nanoparticle does not dissolve in common solvents like chloroform [285]. Thus, its dispersion in the PIM-1/chloroform solution to prepare an MMM is feasible. Thanks to its imidazole functionalities, the nanoparticles form hydrogen bonds with PIM-1, which improve their dispersion in the PIM-1 matrix. PIM-1/BILP-10 MMM with 30 wt% filler has a high CO₂ permeability (increased from 4700 to 7200 Barrer, meaning 53% improvement). Not only the voids at the PIM-1/BILP-10 interface, but also pathways inside the porous structure of the BILP-10 contribute to the increase of the free volume of the MMM. Up to 30 wt% of the filler loading, the CO₂ permeability increases monotonously, which is ascribed to the generation

of more free volumes in the system. However, a filler loading above this critical value leads to a permeability reduction. For example, a membrane containing 40 wt% of the BILP-10 shows CO₂ permeability of 5,100 Barrer. CO₂/N₂ selectivity of 19.3 for pure PIM-1 decreases to 15.1 and 15.3 for 17.0 and 30.0 wt% filler loadings, respectively. The selectivity reduction is due to the presence of extra pathways created by the porous filler letting N₂ diffusion and consequently causing selectivity reduction. The best MMM (30 wt% BILP-10) in real isobaric permeation test using flue gas consisting 80% N₂, 10% CO₂, 9% O₂, 10 ppm NO₂, and 1.3 ppm SO₂ showed a high CO₂ permeability of 4300 Barrer but a moderate CO₂/N₂ selectivity of 17 over 15 h test time. Thus, incorporating the crosslinked organic fillers which simultaneously bear two kinds of amine groups into PIM-1 cannot increase the moderate selectivity of PIM-1 sufficiently.

Figure 28B shows that hyper-crosslinked polymeric nanoporous particles (HCP) can be used as the dispersed phase in PIM-1 to suppress its aging. HCP polystyrene particles with an average diameter of 55 nm can be synthesized by emulsion polymerization and incorporated into PIM-1. The advantage of emulsion polymerization over other conventional methods for preparing nanoparticles is its ability in precise control of nanoparticle size [286]. Thus, the use of non-aggregated, narrow-size-distributed nanoparticles obtained by emulsion polymerization in a MMM does not leave large polymer/particle interfacial defects. This means that non-selective diffusion routes which sacrifice selectivity are not created. The CO₂ permeation of the MMMs containing such HCP polystyrene filler increases monotonously from 8,000 to about 21,000 Barrer upon the addition of nearly 22 wt% of the filler. However, the CO₂/N₂ selectivity decreases from 15.0 to 9.5 under this circumstance [272]. The main reason behind such a significant increase in the CO₂ permeability is the high surface area of the HCP, which is two times greater than the

surface area of the pure PIM-1, 1,700 vs. 750-850 m²/g. So, as the filler concentration increases in MMMs, their CO₂ permeability improves.

The aging of the HCP polystyrene/PIM-1 membranes can be also minimized by using such HCP fillers. The pores of the HCP fillers are more stable than the pores of other usual nanoporous fillers due to their crosslinked structure. Thus, the pores do not collapse over time easily and thereby endow the MMMs with high aging resistance. On the other hand, ethanol treatment, which is used as a technique for improving permeability affects aging resistance negatively. For example, CO₂ permeation loss of an MMM cast from dichloromethane, which contains 16.67 wt% HCP filler after 150 days is about 9.4%, while for the same membrane over the same period the CO₂ permeation loss increases to 28% just due to the ethanol treatment. As aging decreases N₂ permeability of the MMMs more than their CO₂ permeability, their CO₂/N₂ selectivities increase over time. Interestingly, PIM-1 thin-film nanocomposite (TFN) membranes containing 60 wt% of HCP can be produced [287]. The Maxwell model can be used to predict CO₂ permeability of PIM-1/HCP membranes.

8.4. PIM Membranes Containing 2D Nanoparticles

Two dimensional (2D) nanomaterials such as graphene, graphitic carbon nitride nanosheets (g-C₃N₄) and MXene are in the form of a single- or few-atomic-layer flakes. 2D nanoparticles significantly improve the ability of free-standing PIM-based MMMs for CO₂ removal applications. For example, the addition of 1 wt% of the g-C₃N₄ nanosheets to the PIM-1 increased the FFV of the membrane from 22 to 24.2% and decreased the density of the membrane from 1.117 to 1.086 g/cm³ [288]. The latter values, however, changed to 22.9% and 1.105 g/cm³ as the filler content increases to 2 wt%. The addition of up to 1 wt% of the filler decreased the packing of PIM-1 chains, but increased FFV, creating more passages for gas transport. On the other hand, at a high

loading level around 1.5 and 2.0 wt%, restacking of nanosheets lowered FFV, increased the membrane density, and decreased the number of pathways for gas transport. The CO₂ permeability of the pure "as-cast" PIM-1 membranes was 3,425 Barrer. The permeability increased to 5,785 Barrer with the addition of 1 wt% of the nanosheets and decreased to 3,381 Barrer (which is lower than that of pure PIM-1) with the addition of 2 wt% of the filler [288].

Similar to the FFV analysis, the improvement in CO₂ permeability at low filler concentrations can be attributed to the reduced PIM-1 chain packing and increased free volume caused by the filler. On the other hand, decreased permeability at high filler contents can be ascribed to the blockage of interconnected, porous pathways of the PIM-1 matrix. The effect of the filler level on the CO₂/N₂ and CO₂/CH₄ selectivities is, however, completely different. For both gas mixtures, selectivity decreases monotonously as the filler content increases from 0.0 to 1.5 wt% mainly due to the creation of non-selective voids at the filler/polymer interface [288]. In contrast, the MMM with 2.0 wt% of g-C₃N₄ has a little improved selectivity but almost similar CO₂ and CH₄ permeabilities to those of pure PIM-1[288]. In other words, the MMM follows the general selectivity-permeability trade-off rule. Methanol treatment of g-C₃N₄/PIM-1 membranes affects their permeability significantly. For all filler levels, the permeability doubled. For example, CO₂ permeability of 'as-cast' MMM containing 1 wt% g-C₃N₄ increases from 5,785 to 10,528 Barrer upon methanol treatment [288]. This signifies that methanol treatment affects chain packing and chain arrangement severely.

From the selectivity point of view, alcohol-treatment decreases selectivity in comparison with the 'as-cast' MMMs. However, both 'as-cast' and 'alcohol-treated' membranes show similar trends toward filler loading. So, it seems 2D, ultra-microporous fillers such as g-C₃N₄ are ideal candidates for MMMs manufacturing due to their high surface area and their ability in debundling

the PIM-1 chains. They can improve permeability at concentrations as low as 1 wt% thanks to their high aspect ratio. Aging and thermal stability are other properties that are improved by the incorporation of 2D fillers.

8.5. Membranes Containing Covalent Organic Frameworks (COFs)

Porous micron-sized aromatic framework particles like PAF-1 can mitigate the aging of PIM-1 [273]. These particles have a surface area around 5,200 m²/g and possess great affinity for CO₂. When they are incorporated into PIM-1, they anchor to the bulky moieties of the polymer, freezing the free volume of as-cast membranes, and suppressing the aging. In other words, several segments of PIM-1 chains are adsorbed in the pores of the porous filler keeping the PIM-1 chains unpacked over time.

Figure 28D shows the building block of the PAF-1 and displays schematically its incorporation into a PIM-1 membrane. The schematic shows how aging causes a decrease in free volume in the absence of the PAF-1 and how the aging phenomenon is suppressed in the presence of the PAF-1. PIM-1/PAF-1 MMMs show just a 7% decrease in permeability after 240 days. During this period, however, pure PIM-1 shows a 62% decrease in the CO₂ permeability [273]. In addition, PIM-1/PAF-1 has a high CO₂/CH₄ selectivity of around 20 and a high CO₂ permeability of about 15,000 Barrer [273].

A porous nanoparticle named SNW-1 can be synthesized thorough the reaction of melamine and terephthalaldehyde [263]. The nanoparticle consists of many −NH groups that facilitate CO₂ adsorption when used as the dispersed phase in the PIM-1 matrix. Moreover, the nanoparticles are dispersed homogenously in the PIM-1 matrix due to the formation of hydrogen bonds between −NH groups of the SNW-1 and C≡N and dioxane rings of the PIM-1. The surface

area of the filler is about 780 m²/g and its CO₂ uptake at pressures of 2 and 30 bars have been reported to be 40 and 161 cm³/g, respectively [263]. Because of the high specific surface area, high microporosity, and amine groups of the filler, SNW-1 containing MMM are suitable for CO₂ removal. 10 wt% of SNW-1 was its optimum loading for the fabrication of high-performance nanocomposite membranes for CO₂ removal. CO₂ permeability increases monotonously from 3,672 (for pure PIM-1) to 7,553 Barrer for PIM-1/SNW-1 (10 wt%) [263]. However, a further increase in the filler content does not change the selectivity significantly, while it decreases the CO₂ permeability from 7,954 to 6,460 Barrer [263]. In the range of the SNW-1 < 10 wt%, the main reason for improving CO₂ permeability is an increase in the free volume of the matrix confirmed by augmentation in the d-spacing of the PIM-1 chains. In other words, the CO₂ permeability is improved due to increased CO₂ diffusivity coefficient. However, at the higher SNW-1 loading, about 20 wt%, diffusion pathways created by the PIM-1 are blocked by the SNW-1 causing permeability decline. As for CO₂/CH₄ and CO₂/N₂ selectivities of the MMMs, 10 wt% addition of the SNW-1 to the PIM-1 caused 27.4 and 37.6% improvements compared to pure PIM-1, respectively [263]. The main reason behind such increases in selectivities is the establishment of acid-base interactions between -NH groups of the SNW-1 and CO₂ molecules.

8.6. Membranes Containing Metal-organic Frameworks (MOFs)

The addition of a MOF to MMMs improves CO₂ permeability without sacrificing the CO₂/N₂ selectivity through three different methods. First, the MOFs themselves have a porous structure. So, CO₂ molecules can directly diffuse through the MOFs' channels when a high amount of the filler is loaded. Second, their presence in the PIM-1 matrix can produce more free volume in the PIM-1/MOF interface. Third, MOFs can be functionalized to show high affinity toward CO₂ molecules, thereby improving the gas uptake of the MMMs. MOFs have organic-inorganic nature

and their presence in MMMs leads to the generation of less non-selective macro-voids [289, 290]. Having this background, various Ti_xUiO -66 (x= 1, 5, 10, 15) can be synthesized from UiO-66 by post-synthetic transmetallation [291]. The presence of the titanium in the molecular structure of the filler improves the polymer/filler interactions.

Figure 28E shows how the titanium exchange improves the interactions of the MOF with the PIM-1 and consequently its dispersion in the matrix. Ti substitution decreases the crystallinity of the UiO-66 and gives it a higher chance to interact with the PIM-1's nucleophilic groups and Ti^{IV}/Zr^{IV} metal sites [291]. The Ti₅UiO-66 provides the best CO₂ permeability compared to all other fillers of this family including UiO-66, Ti₁UiO-66, Ti₁UiO-66, and Ti₁₅UiO-66 [291]. When 5 wt% of the Ti₅UiO-66 is added to PIM-1, the CO₂ permeability increases from around 3,800 to 13,500 Barrer, representing a 274% permeability improvement without a selectivity loss [291]. Under these circumstances, the CO₂/N₂ selectivity remains in the range of 20 to 24 even in long term periods [291].

PIM-1 is a hydrophobic material consisting of aromatic repeat units. It is immiscible with hydrophilic nanomaterials such as silicalite-1 crystals (MFI). To obtain fine dispersion of the filler in the PIM-1 matrix without detecting any interfacial voids, the outer surface of the silicalite-1 crystals must be functionalized by aromatic moieties, -(CH₂)₂Ph. A 35.5 vol.% addition of the filler to PIM-1 decreases the CO₂ permeability from 4390 (for the pure polymer) to 2,530 Barrer (for the MMMs) while increases the CO₂/N₂ selectivity from 24 to 30 [292]. The decrease in the permeability and the increase in the selectivity imply that MMMs containing MFI crystals are less permeable but more selective compared to PIM-1. This indicates the absence of voids at the PIM-1/MFI interface and filler agglomeration.

Motivated by the high specific surface area of the MIL-101 (4000 m²/g) and its high thermal and chemical stabilities [293], the porous nanoparticles can be incorporated into the PIM-1 matrix to prepare MMMs [293]. 33 vol.% of the MIL-101 is loaded into the PIM-1 matrix, as it is expected that gas transport improvements happen in loading levels only higher than 20 vol.%. The strong interactions of the filler and the PIM-1 matrix originate from the strong non-covalent bond formation between dioxane groups of PIM-1 and metal cations in the MIL-101 [293]. CO₂ permeabilities of 3,250 and 8,440 Barrer have been reported for PIM-1 and PIM-MIL-101, respectively [293]. Also, the CO₂/N₂ selectivity has been reported to increase from 19 to 36 upon the addition of the filler. Here, the CO₂ permeability improvement is mainly attributed to the diffusivity coefficient enhancement of the CO₂, as its value increased from 4.1×10⁻⁷ to 8.4×10⁻⁷ cm²/s, while the CO₂ solubility coefficient remained unchanged upon the addition of the filler [293]. As a result, it can be concluded that the mesoporous MIL-101 nanoparticles are effective fillers, as they can concurrently improve permeability and selectivity of the PIM-1.

To develop highly efficient PIM-based MMMs containing MOFs for CO₂ separation, various ionic liquids (ILs) can be incorporated into pores of MOFs. For example, amine-containing ILs [C₃NH₂bim][Tf₂N] (TSIL) can be incorporated into a special kind of amine-functionalized MOF, NH₂-MIL-101(Cr), to obtain a nanoporous filler and then add the filler to PIM-1 to fabricate a MMM, which surpasses the 2008 Robeson upper bounds. Figure 28F shows the manufacturing steps of the MMMs and the mechanism by which the PIM-1 based MMMs separate components of a CO₂/N₂ gas mixture. Unsaturated metal sites of the MOFs can be considered as Lewis acids; they are able to anchor the ILs to prevent their leakage in practical applications. Besides, the presence of amine groups on the MOFs facilitates their homogenous dispersion in the PIM-1 matrix. The optimum permeability and selectivity were achieved upon 5 wt% loading of the TSIL-

containing MOF, which caused 23% improvement in CO₂ permeability and 119% (from 17 to 37) enhancement in CO₂/N₂ selectivity, compared to the pure PIM-1 [275]. Such a significant improvement in the MMMs performance can be attributed to the increase in the internal space of the MMMs and the facile CO₂ transport through the MOF's already available channels. Thanks to the presence of amine groups, TSIL is a CO₂-philic material but does not show any affinity towards N₂. When it anchors on the MOF surface, it decreases the pore volume of the MOF, which leads to a reduction in the adsorption capacity of both CO₂ and N₂. However, this reduction is more significant for N₂, as there is no affinity between N₂ and the TSIL. Besides, the measured solubility values show a slight decrease in the N₂ solubility coefficient, confirming the repulsion of N₂ by the TSIL-containing MOF. At higher loadings, like 10 wt%, several voids are formed at the filler/PIM-1 interface. These voids create a very easy way for N₂ molecules to cross over the membrane resulting in a CO₂/N₂ selectivity reduction. As a result, three different factors can be mentioned for such extraordinary performance of this MMM. First, IL plays an important role in the system, as it is a selective CO₂ carrier. Second, the filler itself has a porous structure, which increases the CO₂ permeability. Third, the NH₂-MIL-101(Cr) can control the dispersion of the IL to create more active sites for gas molecules.

Amine-functionalized MOFs such as NH₂-UiO-66 (functionalized with amino group) and UiO-66-(COOH)₂ (functionalized with two carboxylic groups) can be embedded into PIMs with different moieties to separate CO₂/N₂ and CO₂/CH₄ gas mixtures efficiently [294]. As the pure PIM-1 intrinsically shows high CO₂ permeability, the main aim here is improving PIM-1 selectivity via the addition of the MOFs. The MOFs size can be adjusted from micron-size to nanosize through water modulation and functionalization [294]. The dispersion of the nano-size MOFs in the PIM-1 matrix is such fine that it creates a fully transparent film in contrast to the micron-

size counterpart. Considering just the effect of UiO-66 particle size on gas transport properties, very different behavior is observed between micron- and nano-size particles [294]. At a high MOFs loading level, the MMMs containing micron-size MOFs have double permeability and a little bit decrease in selectivity, compared to pure PIM-1, which is a usual behavior caused by the generation of non-selective voids in the MOFs/PIM interface [294]. On the other hand, the high loading level of the nano-size UiO-66 causes a decrease in the permeability and an increase in the ideal selectivity [294].

The rigidification of PIM-1 chains upon the addition of UiO-66 causes the selectivity increase and permeability decrease. However, at a low level of filler loading, the permeability decrease is negligible. The improvements are more significant in the case of the addition of amine-functionalized, nano-size UiO-66 (UiO-66-NH₂) and the optimum permeability and selectivity are obtained in the filler loading range of 5-10 wt%. Increasing more UiO-66-NH₂ than this optimum range decreases permeability due to the formation of non-porous aggregates of the nano-size MOFs. Upon 5-10 wt% addition of the nano-sized UiO-66-NH₂, the MMMs easily surpass the 2008 CO₂/N₂ Robeson upper bound and reach ideal selectivities of 27 and 28 for CO₂/N₂ and CO₂/CH₄, respectively. They also keep their high permeability thanks to the existence of additional gas diffusion paths created by the porous MOF. As a result, it should be emphasized that not only the functionality but also the size of the filler affects the MMMs performance. Nano-sized fillers have a good dispersion in the PIM-1 matrix. They reduce the possibility of forming non-selective voids, which leads to selectivity improvement. Such functionalized UiO-66-NH₂ nanoparticles also do not sacrifice permeability at the expense of selectivity [294].

The properties of AO-PIM-1 are excellent to host NH₂-UiO-66 for making MMMs. To synthesize AO-PIM-1, all or some of the -CN groups of PIM-1 should be converted into -CN₂OH₃

and the conversion extent depends on the modification reaction duration [295]. 53% and 66% of the –CN groups of PIM-1 were replaced with amidoxime groups when it was subjected to the modification reactions for 1.5 or 3.0 h, respectively. It is necessary to point out here that as the population of amidoxime groups in PIM-1 chain increases, the selectivity also increases, whereas permeability decreases. After PIM-1 modification, the formation of a perfect interface between the filler and the polymeric matrix guarantees an excellent CO₂ capture by the membrane [295]. It is believed that strong hydrogen bonds are formed between amine groups of the MOF and amidoxime groups of the polymer. These strong interactions between the filler and the polymer, at 30 wt% of the filler, not only increases CO₂ permeability up to 8,425 Barrer but also keeps the CO₂/N₂ and CO₂/CH₄ selectivities at 27.5 and 23.0, respectively [295].

Comparing the diffusivity and solubility data, it can be observed that the addition of 30 wt% of the filler increases the diffusivity coefficient 10 times, whereas the solubility coefficient is not affected upon the addition of the filler. The CO₂ permeability of the AO-PIM-1/NH₂-UiO-66 decreased from 8,425 to 5,800 Barrer after 31 days (showing just 31% permeability loss) and remained constant in the next 80 days [295]. This shows the establishment of strong hydrogen interactions between the filler and the polymer, which lowers the production of non-selective voids, suppresses the generation of the undesired channels, and reduces the aging problems as well. To reach the best MMMs performance, it is necessary to modify both the filler and the PIM-1 chains simultaneously.

MFM-300 (V^{III}) can be distributed homogenously in the PIM-1 matrix and has a good affinity towards it. The addition of the MOF increases CO₂ permeation due to chemical affinity between CO₂ molecules and one-dimensional pore channels of the MOF. At 25 wt% loading of the MOF, the CO₂ permeability was reported to be 4,617 Barrer and the CO₂/N₂ selectivity 21.3

[296]. For the CO₂/N₂ gas mixture, the MMMs show very high performance, located above the 2008 Robeson upper bound. As a result, porous MFM-300 (V^{III}) containing hydroxyl groups seems to be a good MOF for incorporation into PIM-1 to fabricate MMMs for CO₂/N₂ applications.

It has been shown that MOFs addition and methanol treatment make the MMMs more permeable. In the case of both pure PIM-1 and the MMMs, the permeability increase upon the methanol treatment is attributed to simultaneous solvent extraction and free-volume generation. The filler incorporation improves the diffusivity coefficient but has little effect on the solubility coefficient. The addition of UiO-66 and UiO-66-(COOH)₂ increases CO₂ permeability, while slightly decreases the CO₂/CH₄ selectivity. However, not only does the UiO-66-(NH₂)/PIM-1 MMM show higher CO₂ permeability compared to the pure PIM-1 but also keeps the CO₂/CH₄ selectivity in the same selectivity range of pure PIM-1. This may be ascribed to the ability of NH₂ for improving the compatibility between UiO-66 and PIM-1. Thus, an appropriate filler is the one that improves permeability without sacrificing selectivity [297].

To fabricate membranes for natural gas purification, sheet-like MOFs were added to PIM-1 [298]. Such an MOF is copper 1,4-benzenedicarboxylate nanosheets, CuBDC-ns MOF, which is a 2D layered MOF. It can establish a large interface with PIM-1 chains. Moreover, it has a pore size of 5.2 Å, which is large enough for CO₂ diffusion while small enough for blocking CH₄ molecules. The MOF also shows more affinity towards CO₂ rather than CH₄. A 660 nm thick membrane containing 10 wt% of the MOF has CO₂ permeance of 407 GPU and CO₂/CH₄ selectivity of 15.6. It is worth to note here that ultrathin membranes made via spin coating method have improved gas transport properties compared with thick membranes obtained through conventional solution casting method. In addition, shear forces exerted on 2D nanosheets during the spin coating process orient the selective pores of the MOF in a direction where permeation

driving force and gas flux exist. So, it seems that incorporating 2D MOF particles and taking the advantage of spin coating method are good strategies to develop efficient gas-separating membranes.

The addition of ZIF-8 to PIM-1 can improve its CO₂ permeability and the CO₂/CH₄ selectivity [268]. The main reason behind the permeability improvement is improved diffusivity coefficient. In comparison to solid impermeable SiO₂ nanoparticles, ZIFs nanoparticles are tunable in terms of particle size and functionality. Thus, their addition to PIM-1 leads to an MMM surpassing the 2008 Robeson upper bounds. PIM-1 has very high CO₂ solubility coefficient but low CO₂ diffusivity coefficient. The addition of the ZIF-8 nanoparticles does not alter the solubility coefficient but improves the diffusivity coefficient of PIM-1[268]. This is a feature that ZIF-8 nanoparticles have but other nanoparticles like silica do not. The CO₂ permeability increases from 4,390 Barrer for pure as-cast PIM-1 to 6,300 Barrer for as-cast PIM-1 matrix containing 43 vol.% ZIF-8, though the relationship between filler content and permeability is not monotonous [268]. Moreover, the CO₂/CH₄ selectivity increased from 14.2 to 14.7. The maximum selectivity happens at 28 vol.% of ZIF-8 where the selectivity value is 18.6. In the case of alcohol-treated PIM-1/ZIF-8 MMMs, a monotonous relationship exists between CO₂ permeability and ZIF-8 loading level; the permeability increases from 12,600 to 19,350 Barrer upon the addition of 43 vol.% ZIF-8 [268]. However, the CO₂/CH₄ selectivity of the membranes decreases monotonously from 17 to 7.3 upon the addition of 43 vol.% ZIF-8 [268]. Both as-cast and ethanol-treated PIM-1/ZIF-8 MMMs surpass the 2008 CO₂/CH₄ Robeson upper bound [268]. In general, this research shows that in the case of using porous, permeable particles like ZIF-8, the diffusion coefficient of CO₂ in the PIM-1 based MMM increases as more gas molecules can diffuse through the cavities of the filler [268].

TOX-PIMs are a family of PIM-1s, which are crosslinked by a thermo-oxidative process. Membranes that have such crosslinked PIM-1 chains show high CO₂/CH₄ selectivity up to 70. However, their CO₂ permeability is low (less than 1,000 Barrer). The addition of nano-porous fillers can compensate for the low permeabilities. Over two years, the selectivity of such membranes increases, while their permeabilities decrease slightly. However, after two years, they showed two orders of magnitude higher gas transport properties than the pure PIM-1 [276]. Song et al. [276] added non-porous SiO₂ and microporous ZIF-8 nanoparticles to the PIM-1 matrices and exposed the system to the thermal oxidation crosslinking at the presence of oxygen at 350-450 °C. Figure 28a schematically presents the manufacturing steps of such MMMs. Usually, the crosslinking reaction decreases permeability, and this reduction is more significant for larger molecules (CH₄ and N₂) than smaller ones (CO₂ and H₂). The CO₂ permeability increases and CO₂/N₂ and CO₂/CH₄ selectivities decrease with the addition of up to 20 wt% ZIF-8 or silica. The CO₂/N₂ selectivity has been reported to decrease significantly in the range of 0–5 wt% of the ZIF-8 and remains ~27 in the filler range of 5-20 wt% [276]. However, the CO₂/CH₄ selectivity slightly decreased from 38 to 27 in the filler range of 5-20 wt% [276]. The improvement in the CO₂ permeability is mainly due to the improved diffusivity coefficient. As it is known, solubility and diffusivity coefficients both contribute to the permeability, but solubility tests, in this case, show that no significant difference exists between the solubility coefficients of PIM-1, TOX-PIM-1, and SiO₂/ZIF-8-TOX-PIM-1. Thus, the improved CO₂ permeability is due to the diffusivity coefficient augmentation, which is caused by the generation of extra channels and heterogeneous interfaces upon the addition of the filler.

8.7. Effect of Filler Geometry on PIM-based MMMs Performance for CO₂ Separation

Nanofiller geometry has a significant effect on the gas separation performance of MMMs. In this section, the permeability of graphene/PIM-1 is compared with those of MMMs made from PIM-1/fumed silica [252] and PIM-1/PEG-functionalized MWCNT (f-MWCNT) [264]. All of these three nanoparticles suppress PIM-1 aging through decreasing conformational freedom and chain packing. However, the level of aging suppression depends on the fillers loading level. In the case of PIM-1/f-MWCNT, the highest permeability is achieved with the addition of 1 vol.% of the filler, while in the case of the fused silica, the highest permeability is achieved at 24 vol.% filler addition. In a direct contrast, just 0.05 vol.% of the graphene in PIM-1 leads to the highest permeation. These results imply that not only the available surface area of the filler but also the curvature of the surface affect the permeability of the MMMs. Silica is a spherical nanoparticle, f-MWCNT is a cylindrical one, while graphene is a planar filler. The different loading levels of each nanofiller at which the maximum permeability happens points out to the different accessible surface areas that each nanofiller provides. While both of silica and f-MWCNT have surface areas around 250 m²/g, the maximum permeability occurs at 24 vol.% silica incorporation while for f-MWCNT that value is 1 vol.% [264]. For a single graphene sheet, the theoretical surface area is about 2,630 m²/g, and for a few layers of graphene, it is lower but high enough to endow the highest permeability by just 0.05 vol.% addition. The MMMs fabricated by planar few-layer graphene fillers retained its CO₂ permeability after 8 months [299]. The membrane containing 0.164 vol.% of the graphene showed an initial CO₂ permeability of 7,830 Barrer [299]. This membrane maintained a major portion of its permeability after 8 months; its CO₂ permeability decreased to 5,680 Barrer at the end of the period. On the other hand, the CO₂ permeability of the pure PIM-1 decreased from 5,120 to 3,670 Barrer in this period [299]. As a result, it can be concluded that the ability of fillers for

preventing chain packing increases in the order of spherical, cylindrical, and planar fillers [299].

Table 8 summarizes the effects of different nanoparticles on the CO₂ separation performance of PIM membranes.

Table 8. Performances of PIM-based MMMs for CO₂ separation.

Membrane	Permeability (Barrer)			Selectivity		Ref
	CO ₂	CH ₄	N_2	CO ₂ /CH ₄	CO_2/N_2	1
PIM-1	5,040	288	244	17.5	20.6	[276]
PIM-1/30 wt% ZIF-8	6,424	370	304	17.4	21.1	
PIM-1	5,040	288	244	17.5	20.6	[276]
PIM-1/40 wt% SiO ₂	8,505	830	581	10.2	14.6	
TOX-PIM-1	1,104	16	30	69.2	36.6	[276]
TOX-PIM-1/20 wt% ZIF-8	3,944	147	139	26.8	28.3	
TOX-PIM-1	1,104	16	30	69.2	36.6	[276]
PIM-1/20 wt% SiO ₂	2,615	80	101	32.5	26.0	
PIM-1	6,576	536	351	12.3	18.7	[262]
PIM-1/20 wt% MOF-74	21,269	1114	742	19.1	28.7	
PIM-1	6,576	536	351	12.3	18.7	[238]
PIM-1/20 wt% UiO-66-NH ₂	12,498	392	230	31.9	54.2	
PIM-1	6,211	401	279	15.5	22.2	[264]
PIM-1/1.0 wt% f-MWCNTs	7,813	785	417	9.9	18.7	
PIM-1	6,211	401	279	15.5	22.2	[264]
PIM-1/1.0 wt% SWCNTs	15,721	1820	949	8.6	16.5	
PIM-1	3,425	229	148	15.0	23.1	[288]
PIM-1/1.0 wt% g-C ₃ N ₄	5,785	503	354	11.5	16.3	
PIM-1	3,795	315	198	12.0	19.0	[279]
PIM-1/10 wt% PEG-POSS	1,309	44	43	30.0	31.0	
PIM-1	3,295	322	164	10.2	20.1	[300]
PIM-1/30 wt% ZIF-71	8,377	750	457	11.2	8.3	
UV-PIM	1,233	36	41	34.1	29.8	[300]
UV-PIM/30 wt% ZIF-71	3,459	97	129	35.6	26.9	

9. Potential of PIM Membranes for Industrial Implementations

Nonlinear sorption; that is, the dependence of permeability on pressure, causes a membrane to show different behaviors in mixed gas and pure gas permeation tests. To evaluate the potential of PIMs in industrial-scale CO₂ separation processes, a prototype PIM-1 membrane was studied and was found to show a CO₂/CH₄ selectivity of 8 and a mixed-CO₂ permeability of 4,500 Barrer, under a CO₂ partial pressure of 10 bar [200]. Up to an operating pressure of 77 bar, the modified glassy AO-PIM-1 membrane demonstrated a unique separation performance with a ternary mixture feed containing CO₂ and H₂S [301]. Similarly, up to an operating pressure of 48 bar, an OH-functionalized PIM (PIM-6FDA-OH) membrane was used successfully for the separation of an aggressive sour natural gas containing H₂S and CO₂ [302].

Ladder PIM-Trip-TB is another polymer suitable for fabricating membranes that are able to separate CH₄ and CO₂ mixed gases [303]. Its membranes are promising candidates for reducing greenhouse gas emissions, producing clean energy and proposing the 2018 mixed-gas CO₂/CH₄ upper bound (Figure 29a) [89]. As an instance, large scale production of AO-PIM membranes can be practiced for fabricating composite structures or integrally skinned asymmetric membranes with hollow-fiber or flat-sheet geometries.

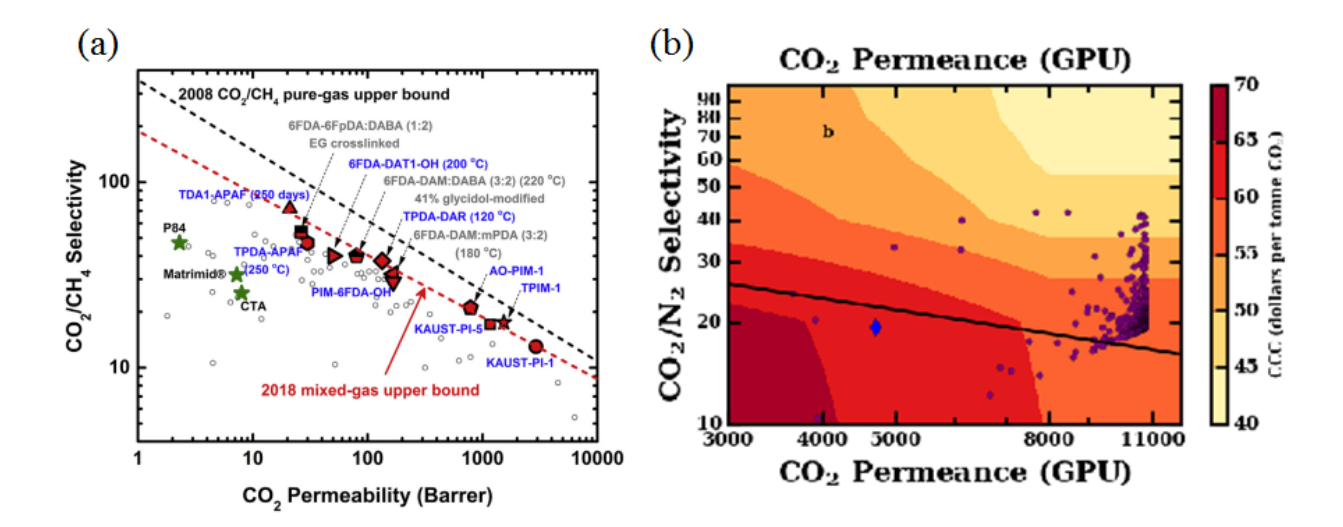


Figure 29. (a) Pure- and mixed-gas CO₂/CH₄ separation performance of PIM membranes, and (b) performance of PIM-based membrane for CO₂/N₂ separation and its relationship with carbon capture cost (CCC) [89, 304]. (a) Reprinted with permission from Wang Y, Ma X, Ghanem B, Alghunaimi F, Pinnau I, Han Y. Polymers of intrinsic microporosity for energy-intensive membrane-based gas separations, Materials Today Nano, 3:69-95. (2018). Copyright 2018 Elsevier. (b) Reprinted with permission from Budhathoki S, Ajayi O, Steckel JA, Wilmer CE., High-throughput computational prediction of the cost of carbon capture using mixed matrix membranes. Energy & Environmental Science. 12:1255-64. (2019). Copyright 2019 Royal Chemical Society.

Consequently, CO₂-selective ultra-permeable PIM membranes have received growing attention in recent years for carbon capture and bio/natural gas upgrading owing to the intrinsic efficiency of separations. Future progresses to commercialize these membranes should focus on the preparation of AO-PIM-1 as TFC or asymmetric hollow-fiber membranes. Regarding industrial-scale production, gas separation membranes with appropriate mechanical properties are required to assure the feasibility of their fabrication as thin films that are installed in spiral-wound or hollow-fiber modules. PIM-1 has sufficient elasticity to withstand the elastic deformations during gas separation [305].

High robust membranes can be fabricated from PIM-PIs. KAUST-PI-1 demonstrates higher Young's modulus and tensile strength at break than PIM-1 and PIM-PI-1. However, KAUST-PI-1 cannot sustain high strains. PIM-PI, PIM-EA-TB, and EA-DMN have satisfactory mechanical properties with respect to commercial CA membranes (Table 9). Efforts for commercialization require membrane scale-up in the form of TFC or integrally-skinned asymmetric membranes. To decrease the membrane surface required for a special separation, the use of highly permeable membranes with thin selective layers is crucial [306]. For practical applications, a thin layer is put over microporous support to fabricate a TFC membrane [26, 307, 308]. The thin film acts as a selective layer, which controls the separation properties and the support provides mechanical strength required for industrial applications [309]. Techno-economic evaluation predicts that the cost of CO₂ capture by a PIM-1 membrane is dependent on its performance (\$64 per ton of removed CO₂) [304]. Increasing CO₂ permeance of a membrane to 8,000 GPU with a CO₂/N₂ selectivity of 38 can decrease the cost of CO₂ capture to less than \$50 per ton of removed CO₂ (Figure 29b).

Table 9. Mechanical properties of several PIM membranes.

Polymer	Young	Tensile	Elongation at	Ref.
	modulus	Strength at	break (%)	
	(GPA)	break (MPa)		
PIM-1	0.868	48.0	10.0	[125]
KAUST-PI-1	2.460	94.0	5.9	[125]
PIM-PI-1	1.620	61.0	69.0	[125]
EA-DMN	0.836	63.1	30.0	[310]
EAD-DMN	0.999	55.4	14.5	[310]
PIM-EA-TB	1.030	44.0	43.0	[243]
CA	1.220	49.0	53.0	[311]
Matrimid-5218	2.896	85.0	49.0	[125]

10. Critical Insight into Gaps and Areas of Weakness

Engineering of PIM membranes for gas separations through polymer chemistry is a fast-evolving field of research. The availability of numerous starting monomers provides a large degree of freedom for tuning properties of PIMs, including the packing structure and membrane properties. However, the use of expensive reagents, complex synthesis procedures, and low yields are barriers hindering the wide-spread use of PIM membranes. For industrial applications, the low stability (physical aging and plasticization), and low scalability of PIMs are additional challenges. Fortunately, these challenges can be tackled by tailoring the molecular structure, rigidity, microporosity, and chemistry of PIMs during their synthesis. These abilities require the improvement of technical knowledge to a level that permits systematic preparation of PIMs with desirable chain stiffness, functional groups, interchain rigidity, and pore size distribution. Some of these properties work against each other. Thus, systematic procedures are needed to synthesize PIMs with an optimum combination of all properties. They include procedures for introducing CO₂-philic groups into the polymers structure and incorporating suitable contortion sites, adjusting physiochemical properties of PIMs enabling the separation of gas components based on their molecular sizes and solubilities, achieving long-term stability, and incorporating contorted moieties into other classes of polymers. In designing new molecular structures or modifying already existing PIMs, membrane processability should be considered. Any crosslinked structure or long branches for improving gas transport properties should not limit the processability of PIMs. Several post-processing methods such as thermal treatment and crosslinking can be used to

improve physical aging and plasticization resistance. However, membranes modified by these methods are not scalable and suffer from brittleness.

In terms of geometry, the trend is towards designing hollow fiber PIM membranes rather than flat sheet counterparts. Any modification that facilitates the processing of PIMs in the form of hollow fiber is highly favorable, as fiber spinning of existing PIMs is more difficult than commercial polymers. While integrating different moieties with various levels of rigidity into PIMs structures provides high degrees of intrachain rigidity, the resulting PIMs have not been studied adequately. Further improvements can be achieved by studying structure—physical property and physical property—transport property relationships of PIM membranes, as these relationships are still not well understood. New PIM membranes with satisfactory gas selectivities can be fabricated using a combination of diffusivity- and solubility-controlled approaches. However, balancing the chain mobility and segments affinity are still a challenging.

There has been extensive research studies to develop new facilitated-transport PIM membranes with improved selectivity and aging and plasticization resistance. Although these membranes suffer from drying and carrier saturation, they are suitable for use at room temperatures and low pressures at which other membranes demonstrate low performances. Membranes stability and performance can be tailored by surface modifications especially in asymmetric membranes. Solubility-controlled PIM membranes have potential to enhance CO₂ selectivity without adding extra processing difficulties and costs related to membranes fabrication. Continued research to achieve long term stability is crucial for developing solubility-controlled membranes appropriate for industrial applications.

Many approaches have been proposed to mitigate physical aging and plasticization, and improve gas sieving abilities of free-standing PIM membranes. Future endeavor in the area of TFC

PIM membranes include applying these approaches to thin films and testing the films over a commercially useful period. Continuous studies on TFC membranes will generate data needed to plot CO₂ permeance *vs.* CO₂/N₂ and CO₂/CH₄ selectivities. Note that the alcohol soaking technique which has been used widely for PIM membranes may detach the thin film from the support.

There is a need for testing PIM membranes under conditions that more closely resemble the real practical environments, as gas transport properties of PIM membranes have mostly been tested under pure gas conditions. In addition, flue and natural gases contain minor components like CO, H₂S, and water, which may affect the membranes' performance and stability. The effects of these components should be taken into consideration in future studies. Another less explored area is PIM-based blend membranes. There is a need for exploring different polymers, blended with PIMs, to investigate their gas transport properties, phase behavior, compatibility, and mechanical and thermal strengths.

Of demand are more accurate atomistic molecular simulation techniques that can accurately predict a membrane's gas separation properties. These techniques facilitate the interpretation of experimental data and screening of potential PIMs for membrane applications before experimentally fabricating them. An accurate molecular simulation technique can estimate the effect of different functionalizations on CO₂ separation properties of PIM membranes. Besides, the monomer type, the effect of the backbone's rigidity, and the introduction of bulky side groups on microporosity can be analyzed computationally. Also, these techniques can help establish structure-property relationships and guide experimentalists in their search for optimal designs. However, in simulating PIM membranes there are currently challenges such as the occurrence of plasticization and swelling, which change microporous polymers' structure from static to dynamic. Thus, future modeling efforts should focus on developing easy-to-run, fast, accurate modeling

techniques that are capable of accounting for these dynamic phenomena. Besides, insights can be gained by developing data-driven models such as machine learning models trained with the vast available experimental data sets. These models and the resulting data analytics can facilitate the discovery of new PIM membranes.

Despite appealing features of PIM-based MMMs, restricting the movement of polymer chains in the filler's vicinity may create non-selective voids at the filler/polymer interface. Many surface modifications have been introduced to overcome these problems. However, there is no accurate-enough technique to quantify the extent of interactions between particles and PIMs chains in MMMs under the current knowledge. There is a need for developing quantitative characterization methods to measure the change in such interactions. Also, there is a need for further investigating the effects of the particle size and shape on the CO₂ performance of PIM-based MMMs. The use of very thin films (< 1µm) as an active layer of membranes is very attractive. So, investigating membranes containing 2D nanomaterials can be a hot topic. More investigations are needed to develop PIM-based MMMs which simultaneously have fine particle dispersion, no agglomeration, low level of unselective voids and chain rigidification, easy processability, and economic feasibility for large-scale production.

11. Concluding Remarks

Strategies that have been applied to adjust the gas transport properties of PIM membranes were reviewed. Incorporating highly rigid moieties into the polymer backbone and interlocking moieties increase the backbone rigidity and consequently improve the gas transport properties. Attaching extended substituents to bridged bicyclic moieties creates 2D ribbon-shaped chains, which provide ultra-permeability. For example, the attachment of various substituents to BTrip moiety of PIM membranes endows the membranes with gas separation performances that are above the newest

CO₂/CH₄ and CO₂/N₂ upper bounds. Such strategies can improve the permeability of PIM membranes, making them suitable for CO₂ removal from fuel and flue gases. However, most of highly permeable PIM membranes show selectivities below 40, which has been recommended for CO₂ separation [312]. Incorporating new moieties and cleverly designing the PIM backbone are effective methods for balancing permeability and selectivity. There is a commercial need for integrally-skinned asymmetric membranes with a very thin selective layer of <200 nm placed on a large support layer. Also, new membrane modules that improve mass transport and are suitable for the TFC membranes are needed.

In the case of polyimides, it was discussed how stable, contorted, and kinked polymer structures endow membranes with energy-efficient gas separation performance and excellent properties such as processability, thermal and mechanical stabilities, and feasibility. These properties permit performing different kinds of post-modification reactions and adjustments. Better understanding of structure-property relationships will enable the design of the advanced membrane materials that are commercially viable. In PIM-PIs, the form of the side chains attached to the dianhydrides or diamines influences membrane gas separation properties. It can also affect membrane characteristics, inter-chain molecular interactions, chain packing, and pore-size distribution, which affect the trade-off between permeability and selectivity of the membranes.

The PIM-PIs membranes prepared from diamines containing a rigid moiety are unable to surpass the CO₂/N₂ and CO₂/CH₄ upper bounds. Incorporating bridged bicyclic moieties into dianhydride molecules, connecting short and bulky bridgehead substituents to the moiety, and limiting the rotation around the imide bond via utilizing short diamines bearing branched groups endow PIM-PIs with ultra-microporous structures and consequently lead to the fabrication of membranes, performances of which will be above the 2008 Robeson upper bounds but still below

the 2019 upper bounds. The fabrication of efficient membranes requires controlling materials properties at the nano and molecular scales. Thermal treatment at optimum temperatures via TR and TC processes, and the fabrication of CMS membranes from PIM-PIs are notable strategies for surpassing the 2008 Robeson upper bounds. Also, PIM membrane post-modification methods — such as thermal crosslinking, controlled thermal-oxidative crosslinking, UV-crosslinking, and twisting the porous network toward ultra-microporosity using appropriate chemical functionalization — allow for surpassing the 2008 Robeson upper bounds. Embedding functionalized nanomaterials in the PIM matrices endows fixed facilitated transport membranes and MMMs with synergetic properties that provide the PIM-based nanocomposite membranes with excellent gas separation performance. Most of PIM-based MMMs have been made of PIM-1. However, other PIM polymers especially PIM-PIs can be used to fabricate other types of PIM-based MMMs.

Exposure of PIM membranes to gas steams containing CO₂ at high pressures can lead to selectivity loss stemming from plasticization. Making a balance between inter- and intra-chain rigidities is necessary to mitigate plasticization. Effective approaches to mitigate physical aging include an appropriate design of the polymer backbone architecture, post-modification, and nanomaterial addition. The formation of porous polymers with flexible backbones and rigid side chains represents a promising new family of materials for addressing physical aging and plasticization. New materials are required with excellent stability against aging and plasticization to minimizing their degradation over harsh thermal and chemical conditions. The brittleness of PIM membranes can be addressed by blending them with other polymers that have excellent flexibility and toughness. The plasticization problem of PIM membranes can also be addressed by

blending. These areas are evolving very fast, enabling the fabrication of more robust, higher performance gas-separation membranes.

References

- [1] Merkel TC, Wei X, He Z, White LS, Wijmans J, Baker RW. Selective exhaust gas recycle with membranes for CO2 capture from natural gas combined cycle power plants. Industrial & Engineering Chemistry Research. 2012;52:1150-9.
- [2] Hajilary N, Rezakazemi M, Shahi A. CO2 emission reduction by zero flaring startup in gas refinery. Materials Science for Energy Technologies. 2020;3:218-24.
- [3] Hajilary N, Shahi A, Rezakazemi M. Evaluation of socio-economic factors on CO2 emissions in Iran: Factorial design and multivariable methods. Journal of Cleaner Production. 2018;189:108-15.
- [4] Sadeghi M, Talakesh MM, Arabi Shamsabadi A, Soroush M. Novel Application of a Polyurethane Membrane for Efficient Separation of Hydrogen Sulfide from Binary and Ternary Gas Mixtures. ChemistrySelect. 2018;3:3302-8.
- [5] Sohaib Q, Muhammad A, Younas M, Rezakazemi M. Modeling pre-combustion CO2 capture with tubular membrane contactor using ionic liquids at elevated temperatures. Separation and Purification Technology. 2020;241:116677.
- [6] Zhou J, Jin Z, Luo KH. The role of brine in gas adsorption and dissolution in kerogen nanopores for enhanced gas recovery and CO2 sequestration. Chemical Engineering Journal. 2020:125704.
- [7] Hu L, Chen L, Peng X, Zhang J, Mo X, Liu Y, et al. Bifuctional metal-doped ZIF-8: a highly efficient catalyst for the synthesis of cyclic carbonates from CO2 cycloaddition. Microporous and Mesoporous Materials. 2020:110123.
- [8] Halmann MM. Chemical Fixation of Carbon DioxideMethods for Recycling CO2 into Useful Products: CRC press; 1993.
- [9] Shirazian S, Marjani A, Rezakazemi M. Separation of CO2 by single and mixed aqueous amine solvents in membrane contactors: fluid flow and mass transfer modeling. Engineering with Computers. 2012;28:189-98.
- [10] Figueroa JD, Fout T, Plasynski S, McIlvried H, Srivastava RD. Advances in CO 2 capture technology—the US Department of Energy's Carbon Sequestration Program. International journal of greenhouse gas control. 2008;2:9-20.
- [11] Du N, Park HB, Dal-Cin MM, Guiver MD. Advances in high permeability polymeric membrane materials for CO 2 separations. Energy & Environmental Science. 2012;5:7306-22.
- [12] Shamsabadi AA, Kargari A, Farshadpour F, Laki S. Mathematical modeling of CO2/CH4 separation by hollow fiber membrane module using finite difference method. Journal of Membrane and Separation Technology. 2012;1:19-29.
- [13] Saedi S, Madaeni SS, Shamsabadi AA. PDMS coated asymmetric PES membrane for natural gas sweetening: Effect of preparation and operating parameters on performance. The Canadian Journal of Chemical Engineering. 2014;92:892-904.
- [14] Hajilary N, Rezakazemi M. Ethylene glycol elimination in amine loop for more efficient gas conditioning. Chemistry Central Journal. 2018;12:120.
- [15] Soroush E, Mesbah M, Hajilary N, Rezakazemi M. ANFIS modeling for prediction of CO2 solubility in potassium and sodium based amino acid Salt solutions. Journal of Environmental Chemical Engineering. 2019;7:102925.
- [16] Soroush E, Shahsavari S, Mesbah M, Rezakazemi M, Zhang Ze. A robust predictive tool for estimating CO2 solubility in potassium based amino acid salt solutions. Chinese Journal of Chemical Engineering. 2018;26:740-6.
- [17] Rezakazemi M, Heydari I, Zhang Z. Hybrid systems: Combining membrane and absorption technologies leads to more efficient acid gases (CO2 and H2S) removal from natural gas. Journal of CO2 Utilization. 2017;18:362-9.

- [18] Mesbah M, Shahsavari S, Soroush E, Rahaei N, Rezakazemi M. Accurate prediction of miscibility of CO2 and supercritical CO2 in ionic liquids using machine learning. Journal of CO2 Utilization. 2018;25:99-107.
- [19] Dashti A, Riasat Harami H, Rezakazemi M, Shirazian S. Estimating CH4 and CO2 solubilities in ionic liquids using computational intelligence approaches. Journal of Molecular Liquids. 2018;271:661-9.
- [20] Hajilary N, Rezakazemi M, Shirazian S. Biofuel types and membrane separation. Environmental Chemistry Letters. 2019;17:1-18.
- [21] Rezakazemi M, Khajeh A, Mesbah M. Membrane filtration of wastewater from gas and oil production. Environmental Chemistry Letters. 2018;16:367-88.
- [22] Razavi SMR, Rezakazemi M, Albadarin AB, Shirazian S. Simulation of CO2 absorption by solution of ammonium ionic liquid in hollow-fiber contactors. Chemical Engineering and Processing: Process Intensification. 2016;108:27-34.
- [23] Hajilary N, Rezakazemi M. CFD modeling of CO2 capture by water-based nanofluids using hollow fiber membrane contactor. International Journal of Greenhouse Gas Control. 2018;77:88-95.
- [24] Zhang Z, Chen F, Rezakazemi M, Zhang W, Lu C, Chang H, et al. Modeling of a CO2-piperazine-membrane absorption system. Chemical Engineering Research and Design. 2018;131:375-84.
- [25] Rezakazemi M, Darabi M, Soroush E, Mesbah M. CO2 absorption enhancement by water-based nanofluids of CNT and SiO2 using hollow-fiber membrane contactor. Separation and Purification Technology. 2019;210:920-6.
- [26] Sridhar S, Aminabhavi TM, Mayor SJ, Ramakrishna M. Permeation of Carbon Dioxide and Methane Gases through Novel Silver-Incorporated Thin Film Composite Pebax Membranes. Industrial & Engineering Chemistry Research. 2007;46:8144-51.
- [27] Sadeghi A, Nazem H, Rezakazemi M, Shirazian S. Predictive construction of phase diagram of ternary solutions containing polymer/solvent/nonsolvent using modified Flory-Huggins model. Journal of Molecular Liquids. 2018;263:282-7.
- [28] Muhammad A, Younas M, Rezakazemi M. CFD simulation of copper(II) extraction with TFA in non-dispersive hollow fiber membrane contactors. Environmental Science and Pollution Research. 2018;25:12053-63.
- [29] Rezakazemi M, Maghami M, Mohammadi T. High Loaded Synthetic Hazardous Wastewater Treatment Using Lab-Scale Submerged Ceramic Membrane Bioreactor. Periodica Polytechnica Chemical Engineering. 2018;62:299-304.
- [30] Galizia M, Chi WS, Smith ZP, Merkel TC, Baker RW, Freeman BD. 50th anniversary perspective: polymers and mixed matrix membranes for gas and vapor separation: a review and prospective opportunities. Macromolecules. 2017;50:7809-43.
- [31] Ahmadpour E, Shamsabadi AA, Behbahani RM, Aghajani M, Kargari A. Study of CO2 separation with PVC/Pebax composite membrane. Journal of Natural Gas Science and Engineering. 2014;21:518-23.
- [32] Lin H, He Z, Sun Z, Kniep J, Ng A, Baker RW, et al. CO 2-selective membranes for hydrogen production and CO 2 capture—Part II: Techno-economic analysis. Journal of Membrane Science. 2015;493:794-806.
- [33] Cowan MG, Gin DL, Noble RD. Poly (ionic liquid)/lonic Liquid Ion-Gels with High "Free" Ionic Liquid Content: Platform Membrane Materials for CO2/Light Gas Separations. Accounts of chemical research. 2016;49:724-32.
- [34] Rezakazemi M. CFD simulation of seawater purification using direct contact membrane desalination (DCMD) system. Desalination. 2018;443:323-32.
- [35] Dadashi Firouzjaei M, Arabi Shamsabadi A, Aghapour Aktij S, Seyedpour SF, Sharifian Gh M, Rahimpour A, et al. Exploiting Synergetic Effects of Graphene Oxide and a Silver-based Metal-Organic Framework to Enhance Antifouling and Anti-biofouling Properties of Thin Film Nanocomposite Membranes. ACS applied materials & interfaces. 2018.

- [36] Saberi S, Shamsabadi AA, Shahrooz M, Sadeghi M, Soroush M. Improving the Transport and Antifouling Properties of Poly (vinyl chloride) Hollow-Fiber Ultrafiltration Membranes by Incorporating Silica Nanoparticles. ACS omega. 2018;3:17439-46.
- [37] Rezakazemi M, Shirazian S. Separation Performance of Nanostructured Ceramic Membranes: Analytical Model Development. Journal of Non-Equilibrium Thermodynamics2018. p. 245.
- [38] Rezakazemi M, Mirzaei S, Asghari M, Ivakpour J. Aluminum Oxide Nanoparticles for Highly Efficient Asphaltene Separation from Crude Oil Using Ceramic Membrane Technology. Oil & Gas Science and Technology Rev IFP Energies nouvelles. 2017;72.
- [39] Fasihi M, Shirazian S, Marjani A, Rezakazemi M. Computational fluid dynamics simulation of transport phenomena in ceramic membranes for SO2 separation. Mathematical and Computer Modelling. 2012;56:278-86.
- [40] Shirazian S, Rezakazemi M, Marjani A, Rafivahid MS. Development of a mass transfer model for simulation of sulfur dioxide removal in ceramic membrane contactors. Asia-Pacific Journal of Chemical Engineering. 2011;7:828-34.
- [41] Rehman WU, Muhammad A, Khan QA, Younas M, Rezakazemi M. Pomegranate juice concentration using osmotic distillation with membrane contactor. Separation and Purification Technology. 2019;224:481-9.
- [42] Rezakazemi M, Marjani A, Shirazian S. Organic solvent removal by pervaporation membrane technology: experimental and simulation. Environmental Science and Pollution Research. 2018;25:19818-25.
- [43] Dashti A, Asghari M, Dehghani M, Rezakazemi M, Mohammadi AH, Bhatia SK. Molecular dynamics, grand canonical Monte Carlo and expert simulations and modeling of water—acetic acid pervaporation using polyvinyl alcohol/tetraethyl orthosilicates membrane. Journal of Molecular Liquids. 2018;265:53-68.
- [44] Rezakazemi M, Shahidi K, Mohammadi T. Synthetic PDMS composite membranes for pervaporation dehydration of ethanol. Desalination and Water Treatment. 2015;54:1542-9.
- [45] Esfandiari A, Hosseini Monjezi A, Rezakazemi M, Younas M. Computational fluid dynamic modeling of water desalination using low-energy continuous direct contact membrane distillation process. Applied Thermal Engineering. 2019;163:114391.
- [46] Ayaz M, Muhammad A, Younas M, Khan AL, Rezakazemi M. Enhanced Water Flux by Fabrication of Polysulfone/Alumina Nanocomposite Membrane for Copper(II) Removal. Macromolecular Research. 2019;27:565-71.
- [47] Rezakazemi M, Shirazian S. Gas permeation prediction through polymeric membranes using compressible regular solution theory. International Journal of Hydrogen Energy. 2018;43:22357-64.
- [48] Rezakazemi M, Maghami M, Mohammadi T. Wastewaters treatment containing phenol and ammonium using aerobic submerged membrane bioreactor. Chemistry Central Journal. 2018;12:79.
- [49] Dashti A, Harami HR, Rezakazemi M. Accurate prediction of solubility of gases within H2-selective nanocomposite membranes using committee machine intelligent system. International Journal of Hydrogen Energy. 2018;43:6614-24.
- [50] Tavasoli E, Sadeghi M, Riazi H, Shamsabadi AA, Soroush M. Gas Separation Polysulfone Membranes Modified by Cadmium-based Nanoparticles. Fibers and Polymers. 2018;19:2049-55.
- [51] Rungta M, Wenz GB, Zhang C, Xu L, Qiu W, Adams JS, et al. Carbon molecular sieve structure development and membrane performance relationships. Carbon. 2017;115:237-48.
- [52] Rezakazemi M, Mosavi A, Shirazian S. ANFIS pattern for molecular membranes separation optimization. Journal of Molecular Liquids. 2019;274:470-6.
- [53] Rezakazemi M, Hemmati A, Shirazian S. Cellulose Acetate Polymeric Membrane Fabrication by Nonsolvent-Induced Phase Separation Process: Determination of Velocities of Individual Components. Journal of Non-Equilibrium Thermodynamics2019. p. 71-80.

- [54] Pandey P, Chauhan R. Membranes for gas separation. Progress in Polymer Science. 2001;26:853-93.[55] Wijmans J, Baker R. The solution-diffusion model: a review. Journal of membrane science.1995;107:1-21.
- [56] Najafi M, Sadeghi M, Shamsabadi AA, Dinari M, Soroush M. Polysulfone Membranes Incorporated with Reduced Graphene Oxide Nanoparticles for Enhanced Olefin/Paraffin Separation. ChemistrySelect. 2020;5:3675-81.
- [57] Sadrzadeh M, Rezakazemi M, Mohammadi T. Chapter 19 Fundamentals and Measurement Techniques for Gas Transport in Polymers. In: Thomas S, Wilson R, S AK, George SC, editors. Transport Properties of Polymeric Membranes: Elsevier; 2018. p. 391-423.
- [58] Sridhar S, Smitha B, Aminabhavi TM. Separation of Carbon Dioxide from Natural Gas Mixtures through Polymeric Membranes—A Review. Separation & Purification Reviews. 2007;36:113-74.
- [59] Yavari M, Le T, Lin H. Physical aging of glassy perfluoropolymers in thin film composite membranes. Part I. Gas transport properties. Journal of Membrane Science. 2017;525:387-98.
- [60] Merkel TC, Zhou M, Baker RW. Carbon dioxide capture with membranes at an IGCC power plant. Journal of membrane science. 2012;389:441-50.
- [61] Arabi Shamsabadi A, Pournaghshband Isfahani A, Khoshhal Salestan S, Rahimpour A, Ghalei B, Sivaniah E, et al. Pushing Rubbery Polymer Membranes to be Economic for CO2 Separation: Embedment with Ti3C2Tx MXene Nanosheets. ACS Applied Materials & Interfaces. 2019.
- [62] Livingston A, Baker R. Membranes from academia to industry. Nat Mater. 2017;16:280-2.
- [63] Shamsabadi AA, Behbahani RM, Seidi F, Soroush M. Physical aging of polyetherimide membranes. Journal of Natural Gas Science and Engineering. 2015;27:651-60.
- [64] Robeson LM. The upper bound revisited. Journal of Membrane Science. 2008;320:390-400.
- [65] Freeman BD. Basis of permeability/selectivity tradeoff relations in polymeric gas separation membranes. Macromolecules. 1999;32:375-80.
- [66] Shamsipur H, Dawood BA, Budd PM, Bernardo P, Clarizia G, Jansen JC. Thermally rearrangeable PIM-polyimides for gas separation membranes. Macromolecules. 2014;47:5595-606.
- [67] Ogieglo W, Puspasari T, Ma X, Pinnau I. Sub-100 nm carbon molecular sieve membranes from a polymer of intrinsic microporosity precursor: Physical aging and near-equilibrium gas separation properties. Journal of Membrane Science. 2020;597:117752.
- [68] Shamsabadi AA, Riazi H, Soroush M. Mixed Matrix Membranes for CO2 Separations: Membrane Preparation, Properties, and Separation Performance Evaluation. Current Trends and Future Developments on (Bio-) Membranes: Elsevier; 2018. p. 103-53.
- [69] Sadeghi M, Isfahani AP, Shamsabadi AA, Favakeh S, Soroush M. Improved gas transport properties of polyurethane—urea membranes through incorporating a cadmium-based metal organic framework. Journal of Applied Polymer Science. 2019:48704.
- [70] Sadeghi M, Shamsabadi AA, Ronasi A, Isfahani AP, Dinari M, Soroush M. Engineering the dispersion of nanoparticles in polyurethane membranes to control membrane physical and transport properties. Chemical Engineering Science. 2018;192:688-98.
- [71] Swaidan R, Ghanem B, Al-Saeedi M, Litwiller E, Pinnau I. Role of intrachain rigidity in the plasticization of intrinsically microporous triptycene-based polyimide membranes in mixed-gas CO2/CH4 separations. Macromolecules. 2014;47:7453-62.
- [72] Budd PM, Elabas ES, Ghanem BS, Makhseed S, McKeown NB, Msayib KJ, et al. Solution-processed, organophilic membrane derived from a polymer of intrinsic microporosity. Advanced Materials. 2004;16:456-9.
- [73] McKeown NB, Budd PM, Msayib KJ, Ghanem BS, Kingston HJ, Tattershall CE, et al. Polymers of intrinsic microporosity (PIMs): bridging the void between microporous and polymeric materials. Chemistry-A European Journal. 2005;11:2610-20.

- [74] Jue ML, Lively RP. Targeted gas separations through polymer membrane functionalization. Reactive and Functional Polymers. 2015;86:88-110.
- [75] Gemeda AE, De Angelis MG, Du N, Li N, Guiver MD, Sarti GC. Mixed gas sorption in glassy polymeric membranes. III. CO 2/CH 4 mixtures in a polymer of intrinsic microporosity (PIM-1): Effect of temperature. Journal of Membrane Science. 2017;524:746-57.
- [76] Vopička O, De Angelis MG, Du N, Li N, Guiver MD, Sarti GC. Mixed gas sorption in glassy polymeric membranes: II. CO 2/CH 4 mixtures in a polymer of intrinsic microporosity (PIM-1). Journal of Membrane Science. 2014;459:264-76.
- [77] Tiwari RR, Jin J, Freeman B, Paul D. Physical aging, CO 2 sorption and plasticization in thin films of polymer with intrinsic microporosity (PIM-1). Journal of Membrane Science. 2017;537:362-71.
- [78] Li P, Chung T, Paul D. Gas sorption and permeation in PIM-1. Journal of membrane science. 2013;432:50-7.
- [79] McKeown NB, Budd PM. Polymers of intrinsic microporosity (PIMs): organic materials for membrane separations, heterogeneous catalysis and hydrogen storage. Chemical Society Reviews. 2006;35:675-83.
- [80] Satilmis B, Lanč M, Fuoco A, Rizzuto C, Tocci E, Bernardo P, et al. Temperature and pressure dependence of gas permeation in amine-modified PIM-1. Journal of Membrane Science. 2018;555:483-96
- [81] Bhavsar RS, Mitra T, Adams DJ, Cooper AI, Budd PM. Ultrahigh-permeance PIM-1 based thin film nanocomposite membranes on PAN supports for CO2 separation. Journal of Membrane Science. 2018.
- [82] Liang CZ, Liu JT, Lai J-Y, Chung T-S. High-performance multiple-layer PIM composite hollow fiber membranes for gas separation. Journal of Membrane Science. 2018.
- [83] Jue ML, Breedveld V, Lively RP. Defect-free PIM-1 hollow fiber membranes. Journal of Membrane Science. 2017;530:33-41.
- [84] McKeown NB. Polymers of intrinsic microporosity. ISRN Materials Science. 2012;2012.
- [85] McKeown NB. Polymer membranes: Contorted separation. Nature materials. 2016;15:706-7.
- [86] Vopička O, Friess K, Hynek V, Sysel P, Zgažar M, Šípek M, et al. Equilibrium and transient sorption of vapours and gases in the polymer of intrinsic microporosity PIM-1. Journal of membrane science. 2013;434:148-60.
- [87] Genduso G, Ghanem BS, Wang Y, Pinnau I. Synthesis and Gas-Permeation Characterization of a Novel High-Surface Area Polyamide Derived from 1, 3, 6, 8-Tetramethyl-2, 7-diaminotriptycene: Towards Polyamides of Intrinsic Microporosity (PIM-PAs). Polymers. 2019;11:361.
- [88] Comesaña-Gándara B, Chen J, Bezzu CG, Carta M, Rose I, Ferrari M-C, et al. Redefining the Robeson upper bounds for CO 2/CH 4 and CO 2/N 2 separations using a series of ultrapermeable benzotriptycene-based polymers of intrinsic microporosity. Energy & Environmental Science. 2019.
- [89] Wang Y, Ma X, Ghanem B, Alghunaimi F, Pinnau I, Han Y. Polymers of intrinsic microporosity for energy-intensive membrane-based gas separations. Materials Today Nano. 2018;3:69-95.
- [90] Swaidan R, Ghanem B, Pinnau I. Fine-tuned intrinsically ultramicroporous polymers redefine the permeability/selectivity upper bounds of membrane-based air and hydrogen separations. ACS Publications; 2015.
- [91] Rezakazemi M, Sadrzadeh M, Matsuura T. Thermally stable polymers for advanced high-performance gas separation membranes. Progress in Energy and Combustion Science. 2018;66:1-41.
- [92] Low Z-X, Budd PM, McKeown NB, Patterson DA. Gas permeation properties, physical aging, and its mitigation in high free volume glassy polymers. Chemical reviews. 2018;118:5871-911.
- [93] Low Z-X, Budd PM, McKeown NB, Patterson DA. Gas Permeation Properties, Physical Aging, and Its Mitigation in High Free Volume Glassy Polymers. Chemical reviews. 2018.
- [94] Kim S, Lee YM. Rigid and microporous polymers for gas separation membranes. Progress in Polymer Science. 2015;43:1-32.

- [95] Jimenez-Solomon MF, Song Q, Jelfs KE, Munoz-Ibanez M, Livingston AG. Polymer nanofilms with enhanced microporosity by interfacial polymerization. Nature materials. 2016;15:760-7.
- [96] Wang S, Li X, Wu H, Tian Z, Xin Q, He G, et al. Advances in high permeability polymer-based membrane materials for CO 2 separations. Energy & Environmental Science. 2016;9:1863-90.
- [97] Ghanem B, Alghunaimi F, Alaslai N, Ma X, Pinnau I. New phenazine-containing ladder polymer of intrinsic microporosity from a spirobisindane-based AB-type monomer. RSC Advances. 2016;6:79625-30.
- [98] Du N, Robertson GP, Song J, Pinnau I, Thomas S, Guiver MD. Polymers of intrinsic microporosity containing trifluoromethyl and phenylsulfone groups as materials for membrane gas separation. Macromolecules. 2008;41:9656-62.
- [99] Du N, Robertson GP, Pinnau I, Guiver MD. Polymers of intrinsic microporosity derived from novel disulfone-based monomers. Macromolecules. 2009;42:6023-30.
- [100] Du N, Robertson GP, Pinnau I, Guiver MD. Polymers of intrinsic microporosity with dinaphthyl and thianthrene segments. Macromolecules. 2010;43:8580-7.
- [101] Bezzu CG, Carta M, Tonkins A, Jansen JC, Bernardo P, Bazzarelli F, et al. A Spirobifluorene-Based Polymer of Intrinsic Microporosity with Improved Performance for Gas Separation. Advanced Materials. 2012;24:5930-3.
- [102] Bezzu CG, Carta M, Ferrari M-C, Jansen JC, Monteleone M, Esposito E, et al. The synthesis, chain-packing simulation and long-term gas permeability of highly selective spirobifluorene-based polymers of intrinsic microporosity. Journal of Materials Chemistry A. 2018.
- [103] Bezzu CG, Carta M, Ferrari M-C, Jansen JC, Monteleone M, Esposito E, et al. The synthesis, chain-packing simulation and long-term gas permeability of highly selective spirobifluorene-based polymers of intrinsic microporosity. Journal of Materials Chemistry A. 2018;6:10507-14.
- [104] Short R, Carta M, Bezzu CG, Fritsch D, Kariuki BM, McKeown NB. Hexaphenylbenzene-based polymers of intrinsic microporosity. Chemical Communications. 2011;47:6822-4.
- [105] Carta M, Bernardo P, Clarizia G, Jansen JC, McKeown NB. Gas permeability of hexaphenylbenzene based polymers of intrinsic microporosity. Macromolecules. 2014;47:8320-7.
- [106] Halim J, Kota S, Lukatskaya MR, Naguib M, Zhao MQ, Moon EJ, et al. Synthesis and characterization of 2D molybdenum carbide (MXene). Advanced Functional Materials. 2016;26:3118-27. [107] Wang ZG, Liu X, Wang D, Jin J. Tröger's base-based copolymers with intrinsic microporosity for CO 2 separation and effect of Tröger's base on separation performance. Polymer Chemistry. 2014;5:2793-
- [108] Du N, Robertson GP, Pinnau I, Thomas S, Guiver MD. Copolymers of Intrinsic Microporosity Based on 2, 2', 3, 3'-Tetrahydroxy-1, 1'-dinaphthyl. Macromolecular rapid communications. 2009;30:584-8.
- [109] Rose I, Bezzu CG, Carta M, Comesaña-Gándara B, Lasseuguette E, Ferrari MC, et al. Polymer ultrapermeability from the inefficient packing of 2D chains. Nature materials. 2017;16:932-7.
- [110] Yin Y, Guiver MD. Microporous polymers: Ultrapermeable membranes. Nature materials. 2017:16:880.

800.

- [111] He Y, Benedetti FM, Lin S, Liu C, Zhao Y, Ye HZ, et al. Polymers with side chain porosity for ultrapermeable and plasticization resistant materials for gas separations. Advanced Materials. 2019;31:1807871.
- [112] Ghanem BS, Swaidan R, Ma X, Litwiller E, Pinnau I. Energy-efficient hydrogen separation by AB-type ladder-polymer molecular sieves. Advanced Materials. 2014;26:6696-700.
- [113] Xiao Y, Zhang L, Xu L, Chung T-S. Molecular design of Tröger's base-based polymers with intrinsic microporosity for gas separation. Journal of Membrane Science. 2017;521:65-72.
- [114] Carta M, Malpass-Evans R, Croad M, Rogan Y, Jansen JC, Bernardo P, et al. An efficient polymer molecular sieve for membrane gas separations. Science. 2013;339:303-7.

- [115] Zhou J, Zhu X, Hu J, Liu H, Hu Y, Jiang J. Mechanistic insight into highly efficient gas permeation and separation in a shape-persistent ladder polymer membrane. Physical Chemistry Chemical Physics. 2014:16:6075-83.
- [116] Alghunaimi F, Ghanem B, Alaslai N, Swaidan R, Litwiller E, Pinnau I. Gas permeation and physical aging properties of iptycene diamine-based microporous polyimides. Journal of Membrane Science. 2015;490:321-7.
- [117] Carta M, Croad M, Malpass-Evans R, Jansen JC, Bernardo P, Clarizia G, et al. Triptycene induced enhancement of membrane gas selectivity for microporous Tröger's base polymers. Advanced Materials. 2014;26:3526-31.
- [118] Rose I, Carta M, Malpass-Evans R, Ferrari M-C, Bernardo P, Clarizia G, et al. Highly permeable benzotriptycene-based polymer of intrinsic microporosity. ACS Macro Letters. 2015;4:912-5.
- [119] Ghanem BS, Hashem M, Harris KD, Msayib KJ, Xu M, Budd PM, et al. Triptycene-based polymers of intrinsic microporosity: organic materials that can be tailored for gas adsorption. Macromolecules. 2010;43:5287-94.
- [120] Williams R, Burt LA, Esposito E, Jansen JC, Tocci E, Rizzuto C, et al. A highly rigid and gas selective methanopentacene-based polymer of intrinsic microporosity derived from Tröger's base polymerization. Journal of Materials Chemistry A. 2018;6:5661-7.
- [121] Ghanem BS, McKeown NB, Budd PM, Fritsch D. Polymers of intrinsic microporosity derived from bis (phenazyl) monomers. Macromolecules. 2008;41:1640-6.
- [122] Ghanem B, Alaslai N, Miao X, Pinnau I. Novel 6FDA-based polyimides derived from sterically hindered Tröger's base diamines: Synthesis and gas permeation properties. Polymer. 2016;96:13-9.
- [123] Zhang J, Kang H, Martin J, Zhang S, Thomas S, Merkel TC, et al. The enhancement of chain rigidity and gas transport performance of polymers of intrinsic microporosity via intramolecular locking of the spiro-carbon. Chemical Communications. 2016;52:6553-6.
- [124] Comesaña-Gándara B, Chen J, Bezzu CG, Carta M, Rose I, Ferrari M-C, et al. Redefining the Robeson upper bounds for CO 2/CH 4 and CO 2/N 2 separations using a series of ultrapermeable benzotriptycene-based polymers of intrinsic microporosity. Energy & Environmental Science. 2019;12:2733-40.
- [125] Swaidan R, Al-Saeedi M, Ghanem B, Litwiller E, Pinnau I. Rational design of intrinsically ultramicroporous polyimides containing bridgehead-substituted triptycene for highly selective and permeable gas separation membranes. Macromolecules. 2014;47:5104-14.
- [126] Rogan Y, Starannikova L, Ryzhikh V, Yampolskii Y, Bernardo P, Bazzarelli F, et al. Synthesis and gas permeation properties of novel spirobisindane-based polyimides of intrinsic microporosity. Polymer Chemistry. 2013;4:3813-20.
- [127] Luo S, Liu Q, Zhang B, Wiegand JR, Freeman BD, Guo R. Pentiptycene-based polyimides with hierarchically controlled molecular cavity architecture for efficient membrane gas separation. Journal of Membrane Science. 2015;480:20-30.
- [128] Lee M, Bezzu CG, Carta M, Bernardo P, Clarizia G, Jansen JC, et al. Enhancing the Gas Permeability of Tröger's Base Derived Polyimides of Intrinsic Microporosity. Macromolecules. 2016;49:4147-54. [129] Ghanem B, Alghunaimi F, Ma X, Alaslai N, Pinnau I. Synthesis and characterization of novel triptycene dianhydrides and polyimides of intrinsic microporosity based on 3, 3'-dimethylnaphthidine. Polymer. 2016;101:225-32.
- [130] Ma X, Mukaddam M, Pinnau I. Bifunctionalized Intrinsically Microporous Polyimides with Simultaneously Enhanced Gas Permeability and Selectivity. Macromolecular rapid communications. 2016;37:900-4.
- [131] Abdulhamid MA, Lai HW, Wang Y, Jin Z, Teo YC, Ma X, et al. Microporous Polyimides from Ladder Diamines Synthesized by Facile Catalytic Arene–Norbornene Annulation as High-Performance Membranes for Gas Separation. Chemistry of Materials. 2019;31:1767-74.

- [132] Sydlik SA, Chen Z, Swager TM. Triptycene polyimides: soluble polymers with high thermal stability and low refractive indices. Macromolecules. 2011;44:976-80.
- [133] Wiegand JR, Smith ZP, Liu Q, Patterson CT, Freeman BD, Guo R. Synthesis and characterization of triptycene-based polyimides with tunable high fractional free volume for gas separation membranes. Journal of Materials Chemistry A. 2014;2:13309-20.
- [134] Weidman JR, Guo R. The Use of Iptycenes in Rational Macromolecular Design for Gas Separation Membrane Applications. Industrial & Engineering Chemistry Research. 2017;56:4220-36.
- [135] Weidman JR, Luo S, Zhang Q, Guo R. Structure manipulation in triptycene-based polyimides through main chain geometry variation and its effect on gas transport properties. Industrial & Engineering Chemistry Research. 2017;56:1868-79.
- [136] Weidman JR, Luo S, Breier JM, Buckley P, Gao P, Guo R. Triptycene-based copolyimides with tailored backbone rigidity for enhanced gas transport. Polymer. 2017.
- [137] Pournaghshband Isfahani A, Sadeghi M, Wakimoto K, Shrestha BB, Bagheri R, Sivaniah E, et al. Pentiptycene-based polyurethane with enhanced mechanical properties and CO2-plasticization resistance for thin film gas separation membranes. ACS applied materials & interfaces. 2018;10:17366-74.
- [138] Luo S, Stevens KA, Park JS, Moon JD, Liu Q, Freeman BD, et al. Highly CO2-selective gas separation membranes based on segmented copolymers of poly (ethylene oxide) reinforced with pentiptycene-containing polyimide hard segments. ACS applied materials & interfaces. 2016;8:2306-17.
- [139] Ma X, Salinas O, Litwiller E, Pinnau I. Novel spirobifluorene-and dibromospirobifluorene-based polyimides of intrinsic microporosity for gas separation applications. Macromolecules. 2013;46:9618-24. [140] Wang Z, Wang D, Zhang F, Jin J. Tröger's Base-Based Microporous Polyimide Membranes for High-Performance Gas Separation. ACS Macro Letters. 2014;3:597-601.
- [141] Zhuang Y, Seong JG, Do YS, Jo HJ, Cui Z, Lee J, et al. Intrinsically microporous soluble polyimides incorporating tröger's base for membrane gas separation. Macromolecules. 2014;47:3254-62.
- [142] Zhuang Y, Seong JG, Do YS, Lee WH, Lee MJ, Cui Z, et al. Soluble, microporous, Tröger's Base copolyimides with tunable membrane performance for gas separation. Chemical Communications. 2016;52:3817-20.
- [143] Zhuang Y, Seong JG, Do YS, Lee WH, Lee MJ, Guiver MD, et al. High-strength, soluble polyimide membranes incorporating Tröger's Base for gas separation. Journal of Membrane Science. 2016;504:55-65.
- [144] Weidman JR, Luo S, Doherty CM, Hill AJ, Gao P, Guo R. Analysis of governing factors controlling gas transport through fresh and aged triptycene-based polyimide films. Journal of Membrane Science. 2017;522:12-22.
- [145] Lee M, Bezzu CG, Carta M, Bernardo P, Clarizia G, Jansen JC, et al. Enhancing the gas permeability of Troger's base derived polyimides of intrinsic microporosity. Macromolecules. 2016;49:4147-54.
- [146] Wang Z, Wang D, Zhang F, Jin J. Troger's base-based microporous polyimide membranes for high-performance gas separation. ACS Macro Letters. 2014;3:597-601.
- [147] Ma X, Salinas O, Litwiller E, Pinnau I. Pristine and thermally-rearranged gas separation membranes from novel o-hydroxyl-functionalized spirobifluorene-based polyimides. Polymer Chemistry. 2014;5:6914-22.
- [148] Du N, Song J, Robertson GP, Pinnau I, Guiver MD. Linear High Molecular Weight Ladder Polymer via Fast Polycondensation of 5, 5', 6, 6'-Tetrahydroxy-3, 3, 3', 3'-tetramethylspirobisindane with 1, 4-Dicyanotetrafluorobenzene. Macromolecular Rapid Communications. 2008;29:783-8.
- [149] Ghanem BS, McKeown NB, Budd PM, Al-Harbi NM, Fritsch D, Heinrich K, et al. Synthesis, characterization, and gas permeation properties of a novel group of polymers with intrinsic microporosity: PIM-polyimides. Macromolecules. 2009;42:7881-8.

- [150] Rogan Y, Malpass-Evans R, Carta M, Lee M, Jansen JC, Bernardo P, et al. A highly permeable polyimide with enhanced selectivity for membrane gas separations. Journal of Materials Chemistry A. 2014;2:4874-7.
- [151] Ghanem BS, Swaidan R, Litwiller E, Pinnau I. Ultra-Microporous Triptycene-based Polyimide Membranes for High-Performance Gas Separation. Advanced Materials. 2014;26:3688-92.
- [152] Shamsabadi AA, Seidi F, Nozari M, Soroush M. A New Pentiptycene-Based Dianhydride and Its High-Free-Volume Polymer for Carbon Dioxide Removal. ChemSusChem. 2018;11:472-82.
- [153] Ma X, Ghanem B, Salines O, Litwiller E, Pinnau I. Synthesis and effect of physical aging on gas transport properties of a microporous polyimide derived from a novel spirobifluorene-based dianhydride. ACS Macro Letters. 2015;4:231-5.
- [154] Shamsabadi AA, Seidi F, Salehi E, Nozari M, Rahimpour A, Soroush M. Efficient CO 2-removal using novel mixed-matrix membranes with modified TiO 2 nanoparticles. Journal of Materials Chemistry A. 2017;5:4011-25.
- [155] Ma X, Pinnau I. Effect of Film Thickness and Physical Aging on "Intrinsic" Gas Permeation Properties of Microporous Ethanoanthracene-Based Polyimides. Macromolecules. 2018.
- [156] Alghunaimi F, Ghanem B, Alaslai N, Mukaddam M, Pinnau I. Triptycene dimethyl-bridgehead dianhydride-based intrinsically microporous hydroxyl-functionalized polyimide for natural gas upgrading. Journal of Membrane Science. 2016;520:240-6.
- [157] Luo S, Wiegand JR, Kazanowska B, Doherty CM, Konstas K, Hill AJ, et al. Finely tuning the free volume architecture in iptycene-containing polyimides for highly selective and fast hydrogen transport. Macromolecules. 2016;49:3395-405.
- [158] Ghanem BS, McKeown NB, Budd PM, Selbie JD, Fritsch D. High-performance membranes from polyimides with intrinsic microporosity. Advanced Materials. 2008;20:2766-71.
- [159] Ma X, Abdulhamid MA, Pinnau I. Design and synthesis of polyimides based on carbocyclic pseudo-Troger's base-derived dianhydrides for membrane gas separation applications. Macromolecules. 2017;50:5850-7.
- [160] Abbott LJ, Hughes JE, Colina CM. Virtual synthesis of thermally cross-linked copolymers from a novel implementation of polymatic. The Journal of Physical Chemistry B. 2014;118:1916-24.
- [161] Li FY, Xiao Y, Chung T-S, Kawi S. High-performance thermally self-cross-linked polymer of intrinsic microporosity (PIM-1) membranes for energy development. Macromolecules. 2012;45:1427-37.
- [162] Song Q, Cao S, Pritchard RH, Ghalei B, Al-Muhtaseb SA, Terentjev EM, et al. Controlled thermal oxidative crosslinking of polymers of intrinsic microporosity towards tunable molecular sieve membranes. Nature communications. 2014;5:4813.
- [163] Du N, Dal-Cin MM, Robertson GP, Guiver MD. Decarboxylation-induced cross-linking of polymers of intrinsic microporosity (PIMs) for membrane gas separation. Macromolecules. 2012;45:5134-9.
- [164] Sridhar S, Smitha B, Mayor S, Prathab B, Aminabhavi TM. Gas permeation properties of polyamide membrane prepared by interfacial polymerization. Journal of Materials Science. 2007;42:9392-401.
- [165] Park HB, Jung CH, Lee YM, Hill AJ, Pas SJ, Mudie ST, et al. Polymers with cavities tuned for fast selective transport of small molecules and ions. Science. 2007;318:254-8.
- [166] Liu J, Hou X, Park HB, Lin H. High-Performance Polymers for Membrane CO2/N2 Separation. Chemistry-A European Journal. 2016;22:15980-90.
- [167] Smith ZP, Sanders DF, Ribeiro CP, Guo R, Freeman BD, Paul DR, et al. Gas sorption and characterization of thermally rearranged polyimides based on 3, 3'-dihydroxy-4, 4'-diamino-biphenyl (HAB) and 2, 2'-bis-(3, 4-dicarboxyphenyl) hexafluoropropane dianhydride (6FDA). Journal of membrane science. 2012;415:558-67.
- [168] Do YS, Seong JG, Kim S, Lee JG, Lee YM. Thermally rearranged (TR) poly (benzoxazole-co-amide) membranes for hydrogen separation derived from 3, 3'-dihydroxy-4, 4'-diamino-biphenyl (HAB), 4, 4'-oxydianiline (ODA) and isophthaloyl chloride (IPCI). Journal of membrane science. 2013;446:294-302.

- [169] Scholes CA, Ribeiro CP, Kentish SE, Freeman BD. Thermal rearranged poly (benzoxazole-co-imide) membranes for CO 2 separation. Journal of Membrane Science. 2014;450:72-80.
- [170] Jo HJ, Soo CY, Dong G, Do YS, Wang HH, Lee MJ, et al. Thermally rearranged poly (benzoxazole-coimide) membranes with superior mechanical strength for gas separation obtained by tuning chain rigidity. Macromolecules. 2015;48:2194-202.
- [171] Kushwaha A, Dose ME, Smith ZP, Luo S, Freeman BD, Guo R. Preparation and properties of polybenzoxazole-based gas separation membranes: A comparative study between thermal rearrangement (TR) of poly (hydroxyimide) and thermal cyclodehydration of poly (hydroxyamide). Polymer. 2015;78:81-93.
- [172] Liaw D-J, Wang K-L, Huang Y-C, Lee K-R, Lai J-Y, Ha C-S. Advanced polyimide materials: syntheses, physical properties and applications. Progress in Polymer Science. 2012;37:907-74.
- [173] Li S, Jo HJ, Han SH, Park CH, Kim S, Budd PM, et al. Mechanically robust thermally rearranged (TR) polymer membranes with spirobisindane for gas separation. Journal of membrane science. 2013;434:137-47.
- [174] Han SH, Misdan N, Kim S, Doherty CM, Hill AJ, Lee YM. Thermally rearranged (TR) polybenzoxazole: effects of diverse imidization routes on physical properties and gas transport behaviors. Macromolecules. 2010;43:7657-67.
- [175] Han SH, Kwon HJ, Kim KY, Seong JG, Park CH, Kim S, et al. Tuning microcavities in thermally rearranged polymer membranes for CO 2 capture. Physical chemistry chemical physics. 2012;14:4365-73.
- [176] Soo CY, Jo HJ, Lee YM, Quay JR, Murphy MK. Effect of the chemical structure of various diamines on the gas separation of thermally rearranged poly (benzoxazole-co-imide)(TR-PBO-co-I) membranes. Journal of membrane science. 2013;444:365-77.
- [177] Swaidan R, Ma X, Litwiller E, Pinnau I. High pressure pure-and mixed-gas separation of CO 2/CH 4 by thermally-rearranged and carbon molecular sieve membranes derived from a polyimide of intrinsic microporosity. Journal of membrane science. 2013;447:387-94.
- [178] Ma X, Ghanem BS, Pinnau I. O-hydroxy-functionalized diamines, polyimides, methods of making each, and methods of use. Google Patents; 2015.
- [179] Alghunaimi F, Ghanem B, Wang Y, Salinas O, Alaslai N, Pinnau I. Synthesis and gas permeation properties of a novel thermally-rearranged polybenzoxazole made from an intrinsically microporous hydroxyl-functionalized triptycene-based polyimide precursor. Polymer. 2017.
- [180] Fuoco A, Rizzuto C, Tocci E, Monteleone M, Esposito E, Budd PM, et al. The origin of size-selective gas transport through polymers of intrinsic microporosity. Journal of Materials Chemistry A. 2019;7:20121-6.
- [181] Fu S, Sanders ES, Kulkarni S, Chu Y-H, Wenz GB, Koros WJ. The Significance of Entropic Selectivity in Carbon Molecular Sieve Membranes Derived from 6FDA/DETDA: DABA (3: 2) Polyimide. Journal of Membrane Science. 2017.
- [182] Fu S, Wenz GB, Sanders ES, Kulkarni SS, Qiu W, Ma C, et al. Effects of pyrolysis conditions on gas separation properties of 6FDA/DETDA: DABA (3: 2) derived carbon molecular sieve membranes. Journal of Membrane Science. 2016;520:699-711.
- [183] Fu S, Sanders ES, Kulkarni SS, Wenz GB, Koros WJ. Temperature dependence of gas transport and sorption in carbon molecular sieve membranes derived from four 6FDA based polyimides: Entropic selectivity evaluation. Carbon. 2015;95:995-1006.
- [184] Ma X, Swaidan R, Teng B, Tan H, Salinas O, Litwiller E, et al. Carbon molecular sieve gas separation membranes based on an intrinsically microporous polyimide precursor. Carbon. 2013;62:88-96.
- [185] Zhang J, Schott JA, Mahurin SM, Dai S. Porous Structure Design of Polymeric Membranes for Gas Separation. Small Methods. 2017.

- [186] Zhao H, Feng L, Ding X, Tan X, Zhang Y. Gas permeation properties of a metallic ion-cross-linked PIM-1 thin-film composite membrane supported on a UV-cross-linked porous substrate. Chinese Journal of Chemical Engineering. 2018.
- [187] Song Q, Cao S, Zavala-Rivera P, Lu LP, Li W, Ji Y, et al. Photo-oxidative enhancement of polymeric molecular sieve membranes. Nature communications. 2013;4:1918.
- [188] Li FY, Xiao Y, Ong YK, Chung TS. UV-Rearranged PIM-1 Polymeric Membranes for Advanced Hydrogen Purification and Production. Advanced Energy Materials. 2012;2:1456-66.
- [189] Vogiatzis KD, Mavrandonakis A, Klopper W, Froudakis GE. Ab initio Study of the Interactions between CO2 and N-Containing Organic Heterocycles. ChemPhysChem. 2009;10:374-83.
- [190] Patel HA, Yavuz CT. Noninvasive functionalization of polymers of intrinsic microporosity for enhanced CO 2 capture. Chemical Communications. 2012;48:9989-91.
- [191] Noble RD. Generalized microscopic mechanism of facilitated transport in fixed site carrier membranes. Journal of membrane science. 1992;75:121-9.
- [192] Seidi F, Salimi H, Shamsabadi AA, Shabanian M. Synthesis of hybrid materials using graft copolymerization on non-cellulosic polysaccharides via homogenous ATRP. Progress in Polymer Science. 2017.
- [193] Seidi F, Salarabadi MB, Saedi S, Modadi L, Shamsabadi AA, Nikravesh B. Introduction of a novel amino-agarose (AAG) derivative as a fixed facilitated transport carrier to prepare newly asymmetric PES/AAG membranes for CO2 removal. Greenhouse Gases: Science and Technology. 2015;5:701-13. [194] Bai H, Ho WW. Carbon dioxide-selective facilitated transport membranes for hydrogen purification. Production and Purification of Ultraclean Transportation Fuels: ACS Publications; 2011. p. 115-41.
- [195] Saedi S, Madaeni SS, Seidi F, Shamsabadi AA, Laki S. Fixed facilitated transport of CO 2 through integrally-skinned asymmetric polyethersulfone membrane using a novel synthesized Poly (acrylonitrile-co-N, N-Dimethylaminopropyl acrylamide). Chemical Engineering Journal. 2014;236:263-73. [196] Jeon JW, Kim D-G, Sohn E-h, Yoo Y, Kim YS, Kim BG, et al. Highly Carboxylate-Functionalized Polymers of Intrinsic Microporosity for CO2-Selective Polymer Membranes. Macromolecules. 2017;50:8019-27.
- [197] Du N, Robertson GP, Song J, Pinnau I, Guiver MD. High-performance carboxylated polymers of intrinsic microporosity (PIMs) with tunable gas transport properties. Macromolecules. 2009;42:6038-43. [198] Du N, Guiver MD, Robertson GP, Song J. Carboxylated polymers of intrinsic microporosity (PIMs) with tunable gas transport properties. Google Patents; 2014.
- [199] Wu W-H, Thomas P, Hume P, Jin J. Effective Conversion of Amide to Carboxylic Acid on Polymers of Intrinsic Microporosity (PIM-1) with Nitrous Acid. Membranes. 2018;8:20.
- [200] Swaidan R, Ghanem BS, Litwiller E, Pinnau I. Pure-and mixed-gas CO 2/CH 4 separation properties of PIM-1 and an amidoxime-functionalized PIM-1. Journal of Membrane Science. 2014;457:95-102.
- [201] Du N, Park HB, Robertson GP, Dal-Cin MM, Visser T, Scoles L, et al. Polymer nanosieve membranes for CO2-capture applications. Nature materials. 2011;10:372.
- [202] Du N, Robertson GP, Dal-Cin MM, Scoles L, Guiver MD. Polymers of intrinsic microporosity (PIMs) substituted with methyl tetrazole. Polymer. 2012;53:4367-72.
- [203] Mason CR, Maynard-Atem L, Heard KW, Satilmis B, Budd PM, Friess K, et al. Enhancement of CO2 affinity in a polymer of intrinsic microporosity by amine modification. Macromolecules. 2014;47:1021-9. [204] Mason CR, Maynard-Atem L, Al-Harbi NM, Budd PM, Bernardo P, Bazzarelli F, et al. Polymer of intrinsic microporosity incorporating thioamide functionality: preparation and gas transport properties. Macromolecules. 2011;44:6471-9.
- [205] Swaidan R, Ghanem BS, Litwiller E, Pinnau I. Pure-and mixed-gas CO2/CH4 separation properties of PIM-1 and an amidoxime-functionalized PIM-1. Journal of membrane science. 2014;457:95-102.

- [206] Song Q, Cao S, Pritchard RH, Ghalei B, Al-Muhtaseb SA, Terentjev EM, et al. Controlled thermal oxidative crosslinking of polymers of intrinsic microporosity towards tunable molecular sieve membranes. Nature communications. 2014;5:1-12.
- [207] Song Q, Cao S, Zavala-Rivera P, Lu LP, Li W, Ji Y, et al. Photo-oxidative enhancement of polymeric molecular sieve membranes. Nature communications. 2013;4:1-9.
- [208] Fritsch D, Bengtson G, Carta M, McKeown NB. Synthesis and gas permeation properties of Spirobischromane-Based polymers of intrinsic microporosity. Macromolecular Chemistry and Physics. 2011;212:1137-46.
- [209] Luo S, Liu J, Lin H, Kazanowska BA, Hunckler MD, Roeder RK, et al. Preparation and gas transport properties of triptycene-containing polybenzoxazole (PBO)-based polymers derived from thermal rearrangement (TR) and thermal cyclodehydration (TC) processes. Journal of Materials Chemistry A. 2016;4:17050-62.
- [210] Alghunaimi F, Ghanem B, Wang Y, Salinas O, Alaslai N, Pinnau I. Synthesis and gas permeation properties of a novel thermally-rearranged polybenzoxazole made from an intrinsically microporous hydroxyl-functionalized triptycene-based polyimide precursor. Polymer. 2017;121:9-16.
- [211] Saedi S, Madaeni SS, Hassanzadeh K, Shamsabadi AA, Laki S. The effect of polyurethane on the structure and performance of PES membrane for separation of carbon dioxide from methane. Journal of Industrial and Engineering Chemistry. 2014;20:1916-29.
- [212] Saedi S, Madaeni SS, Shamsabadi AA. Fabrication of asymmetric polyethersulfone membranes for separation of carbon dioxide from methane using polyetherimide as polymeric additive. Chemical Engineering Research and Design. 2014;92:2431-8.
- [213] Halder K, Khan MM, Grünauer J, Shishatskiy S, Abetz C, Filiz V, et al. Blend membranes of ionic liquid and polymers of intrinsic microporosity with improved gas separation characteristics. Journal of Membrane Science. 2017;539:368-82.
- [214] Saedi S, Madaeni SS, Seidi F, Shamsabadi AA, Laki S. Synthesis and application of a novel Amino-Starch derivative as a new polymeric additive for fixed facilitated transport of carbon dioxide through an asymmetric polyethersulfone (PES) membrane. International Journal of Greenhouse Gas Control. 2013;19:126-37.
- [215] Robeson LM. Polymer blends in membrane transport processes. Industrial & engineering chemistry research. 2010;49:11859-65.
- [216] Paul DR. Gas transport in homogeneous multicomponent polymers. Journal of membrane Science. 1984;18:75-86.
- [217] Yong W, Li F, Xiao Y, Li P, Pramoda K, Tong Y, et al. Molecular engineering of PIM-1/Matrimid blend membranes for gas separation. Journal of membrane science. 2012;407:47-57.
- [218] Hao L, Li P, Chung T-S. PIM-1 as an organic filler to enhance the gas separation performance of Ultem polyetherimide. Journal of Membrane Science. 2014;453:614-23.
- [219] Hao L, Zuo J, Chung TS. Formation of defect-free polyetherimide/PIM-1 hollow fiber membranes for gas separation. AIChE Journal. 2014;60:3848-58.
- [220] Sekizkardes AK, Kusuma VA, McNally JS, Gidley DW, Resnik K, Venna SR, et al. Microporous polymeric composite membranes with advanced film properties: pore intercalation yields excellent CO 2 separation performance. Journal of Materials Chemistry A. 2018;6:22472-7.
- [221] Zhao S, Liao J, Li D, Wang X, Li N. Blending of compatible polymer of intrinsic microporosity (PIM-1) with Tröger's Base polymer for gas separation membranes. Journal of Membrane Science. 2018;566:77-86.
- [222] Yong WF, Li FY, Chung TS, Tong YW. Molecular interaction, gas transport properties and plasticization behavior of cPIM-1/Torlon blend membranes. Journal of Membrane Science. 2014;462:119-30.

- [223] Yong WF, Chung T-S. Miscible blends of carboxylated polymers of intrinsic microporosity (cPIM-1) and Matrimid. Polymer. 2015;59:290-7.
- [224] Esposito E, Mazzei I, Monteleone M, Fuoco A, Carta M, McKeown NB, et al. Highly Permeable Matrimid®/PIM-EA (H2)-TB Blend Membrane for Gas Separation. Polymers. 2019;11:46.
- [225] Khan MM, Bengtson G, Shishatskiy S, Gacal BN, Rahman MM, Neumann S, et al. Cross-linking of polymer of intrinsic microporosity (PIM-1) via nitrene reaction and its effect on gas transport property. European Polymer Journal. 2013;49:4157-66.
- [226] Du N, Cin MMD, Pinnau I, Nicalek A, Robertson GP, Guiver MD. Azide-based Cross-Linking of Polymers of Intrinsic Microporosity (PIMs) for Condensable Gas Separation. Macromolecular rapid communications. 2011;32:631-6.
- [227] Sekizkardes AK, Kusuma VA, McNally JS, Gidley David W, Resnik K, Venna SR, et al. Microporous polymeric composite membranes with advanced film properties: pore intercalation yields excellent CO2 separation performance. Journal of Materials Chemistry A. 2018;6:22472-7.
- [228] Mei Wu X, Gen Zhang Q, Ju Lin P, Qu Y, Mei Zhu A, Lin Liu Q. Towards enhanced CO2 selectivity of the PIM-1 membrane by blending with polyethylene glycol. Journal of Membrane Science. 2015;493:147-55.
- [229] Liu C, Wilson ST. Membranes Incorporating Microporous Polymers as Fillers. US Patent 7,410,5252008.
- [230] Hou L, Wang Z, Chen Z, Chen W, Yang C. PIM-1 as an organic filler to enhance CO2 separation performance of poly (arylene fluorene ether ketone). Separation and Purification Technology. 2020;242:116766.
- [231] Esposito E, Mazzei I, Monteleone M, Fuoco A, Carta M, McKeown NB, et al. Highly Permeable Matrimid(®)/PIM-EA(H₂)-TB Blend Membrane for Gas Separation. Polymers. 2018;11:46.
- [232] Brunetti A, Cersosimo M, Dong G, Woo KT, Lee J, Kim JS, et al. In situ restoring of aged thermally rearranged gas separation membranes. Journal of Membrane Science. 2016;520:671-8.
- [233] Lau CH, Konstas K, Thornton AW, Liu AC, Mudie S, Kennedy DF, et al. Gas-Separation Membranes Loaded with Porous Aromatic Frameworks that Improve with Age. Angewandte Chemie International Edition. 2015;54:2669-73.
- [234] Teplyakov V, Meares P. Correlation aspects of the selective gas permeabilities of polymeric materials and membranes. Gas Separation & Purification. 1990;4:66-74.
- [235] Jue ML, McKay CS, McCool BA, Finn M, Lively RP. Effect of Nonsolvent Treatments on the Microstructure of PIM-1. Macromolecules. 2015;48:5780-90.
- [236] Tiwari RR, Jin J, Freeman B, Paul D. Physical aging, CO2 sorption and plasticization in thin films of polymer with intrinsic microporosity (PIM-1). Journal of membrane science. 2017;537:362-71.
- [237] Smith SJ, Lau CH, Mardel JI, Kitchin M, Konstas K, Ladewig BP, et al. Physical aging in glassy mixed matrix membranes; tuning particle interaction for mechanically robust nanocomposite films. Journal of Materials Chemistry A. 2016;4:10627-34.
- [238] Tien-Binh N, Rodrigue D, Kaliaguine S. In-situ cross interface linking of PIM-1 polymer and UiO-66-NH2 for outstanding gas separation and physical aging control. Journal of Membrane Science. 2018;548:429-38.
- [239] Bernardo P, Bazzarelli F, Tasselli F, Clarizia G, Mason C, Maynard-Atem L, et al. Effect of physical aging on the gas transport and sorption in PIM-1 membranes. Polymer. 2017;113:283-94.
- [240] Sakaguchi N, Tanaka M, Yamato M, Kawakami H. Superhigh CO2-Permeable Mixed Matrix Membranes Composed of a Polymer of Intrinsic Microporosity (PIM-1) and Surface-Modified Silica Nanoparticles. ACS Applied Polymer Materials. 2019;1:2516-24.
- [241] Scholes CA, Kanehashi S. Polymer of intrinsic microporosity (PIM-1) membranes treated with supercritical CO2. Membranes. 2019;9:41.

- [242] Longo M, De Santo MP, Esposito E, Fuoco A, Monteleone M, Giorno L, et al. Correlating Gas Permeability and Young's Modulus during the Physical Aging of Polymers of Intrinsic Microporosity Using Atomic Force Microscopy. Industrial & Engineering Chemistry Research. 2019.
- [243] Tocci E, De Lorenzo L, Bernardo P, Clarizia G, Bazzarelli F, Mckeown NB, et al. Molecular Modeling and Gas Permeation Properties of a Polymer of Intrinsic Microporosity Composed of Ethanoanthracene and Tröger's Base Units. Macromolecules. 2014;47:7900-16.
- [244] Rochat S, Polak-Kraśna K, Tian M, Mays TJ, Bowen CR, Burrows AD. Assessment of the long-term stability of the polymer of intrinsic microporosity PIM-1 for hydrogen storage applications. International Journal of Hydrogen Energy. 2019;44:332-7.
- [245] Polak-Kraśna K, Fuhrhop C, Rochat S, Burrows A, Georgiadis A, Bowen C, et al. AFM imaging and nanoindentation of polymer of intrinsic microporosity PIM-1. International Journal of Hydrogen Energy. 2017;42:23915-9.
- [246] Zhou H, Jin W. Membranes with Intrinsic Micro-Porosity: Structure, Solubility, and Applications. Membranes. 2019;9:3.
- [247] Zhang C, Koros WJ. Tailoring the transport properties of zeolitic imidazolate frameworks by post-synthetic thermal modification. ACS applied materials & interfaces. 2015;7:23407-11.
- [248] Luo S, Wiegand JR, Gao P, Doherty CM, Hill AJ, Guo R. Molecular origins of fast and selective gas transport in pentiptycene-containing polyimide membranes and their physical aging behavior. Journal of Membrane Science. 2016;518:100-9.
- [249] Kim K, Koh D-Y. Aging: Degradation of Permeability in Microporous Polymeric Membranes. Membrane Journal. 2019;29:191-201.
- [250] Alaslai N, Ma X, Ghanem B, Wang Y, Alghunaimi F, Pinnau I. Synthesis and Characterization of a Novel Microporous Dihydroxyl-Functionalized Triptycene-Diamine-Based Polyimide for Natural Gas Membrane Separation. Macromolecular rapid communications. 2017;38:1700303.
- [251] Ma X, Abdulhamid M, Miao X, Pinnau I. Facile synthesis of a hydroxyl-functionalized troger's base diamine: a new building block for high-performance polyimide gas separation membranes. Macromolecules. 2017;50:9569-76.
- [252] Ahn J, Chung W-J, Pinnau I, Song J, Du N, Robertson GP, et al. Gas transport behavior of mixed-matrix membranes composed of silica nanoparticles in a polymer of intrinsic microporosity (PIM-1). Journal of membrane science. 2010;346:280-7.
- [253] Riasat Harami H, Riazi Fini F, Rezakazemi M, Shirazian S. Sorption in mixed matrix membranes: Experimental and molecular dynamic simulation and Grand Canonical Monte Carlo method. Journal of Molecular Liquids. 2019;282:566-76.
- [254] Riasat Harami H, Amirkhani F, Khadem SA, Rezakazemi M, Asghari M, Shirazian S. Mass transfer through PDMS/zeolite 4A MMMs for hydrogen separation: Molecular dynamics and grand canonical Monte Carlo simulations. International Communications in Heat and Mass Transfer. 2019;108:104259.
- [255] Rezakazemi M, Dashti A, Asghari M, Shirazian S. H2-selective mixed matrix membranes modeling using ANFIS, PSO-ANFIS, GA-ANFIS. International Journal of Hydrogen Energy. 2017;42:15211-25.
- [256] Ahmadpour E, Sarfaraz MV, Behbahani RM, Shamsabadi AA, Aghajani M. Fabrication of mixed matrix membranes containing TiO2 nanoparticles in Pebax 1657 as a copolymer on an ultra-porous PVC support. Journal of Natural Gas Science and Engineering. 2016;35:33-41.
- [257] Rezakazemi M, Ebadi Amooghin A, Montazer-Rahmati MM, Ismail AF, Matsuura T. State-of-the-art membrane based CO2 separation using mixed matrix membranes (MMMs): An overview on current status and future directions. Progress in Polymer Science. 2014;39:817-61.
- [258] Rostamizadeh M, Rezakazemi M, Shahidi K, Mohammadi T. Gas permeation through H2-selective mixed matrix membranes: Experimental and neural network modeling. International Journal of Hydrogen Energy. 2013;38:1128-35.

- [259] Rezakazemi M, Mohammadi T. Gas sorption in H2-selective mixed matrix membranes: Experimental and neural network modeling. International Journal of Hydrogen Energy. 2013;38:14035-41.
- [260] Chen M, Soyekwo F, Zhang Q, Hu C, Zhu A, Liu Q. Graphene oxide nanosheets to improve permeability and selectivity of PIM-1 membrane for carbon dioxide separation. Journal of industrial and engineering chemistry. 2018;63:296-302.
- [261] Alberto M, Luque-Alled JM, Gao L, Iliut M, Prestat E, Newman L, et al. Enhanced organophilic separations with mixed matrix membranes of polymers of intrinsic microporosity and graphene-like fillers. Journal of Membrane Science. 2017;526:437-49.
- [262] Tien-Binh N, Vinh-Thang H, Chen XY, Rodrigue D, Kaliaguine S. Crosslinked MOF-polymer to enhance gas separation of mixed matrix membranes. Journal of Membrane Science. 2016;520:941-50. [263] Wu X, Tian Z, Wang S, Peng D, Yang L, Wu Y, et al. Mixed matrix membranes comprising polymers of intrinsic microporosity and covalent organic framework for gas separation. Journal of Membrane Science. 2017;528:273-83.
- [264] Khan MM, Filiz V, Bengtson G, Shishatskiy S, Rahman MM, Lillepaerg J, et al. Enhanced gas permeability by fabricating mixed matrix membranes of functionalized multiwalled carbon nanotubes and polymers of intrinsic microporosity (PIM). Journal of membrane science. 2013;436:109-20. [265] Sodeifian G, Raji M, Asghari M, Rezakazemi M, Dashti A. Polyurethane-SAPO-34 mixed matrix membrane for CO2/CH4 and CO2/N2 separation. Chinese Journal of Chemical Engineering. 2019;27:322-34.
- [266] Su NC, Sun DT, Beavers CM, Britt DK, Queen WL, Urban JJ. Enhanced permeation arising from dual transport pathways in hybrid polymer–MOF membranes. Energy & Environmental Science. 2016;9:922-31.
- [267] Guo L, Wang X, Leong ZY, Mo R, Sun L, Yang HY. Ar plasma modification of 2D MXene Ti3C2Tx nanosheets for efficient capacitive desalination. FlatChem. 2018;8:17-24.
- [268] Bushell AF, Attfield MP, Mason CR, Budd PM, Yampolskii Y, Starannikova L, et al. Gas permeation parameters of mixed matrix membranes based on the polymer of intrinsic microporosity PIM-1 and the zeolitic imidazolate framework ZIF-8. Journal of Membrane Science. 2013;427:48-62.
- [269] Wang Z, Wang D, Zhang S, Hu L, Jin J. Interfacial design of mixed matrix membranes for improved gas separation performance. Advanced Materials. 2016.
- [270] Moore TT, Koros WJ. Non-ideal effects in organic–inorganic materials for gas separation membranes. Journal of Molecular Structure. 2005;739:87-98.
- [271] Bushell AF, Budd PM, Attfield MP, Jones JTA, Hasell T, Cooper AI, et al. Nanoporous Organic Polymer/Cage Composite Membranes. Angewandte Chemie International Edition. 2013;52:1253-6.
- [272] Mitra T, Bhavsar RS, Adams DJ, Budd PM, Cooper AI. PIM-1 mixed matrix membranes for gas separations using cost-effective hypercrosslinked nanoparticle fillers. Chemical Communications. 2016;52:5581-4.
- [273] Lau CH, Nguyen PT, Hill MR, Thornton AW, Konstas K, Doherty CM, et al. Ending aging in super glassy polymer membranes. Angewandte Chemie International Edition. 2014;53:5322-6.
- [274] Smith SJ, Ladewig BP, Hill AJ, Lau CH, Hill MR. Post-synthetic Ti exchanged UiO-66 metal-organic frameworks that deliver exceptional gas permeability in mixed matrix membranes. Scientific reports. 2015;5:1-6.
- [275] Ma J, Ying Y, Guo X, Huang H, Liu D, Zhong C. Fabrication of mixed-matrix membrane containing metal—organic framework composite with task-specific ionic liquid for efficient CO 2 separation. Journal of Materials Chemistry A. 2016;4:7281-8.
- [276] Song Q, Cao S, Pritchard RH, Qiblawey H, Terentjev EM, Cheetham AK, et al. Nanofiller-tuned microporous polymer molecular sieves for energy and environmental processes. Journal of Materials Chemistry A. 2016;4:270-9.

- [277] Kinoshita Y, Wakimoto K, Gibbons AH, Isfahani AP, Kusuda H, Sivaniah E, et al. Enhanced PIM-1 membrane gas separation selectivity through efficient dispersion of functionalized POSS fillers. Journal of Membrane Science. 2017.
- [278] Konnertz N, Ding Y, Harrison WJ, Budd PM, Schönhals A, Böhning M. Molecular mobility and gas transport properties of nanocomposites based on PIM-1 and polyhedral oligomeric phenethyl-silsesquioxanes (POSS). Journal of Membrane Science. 2017;529:274-85.
- [279] Yang L, Tian Z, Zhang X, Wu X, Wu Y, Wang Y, et al. Enhanced CO2 selectivities by incorporating CO2-philic PEG-POSS into polymers of intrinsic microporosity membrane. Journal of Membrane Science. 2017;543:69-78.
- [280] Rezakazemi M, Vatani A, Mohammadi T. Synthesis and gas transport properties of crosslinked poly(dimethylsiloxane) nanocomposite membranes using octatrimethylsiloxy POSS nanoparticles. Journal of Natural Gas Science and Engineering. 2016;30:10-8.
- [281] Rezakazemi M, Vatani A, Mohammadi T. Synergistic interactions between POSS and fumed silica and their effect on the properties of crosslinked PDMS nanocomposite membranes. RSC Advances. 2015;5:82460-70.
- [282] Yong WF, Kwek KHA, Liao K-S, Chung T-S. Suppression of aging and plasticization in highly permeable polymers. Polymer. 2015;77:377-86.
- [283] Khan MM, Filiz V, Bengtson G, Shishatskiy S, Rahman M, Abetz V. Functionalized carbon nanotubes mixed matrix membranes of polymers of intrinsic microporosity for gas separation. Nanoscale research letters. 2012;7:504.
- [284] Sun H, Gao W, Zhang Y, Cao X, Bao S, Li P, et al. Bis (phenyl) fluorene-based polymer of intrinsic microporosity/functionalized multi-walled carbon nanotubes mixed matrix membranes for enhanced CO2 separation performance. Reactive and Functional Polymers. 2020;147:104465.
- [285] Elliot A. Separation of carbon dioxide from flue gas by mixed matrix membranes using dual phase microporous polymeric constituents. Chemical Communications. 2016;52:11768-71.
- [286] Adelnia H, Gavgani JN, Riazi H, Bidsorkhi HC. Transition behavior, surface characteristics and film formation of functionalized poly (methyl methacrylate-co-butyl acrylate) particles. Progress in Organic Coatings. 2014;77:1826-33.
- [287] Bhavsar RS, Mitra T, Adams DJ, Cooper AI, Budd PM. Ultrahigh-permeance PIM-1 based thin film nanocomposite membranes on PAN supports for CO2 separation. Journal of Membrane Science. 2018;564:878-86.
- [288] Tian Z, Wang S, Wang Y, Ma X, Cao K, Peng D, et al. Enhanced gas separation performance of mixed matrix membranes from graphitic carbon nitride nanosheets and polymers of intrinsic microporosity. Journal of Membrane Science. 2016;514:15-24.
- [289] Younas M, Rezakazemi M, Daud M, Wazir MB, Ahmad S, Ullah N, et al. Recent progress and remaining challenges in post-combustion CO2 capture using metal-organic frameworks (MOFs). Progress in Energy and Combustion Science. 2020;80:100849.
- [290] Ahmadijokani F, Mohammadkhani R, Ahmadipouya S, Shokrgozar A, Rezakazemi M, Molavi H, et al. Superior chemical stability of UiO-66 metal-organic frameworks (MOFs) for selective dye adsorption. Chemical Engineering Journal. 2020;399:125346.
- [291] Smith SJ, Ladewig BP, Hill AJ, Lau CH, Hill MR. Post-synthetic Ti exchanged UiO-66 metal-organic frameworks that deliver exceptional gas permeability in mixed matrix membranes. Scientific reports. 2015;5.
- [292] Mason CR, Buonomenna MG, Golemme G, Budd PM, Galiano F, Figoli A, et al. New organophilic mixed matrix membranes derived from a polymer of intrinsic microporosity and silicalite-1. Polymer. 2013;54:2222-30.

[293] Alentiev AY, Bondarenko G, Kostina YV, Shantarovich V, Klyamkin S, Fedin V, et al. PIM-1/MIL-101 hybrid composite membrane material: Transport properties and free volume. Petroleum Chemistry. 2014;54:477-81.

[294] Ghalei B, Sakurai K, Kinoshita Y, Wakimoto K, Isfahani AP, Song Q, et al. Enhanced selectivity in mixed matrix membranes for CO2 capture through efficient dispersion of amine-functionalized MOF nanoparticles. Nature Energy. 2017;2:nenergy201786.

[295] Wang Z, Ren H, Zhang S, Zhang F, Jin J. Polymers of intrinsic microporosity/metal—organic framework hybrid membranes with improved interfacial interaction for high-performance CO 2 separation. Journal of Materials Chemistry A. 2017.

[296] Morris CG, Jacques NM, Godfrey HG, Mitra T, Fritsch D, Lu Z, et al. Stepwise observation and quantification and mixed matrix membrane separation of CO 2 within a hydroxy-decorated porous host. Chemical Science. 2017;8:3239-48.

[297] Khdhayyer MR, Esposito E, Fuoco A, Monteleone M, Giorno L, Jansen JC, et al. Mixed matrix membranes based on UiO-66 MOFs in the polymer of intrinsic microporosity PIM-1. Separation and Purification Technology. 2017;173:304-13.

[298] Cheng Y, Wang X, Jia C, Wang Y, Zhai L, Wang Q, et al. Ultrathin mixed matrix membranes containing two-dimensional metal-organic framework nanosheets for efficient CO 2/CH 4 separation. Journal of Membrane Science. 2017.

[299] Althumayri K, Harrison WJ, Shin Y, Gardiner JM, Casiraghi C, Budd PM, et al. The influence of few-layer graphene on the gas permeability of the high-free-volume polymer PIM-1. Phil Trans R Soc A. 2016;374:20150031.

[300] Hao L, Liao K-S, Chung T-S. Photo-oxidative PIM-1 based mixed matrix membranes with superior gas separation performance. Journal of Materials Chemistry A. 2015;3:17273-81.

[301] Yi S, Ghanem B, Liu Y, Pinnau I, Koros WJ. Ultraselective glassy polymer membranes with unprecedented performance for energy-efficient sour gas separation. Science Advances. 2019;5:eaaw5459.

[302] Yi S, Ma X, Pinnau I, Koros WJ. A high-performance hydroxyl-functionalized polymer of intrinsic microporosity for an environmentally attractive membrane-based approach to decontamination of sour natural gas. Journal of Materials Chemistry A. 2015;3:22794-806.

[303] Genduso G, Wang Y, Ghanem BS, Pinnau I. Permeation, sorption, and diffusion of CO2-CH4 mixtures in polymers of intrinsic microporosity: The effect of intrachain rigidity on plasticization resistance. Journal of Membrane Science. 2019;584:100-9.

[304] Budhathoki S, Ajayi O, Steckel JA, Wilmer CE. High-throughput computational prediction of the cost of carbon capture using mixed matrix membranes. Energy & Environmental Science. 2019;12:1255-64.

[305] Polak-Kraśna K, Dawson R, Holyfield LT, Bowen CR, Burrows AD, Mays TJ. Mechanical characterisation of polymer of intrinsic microporosity PIM-1 for hydrogen storage applications. Journal of Materials Science. 2017;52:3862-75.

[306] Lin H, Freeman BD. Gas permeation and diffusion in cross-linked poly (ethylene glycol diacrylate). Macromolecules. 2006;39:3568-80.

[307] Yavari M, Maruf S, Ding Y, Lin H. Physical aging of glassy perfluoropolymers in thin film composite membranes. Part II. Glass transition temperature and the free volume model. Journal of Membrane Science. 2017;525:399-408.

[308] Zirehpour A, Rahimpour A, Arabi Shamsabadi A, Sharifian Gh M, Soroush M. Mitigation of thin-film composite membrane biofouling via immobilizing nano-sized biocidal reservoirs in the membrane active layer. Environmental science & technology. 2017;51:5511-22.

[309] Scofield JM, Gurr PA, Kim J, Fu Q, Kentish SE, Qiao GG. Development of novel fluorinated additives for high performance CO 2 separation thin-film composite membranes. Journal of Membrane Science. 2016;499:191-200.

[310] Ma X, Pinnau I. Effect of film thickness and physical aging on "intrinsic" gas permeation properties of microporous ethanoanthracene-based polyimides. Macromolecules. 2018;51:1069-76.

[311] Kujawa J, Rynkowska E, Fatyeyeva K, Knozowska K, Wolan A, Dzieszkowski K, et al. Preparation and Characterization of Cellulose Acetate Propionate Films Functionalized with Reactive Ionic Liquids. Polymers. 2019;11:1217.

[312] Merkel TC, Lin H, Wei X, Baker R. Power plant post-combustion carbon dioxide capture: An opportunity for membranes. Journal of membrane science. 2010;359:126-39.